THE MESSENGER

EL MENSAJERO

Paranal
La Silla
La Serena
Santiago
Munich

No. 95 – March 1999

TELESCOPES AND INSTRUMENTATION

ISAAC at the VLT

A. MOORWOOD, J.-G. CUBY, P. BALLESTER, P. BIEREICHEL, J. BRYNNEL, R. CONZELMANN, B. DELABRE, N. DEVILLARD, A. VAN DIJSSELDONK, G. FINGER, H. GEMPERLEIN, C. LIDMAN, T. HERLIN, G. HUSTER, J. KNUDSTRUP, J.-L. LIZON, H. MEHRGAN, M. MEYER, G. NICOLINI, A. SILBER, J. SPYROMILIO, J. STEGMEIER

ESO

1. Introduction

ISAAC (Infrared Spectrometer and Array Camera) provides for 1–5 µm imaging; 1–2.5 µm polarimetry and 1–5 µm spectroscopy and is the first VLT instrument fully developed by ESO. Figure1 shows it mounted on the adapter/rotator at the Nasmyth B focus of the first of the four 8.2-m VLT Unit Telescopes. ISAAC itself is cryogenically cooled and housed within a 1.6-m diameter vacuum vessel enclosed by the red protective cover seen in this photograph. The large unit to the right, flanked by the two racks of control electronics, is the cable co-rotator system which carries the electrical cables and closed-cycle cooler hoses to the instrument and rotates with it as the telescope tracks objects on the sky. Following integration and extensive testing in Garching, ISAAC was delivered to the Paranal Observatory in June 1998 where it was re-assembled and re-tested in the Integration Laboratory prior to installation on the telescope, as scheduled, on November 14th. First light images were already shown in *The Messenger* 94, 7, and accompanied by a very short article written in the VLT control room while the

Figure 1: ISAAC installed at the Nasmyth B focus of the VLT UT1. The instrument, enclosed in its protective red cover, is attached to the adapter/rotator system at the left and has a total weight of around 1.5 tons. The box at the left contains some of the electronics required for controlling and reading the two infrared array detectors. To the right is the co-rotator system that transfers all the electrical cables and gas hoses for the closed-cycle coolers to the instrument and rotates with it and the adapter. At each side of the co-rotator are cabinets containing electronics for controlling and monitoring the instrument functions and the vacuum and cryogenic system. At the bottom can be seen part of the platform to which the instrument is attached for installation, removal and maintenance activities.

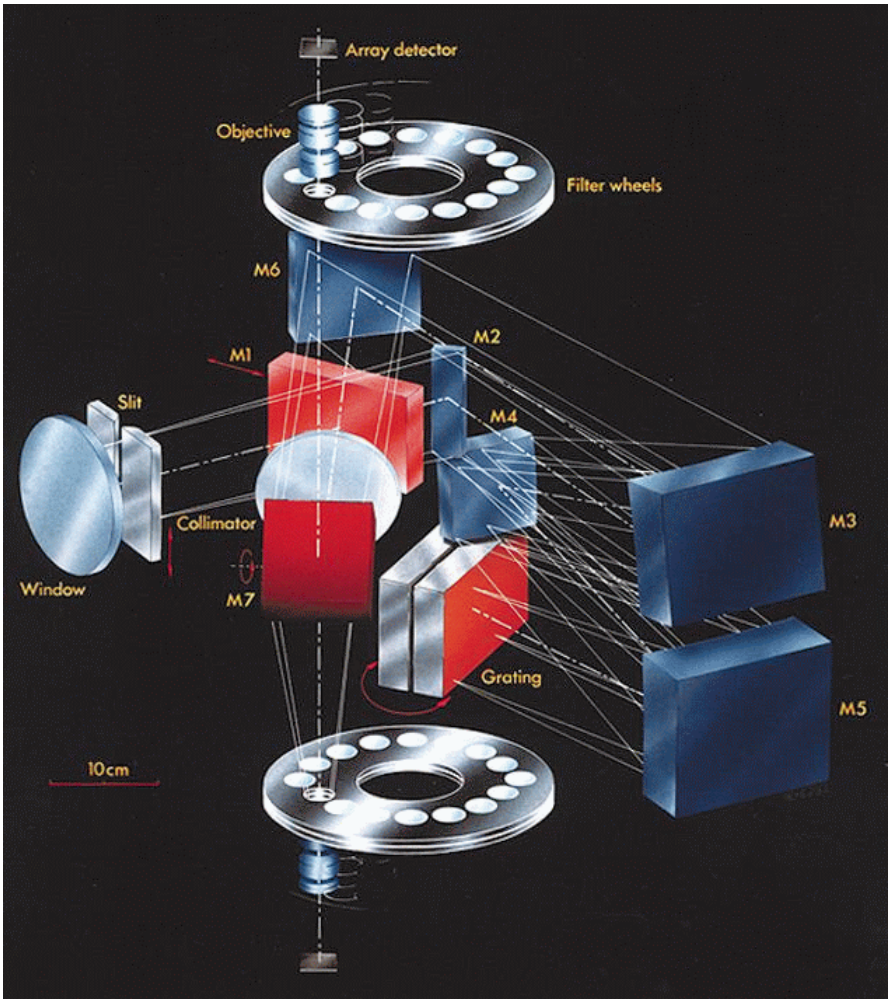

Figure 2: Optical layout of ISAAC. See text for a detailed explanation.

first tests were still in progress. Just prior to the planned start of routine operations on April 1st, it is appropriate here to briefly recall its design and development, report on its performance during the commissioning tests and present some spectra of relatively faint objects which illustrate further the new scientific capabilities now offered by this instrument.

2. Scientific Capabilities

Scientific interest in ISAAC encompasses most topics in modern astronomy from the study of faint outer solar-system bodies to the most distant galaxies and clusters. In these and other areas, such as the study of Brown Dwarfs and low-mass stars, its particular strength lies in the possibility of both making deep imaging observations and surveys and following them up spectroscopically. There is no space here to enter into a detailed discussion of the scientific results and discoveries to be expected. It is, however, interesting to recall that near-infrared imaging and spectroscopy of high redshift galaxies was highlighted in the original ISAAC Design and Implementation Plan of October 1991 as the area which could potentially gain most from such an instrument on a large telescope. More specific topics mentioned were the observation of 'visible' lines for redshift determinations, deep searches for extremely red, possibly primeval galaxies, studies of cluster evolution, etc. Although apparently trivial as a prophecy now, few high z galaxies were actually known at that time and the enormous level of current activity and interest in this area together with the relatively large fraction of ISAAC observing time allocated to it in P 63 is therefore rather comforting. That the required sensitivity can actually be reached is also supported by some of the spectra obtained during commissioning and shown here.

Figure 3: ISAAC with its front vacuum flange removed revealing the slit/mask wheel and the casting used to support its various opto-mechanical functions, including the two cameras which are partly visible to the upper and lower right of the centre.

3. Observational Modes

ISAAC offers the following observational modes:

- Imaging through broad- and narrow-band filters
  - 0.9–2.5 µm with a 2.5 × 2.5′ field of view and 0.147″ pixels
  - 2.5–5 µm with a 40 × 40″ max. field of view and pixels of 0.16″ and 0.08″
- Imaging polarimetry
  - 0.9–2.5 µm using a Wollaston prism with broad-band and a limited set of narrow-band filters
- Spectroscopy at Rs ∼ 500 and 3000 and slit widths of 0.3, 0.6, 1 and 2″
  - 0.9–2.5 µm with a slit length of 2′
  - 2.5–5 µm with a slit length of 40″

The more detailed information required for making an observing proposal can be found on the Web (http://www.eso.org/observing/observing.html).

4. Design and Development

Figure 2 shows the optical layout of ISAAC. It contains two cameras (each comprising 2 filter wheels, an objective wheel and an array detector) one of which is optimised for the 1–2.5 µm and the other for the 2.5–5 µm spectral ranges. For imaging and polarimetry the light entering the window at the left passes through the slit/mask wheel, is diverted by the mirror M1 through the 16-cm-diameter BaF2 collimator/field lens and to the required camera by the M7 selector mirror. For spectroscopy the mirror M1 is retracted, allowing light from the slit to

pass through the spectrometer unit to form an intermediate spectrum close to M6 which is then re-imaged by the selected camera. The spectrometer unit consists of 2 back-to-back mounted gratings – for the low- and medium-resolution modes – and a mirror system comprising three hyperbolic mirrors (M3, M4, M5), which were diamond turned on nickel-coated aluminium and then hand post polished and gold coated. This system is used both to collimate the 10-cm-diameter beam and to form the intermediate spectrum after dispersion at the grating. Attached to the front of the instrument is the pre-slit unit containing a pupil lens, integrating sphere, continuum plus line lamps for flat fielding and wavelength calibration and a technical CCD for slit viewing.

The 1–2.5 µm (SW) 'arm' is equipped with a 1024 × 1024 pixel Hg:Cd:Te array manufactured by the Rockwell International Science Center and the 2.5–5 µm 'arm' with a 256 × 256 InSb array from the Santa Barbara Research Center. Detector control and data acquisition is via the ESO-developed high-speed IRACE system (Meyer et al. 1996).

Most of the moving functions in ISAAC (slit/mask wheel, M1 and M7 selector mirrors, grating, filter and objective wheels) are mounted on paired, angular contact, bearings and driven by 5-phase stepper motors (modified at ESO for cryogenic operation) and stainless steel worm gears acting on Vespel or Nylcast toothed wheels attached to the functions. The linear lens collimator drive employs a preloaded roller screw. Initialisation of the functions is by means of magnetic sensors. In the case of the bearings, the steel balls were replaced by tungsten carbide ones and the separators by self-lubricating Nylcast cages impregnated with 321R from Dow Corning. Because of the inherent difficulty in developing such high-precision moving functions for operation at cryogenic temperatures in vacuum, both the individual components as well as a complete prototype unit were extensively tested before the Final Design Review of the instrument. The various optomechanical functions, including their drive systems, are all supported by a cast aluminium structure surrounded by a radiation shield and attached to the vacuum vessel by two fibreglass 'spiders'. Figure 3 shows ISAAC with the front cover of its vacuum vessel removed and provides a view of the cast structure plus the large slit/mask wheel and parts of the two cameras. Access to the spectrometer is by removing the rear vacuum flange. Total mass of the cryogenically cooled part is 350 kg. Despite this large mass, it can be cooled to its operating temperature of 70 K (and the detectors to as low as 25 K) in 24 hours using a liquid-nitrogen continuous-flow circuit during this phase to boost the cooling power of the two closed-cycle coolers used to maintain the required temperatures during normal operation. Evacuation is by means of a backing pump behind a turbomolecular pump flanged directly onto the vacuum vessel. All cryogenic operations during cool-down and warm-up are controlled automatically by the control system which also monitors temperatures/pressure and sounds safety alarms and/or initiates safety features (e.g. automatic warming up of the detectors in case of loss of cooling power or a rapid pressure rise). Additional details of the design have been given by Moorwood (1996) and of the integration phase in Garching by Lizon (1996).

Figure 4: Colour composite image of the merging galaxy system ESO202–G23 which combines a 1200s ISAAC H (1.65 µm) band exposure with B (1800s) and R (900s) images obtained with the VLT test camera. The field shown here is ∼1.5′ with north at the top and east to the left and the seeing was ∼ 0.4″. Visible are at least one Active Galaxy Nucleus with an associated ionisation cone; a blue star-forming complex to the south; and a complicated pattern of emission resulting from the merger and heavy extinction. Of additional interest is the arc of more distant red galaxies in the lower part of the image.

5. Performance

Based on the commissioning tests and observations made so far, the astronomical performance of ISAAC fully lives up to expectations. The combination of excellent telescope and instrument optical quality delivers fully seeing-limited images with a smallest FWHM so far of 0.28″. The arrays are cosmetically good, the fields 'clean' and flat (to a few per cent before flat fielding), internal flexure is less than 0.5 pixel and the limiting magnitudes are set by the sky + telescope background and the seeing. For observations in the thermal infrared, beyond 2.5 µm, the telescope passed with flying colours its most difficult challenge of performing the active optics corrections while nodding plus chopping and field stabilising with M2.

Given the new maturity of infrared capabilities, it is likely that many scientific programmes will increasingly combine visible and infrared data. As an example, Figure 4 shows a colour composite (B, R, H(1.65 µm)) image of the merging active galaxy system ESO 202-G23 made by combining images obtained with ISAAC and the VLT test camera and which adds to the diagnostic power of the visible or infrared images alone. A selection of other illustrative images has already been presented in *The Messenger* 94, 7 (1998) and on the Web (http://www.eso.org/outreach/press-rel).

Low-resolution spectroscopy at most wavelengths is also background limited by the radiation from the sky and tele-

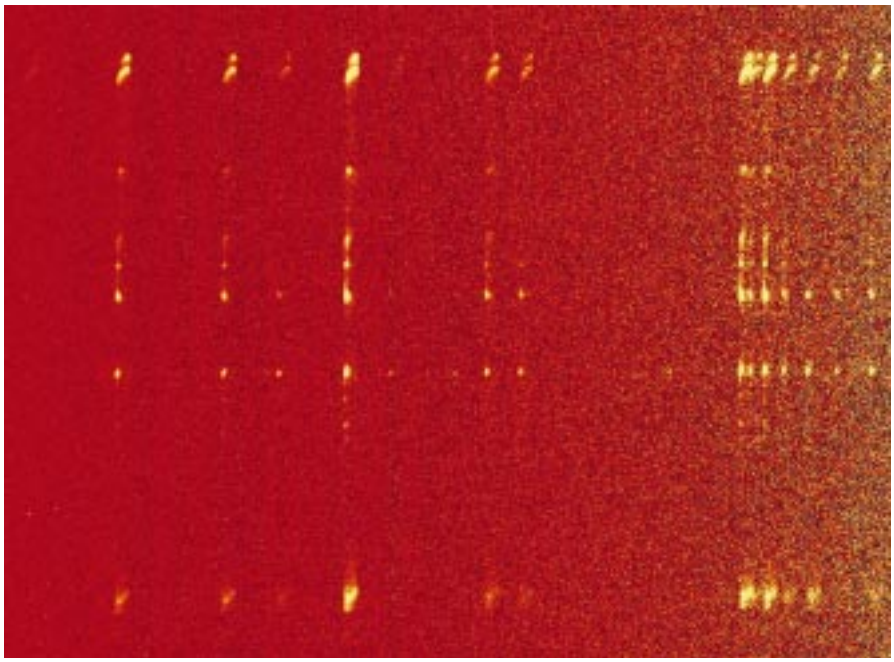

Figure 5: Low-resolution 2–2.5 µm spectral image of HH212 which fully exploits the 2′ long slit. This galactic object is believed to harbour a heavily obscured protostar that has expelled material periodically during it evolution. What is remarkable is the degree of symmetry of the 'bullets' ejected in opposite directions. Each of the 'images' seen here corresponds to a different emission line of interstellar molecular hydrogen that has been excited by the impact of the ejected material.

scope. Examples are shown in Figures 5 and 6 which show a K band spectral image of the fascinating Herbig Haro object HH212 and J, H, K band spectra of the radio galaxy MRC0406-244 plus two extremely red, nearby, galaxies. At medium resolution (R ~ 3000) in the J and H bands, however, regions between the OH sky lines open up where the background continuum has been measured to be extremely low (< 0.1 e^-/s). As the detector dark current is even lower than this, sensitivity in these regions is limited essentially by the detector read noise (< 10 e^-), bad pixels and cosmic rays. This is illustrated by Figure 7 which shows medium-resolution spectra around 1.06 µm of redshifted Hα (+[NII]) emission in two $z \sim 0.62$ galaxies from the CFRS catalogue which are only a few arcsec apart on the sky (Hammer et al. 1995). Finally, Figure 8 shows an example of medium-resolution 'imaging' spectroscopy in the form of a spectrum of SN 1987A obtained through the 2″ slit and with the grating set close to the He I 1.083 µm line.

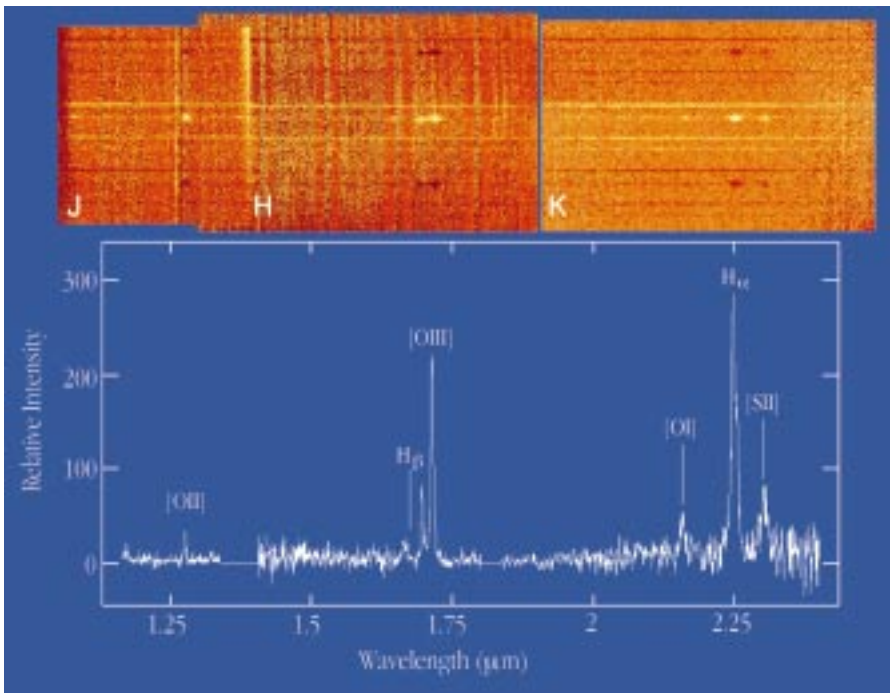

Figure 6: The upper panel shows a montage of low-resolution (R ~ 500) spectral images covering most of the 1–2.5 µm region of the z = 2.4 radio galaxy MRC0406–244 plus two extremely red (R-K > 5) galaxies below and an anonymous one above. Integration times were 2 hours in the J and 1 hour in H and K bands. The negative images of the spectra result from the technique used for sky subtraction, and the vertical stripes are due to increased photon shot noise at the positions of OH night sky lines. The extracted spectrum of the radio galaxy in the lower panel shows the prominent, redshifted, emission lines [OII], Hβ [OIII] (doublet), [OI], Hα and [SII] (doublet) normally observed at visible wavelengths in nearby objects. The apparent absence of these lines in the spectra of the companion red galaxies casts some doubt on the suggested possibility that they are members of a cluster at the same redshift as the radio galaxy.

Because performance is a strong function of mode, wavelength, conditions, etc, it is difficult, and potentially misleading, to summarise it in a few numbers here. The information is available, however, and has been incorporated into the ISAAC Exposure Time Calculators, the ISAAC Users Manual and other information which is available and will be maintained on the Web (http://www.eso.org/observing/observing.html).

6. Observing with ISAAC

Routine observations with ISAAC are planned to start in P 63 on April 1st, 1999. Of course, ISAAC is fully embedded in the VLT operational philosophy and data-flow system as described in detail on the Web (http://www.eso.org/org/dmd). The normal starting point in preparing proposals will probably be to consult the Instrument Description, Users Manual, etc. on the Web and to use the Exposure Time Calculators (ETC) referred to above to assess feasibility and estimate the required integration times. Proposals can then be submitted for either Service or Visitor Mode observations as described in ESO's Announcement for the relevant period. In both cases, the actual observations will be executed at the telescope via Observing Blocks consisting of acquisition and instrument (observation description) templates, which set the various, instrument functions and parameters and control the exposures via a sequencer. Real time feedback on the instrument status and the progress of the observations is provided via the Observing Software display on the instrument workstation and the actual images are displayed on a Real Time Display (RTD). The RTD is also used interactively in some modes e.g. to 'drag' objects seen in the imaging mode into the slit for spectroscopy and to determine pixel values, coordinates, image quality, etc. All raw data are archived as are those reduced by the reduction pipelines whose current status is described separately by Devillard et al. in this issue. Additional observations defined in a Calibration Plan will also be conducted by ESO in order to maintain the instrument performance, analyse trends (e.g. in zero point, dark and flat field variations) and to allow calibration of Service Mode data to a specified level.

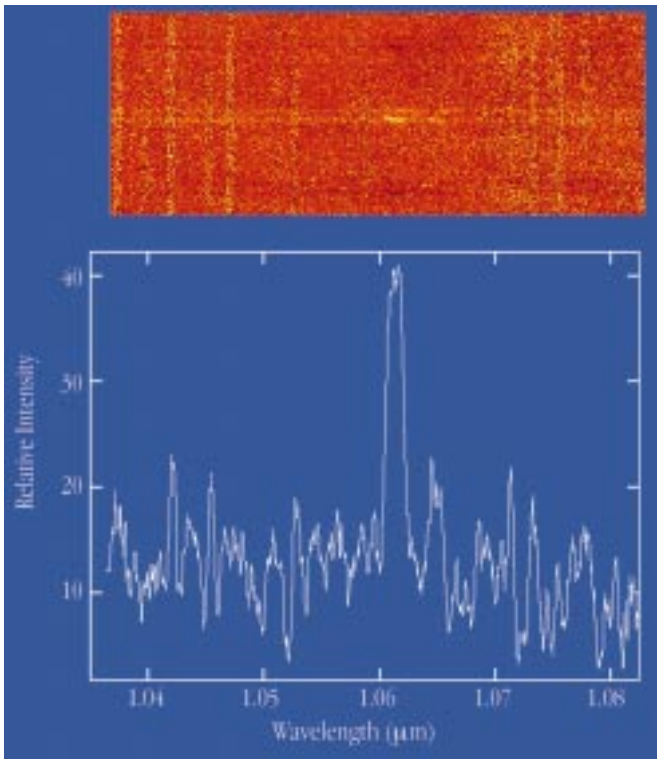

Figure 7: The upper panel shows a medium resolution (R ~ 3000) spectral image around 1.06 μm of two galaxies at z ~ 0.62 selected from the CFRS catalogue. Total exposure time was 1 hour. The lower panel shows the extracted spectrum of the brighter galaxy which, in addition to the continuum, shows bright redshifted Hα and fainter [NII] (to the right) emission lines. As can be seen in the image, the Hα emission appears to be tilted relative to the continuum due to the rotation of the galaxy which can thus be measured to provide an estimate of its mass.

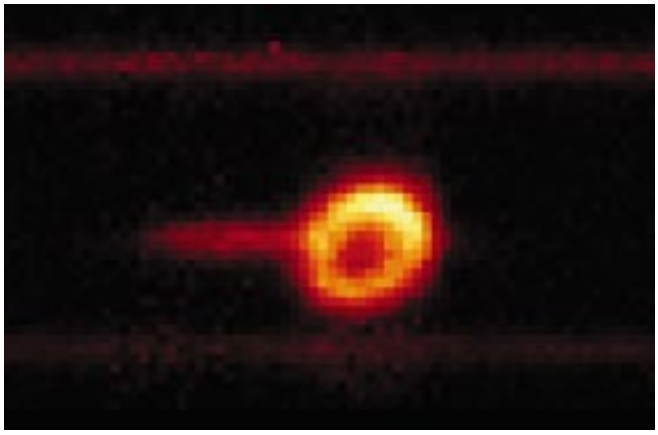

Figure 8: A spectral image of SN 1987A in the HeI (1.083 μm) line obtained in a 20-min exposure using the medium-resolution grating and a 2″ wide slit. The ring is formed of gas blown off the progenitor star during its evolution and which was first photoionised by UV light from the SN and more recently shock ionised by ejecta which, travelling at 30,000 km/s, has only just reached it after a travel time of nearly 12 years. The jet-like feature extending to the left is actually in the spectral dispersion direction and shows the presence of a blue-shifted, high-velocity component that is believed to arise in the ionised ejecta.

7. Acknowledgements

We wish to particularly thank the ISAAC Science Team R. Chini, G. Miley, E. Oliva and J.-L. Puget for their suggestions and encouragement throughout the design and development phase; R. Gilmozzi, P. Gray, M. Petr, G. Rahmer and P. Sansgasset for their support during installation and commissioning on Paranal and J. Alves, P. Amico and M. Kissler-Patig in Garching. Collective thanks are also due to many other people, too numerous to mention individually and within all Divisions of ESO, who have contributed to this project. We are also grateful to L. Tresse and O. Le Fèvre for detailed information on the CFRS galaxy sample.

References

Hammer, F., Crampton, D., Le Fèvre, O., Lilly, S.J. 1995, *ApJ*, **455**,88.

Lizon, J.-L. 1996, *The Messenger*, **86**, 11.

Meyer, M., Finger, G., Mehrgan, H., Stegmeier, J., Moorwood, A.F.M.: 1996, *The Messenger*, **86**, 14.

Moorwood, A.F.M. 1996, In Optical Telescopes of Today and Tomorrow (ed. A. Ardeberg), *SPIE* Vol. 2871, 1146.

amoor@eso.org

ISAAC Pipeline Data Reduction

N. DEVILLARD, Y. JUNG, J.-G. CUBY, ESO

The ISAAC pipeline, just as the pipeline for any other VLT instrument, is built to provide reduced data on site in order to assess their quality as soon as possible. Another version of the same software will also be running in Garching for quality control, trend analysis, and service-observing data-reduction purposes. All instrument pipelines share the same generic structure, taking care of data handling, i.e. transfers and reduction recipe triggering. The recipes themselves are specific to each instrument, they are plug-ins hooked into this generic data-handling structure, and they can be described as specialised tasks attached to an instrument-acquisition template. For more details about pipelines and Data Flow, the reader is referred to the ESO Web pages and corresponding reference documents.

The following instrumental modes are supported in pipeline mode for the first ISAAC period: imaging jitter, twilight flat, darks and bad pixel map creation, illumination frames and zero-point computations. In spectroscopy: NodOnSlit, flat-field, spectroscopic response function, star trace calibration, and slit position. We give here an overview of the algorithms used to reduce the data without user intervention for all these modes, so that observers can get a rough idea of what is done in pipeline mode, what the working domain for the recipes is, what can be obtained in the control-room at runtime, and how to reproduce these reduction processes at their home institute if they wish to.

1. Imaging Mode

Imaging recipes (procedures) are based on the ESO **eclipse** library, mainly to speed up the number-crunching process (see article in *The Messenger* No. 87, p. 19–20). The eclipse library is exportable, compiles on virtually any (recent) Unix machine that has minimum POSIX compatibility, and is available on the Web at the following address: http://www.eso.org/eclipse/

Calibration recipes

Dark frames are acquired through a dedicated template, which stores several dark frames for each possible DIT (Detector Integration Time), and usually

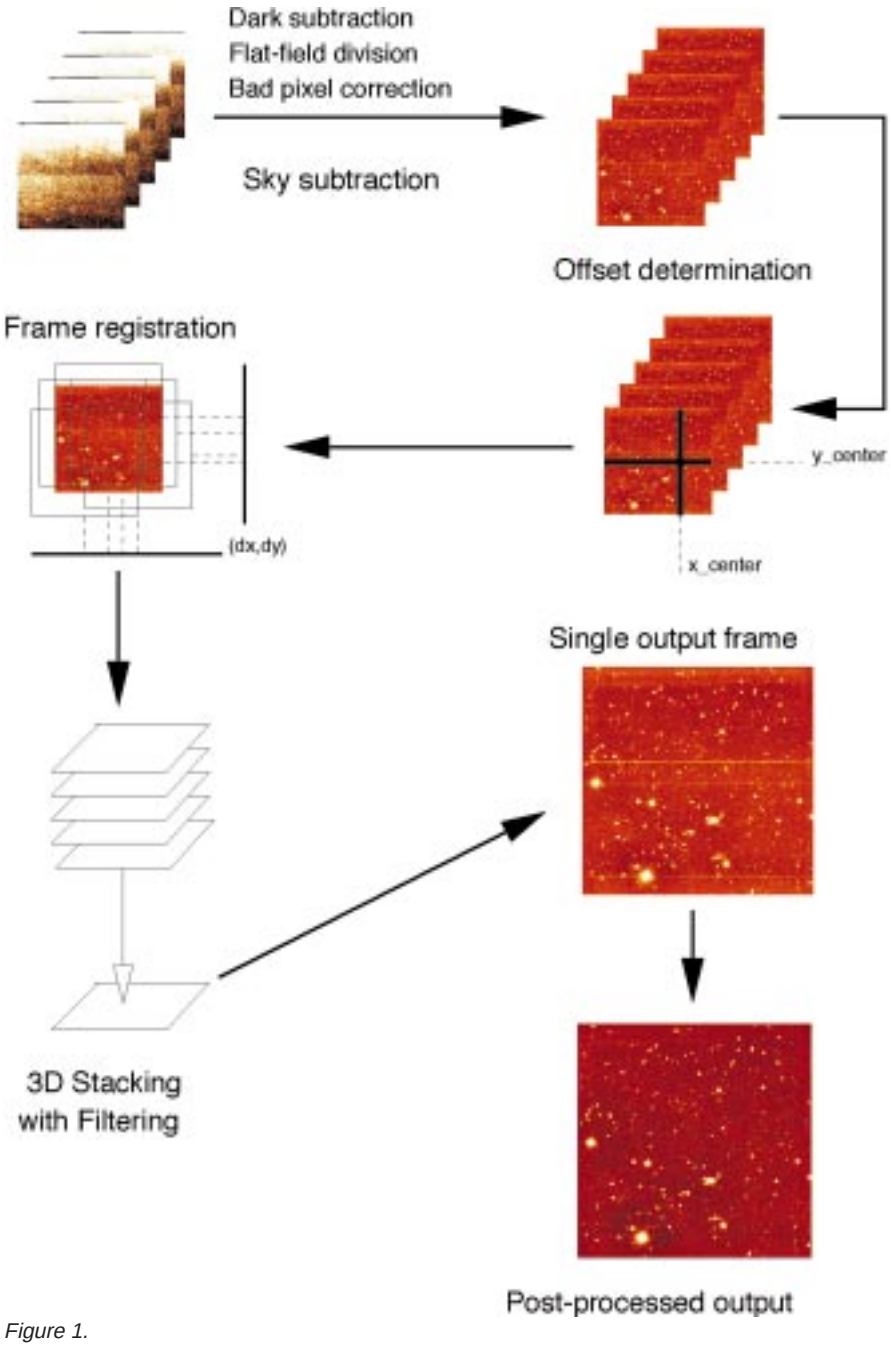

Figure 1.

covers several DIT values. The output of this template is a list of frames containing dark exposures, which need to be sorted out by DIT group and then averaged per group with rejection criteria to avoid cosmics. The output of the **is_darks** procedure is a list of frames, one for each given DIT. Read-out noise is also measured from these frames and the information is written to a readable ASCII file. The associated eclipse routine is **is_darks**. It is recommended to take 5 darks or more per DIT you used during the observation night, so that the computed master dark frame is reasonably reliable.

Twilight flatfields are acquired through a template that observes the sky at dawn or dusk with a constant integration time. Produced frames have an increasing or decreasing signal value that is used to measure detector linearity. For each pixel on the detector, a curve is plotted of the median plane value (x axis) against the individual pixel value in this plane (y axis). This curve shows the pixel's response, from which a robust linear regression provides a pixel gain. The image showing all pixel gains (i.e. the flatfield) is normalised to have an average value of 1. Some criteria can be added later to check that the pixel behaviour is indeed linear, and build a bad pixel map for pixels that have excessively high or low gains, or do not behave linearly at all. The same procedure could be used with any kind of increasing/decreasing signal, which allows to sample the pixels' response at various points. The associated eclipse routine is called **flat**.

Flat-fields are usually corrected for low-frequency variations which are not taken into account by the twilight flat procedure. To compute these variations, a dedicated calibration template is offered. The procedure images a standard star on a grid of 4×4 or 5×5 positions, with the convention that the first acquired frame shall contain the standard at the centre of the image, and subsequent positions be indicated through keywords in the FITS header. Photometry is computed for each star position and a 2d second-degree polynomial is fitted through the obtained surface. An image is generated from this polynomial with an average value of 1. The associated eclipse routine is **is_illum**.

Zero-point acquisitions are done by observing a standard star with wide offsets on the detector. The operator at the instrument is in charge of locating the standard star through finding charts and positioning it at the centre of the array for the very first frame. Subsequent frame offsets are indicated in the FITS header. The recipe identifies the exact position of the standard star up to ± 50 pixels from the centre, computes the number of counts, and relates that measurement to a standard star database. The possible telescope pointing errors are not relevant to this case, because the star has been identified and positioned by human means. This is necessary to ensure that the star is actually in all frames and this is part of the acquisition process for this template. As a consequence, the algorithm does not need automatic astrometric calibration but a simple local peak-finder method. The ideal would be to provide star localisation through un-supervised astrometry; this may be implemented later. The identified infrared star database at this moment contains about 800 star positions with magnitudes in bands J, H, K, Ks, L, M. Some stars have missing information, it is recommended to test out beforehand that the standard star you will be using can actually be found and used from this database. The star search only looks for the closest star in position from RA and DEC information in the header, and computes zero-point information from it. In case of star mismatch (e.g. several standards are in the field), it should be easy to check out that the star used corresponds to the acquired one because all data relative to the used star are given along with the measured values. The standard star database is currently accessible through an eclipse command called **std**. Later on, access should be given through the Web to this list and users should be able to provide their own standards. The associated eclipse routine for zero-point computation is called **is_zerop**. Notice that this method will not apply to standard stars in crowded fields, since it is relying on the assumption that the standard star to look for is the brightest object in the centre of the first frame, a condition that is not fulfilled in that case.

Observation recipes

The main instrumental mode supported by the pipeline is the jittering mode (also known as microscanning). In this mode, no direct sky observation is performed, which maximises observation efficiency. However, a number of as-

sumptions must be fulfilled in order to use this template. The observation procedure is to first centre the first frame on the target, then acquire images with small telescope offsets between frames. The offsets requested to the telescope are stored along in the FITS headers. Of course, the usable part of the data seen through the detector is the intersection of all frames so the offsets should not be too large. On the other hand, the very aim of these offsets is to show what the sky background is to the detector, so offsets should be larger than the largest object on the frame. This means that the method can only be used with relatively small objects, which is typically the case for deep fields. For extended objects or crowded fields, the option is to apply this jittering to two positions: one on the target and another one on an empty field anywhere nearby, the immediate result being a loss of observing efficiency without which no sky subtraction is possible. In this case, we are talking about a jitter+offset mode. The idea in that case is to use the jittered pattern on the (empty) sky frames to filter out all possible remaining object signals and produce a clear sky that is subtracted from object frames. For the moment, the method running in the pipeline is taking a median average of all sky frames and subtracting it from the objects, but that would only work for small numbers of frames. Later implementations will offer various sky filtering algorithms depending on the actual acquisition duration and filter used.

In pure jitter mode (all frames acquired on the object), the instrument has a built-in offset generation method that scatters points optimally with a Poisson distribution law. The generated offsets have the property to be optimally distributed over the possible range of offsets, and thus maximise the chances of being able to filter out the sky background (see the **poisson** command in eclipse). It is recommended to use the *AutoJitter* template unless you have specific needs for the offset values and provide your own to the *GenericOffset* template. Please note that this generic template cannot yet be supported in pipeline mode, because it leaves too many choices to the user to be able to support all possibilities. When we get experience about what is usually requested, some more reduction modes will be implemented for the most usual cases.

The reduction procedure for the jitter algorithm is shown in Figure 1. Pre-processing is done by applying dark subtraction, flatfield division, and bad-pixel correction if these calibration frames are available. The first algorithm step is then to filter out the sky background from raw images. This is done with a 3d-filter with pixel rejection, actually similar to the **imcombine** routine in IRAF. Sky statistics are accumulated at that point and written to an ASCII result file; they should be appended to the output file FITS header in later versions. The second step is to detect the offsets between frames. We need some useful signal in the frames to do that, and the best configuration is to be able to find the same bright object in all consecutive frames. If this is not possible, the algorithm would look for all bright objects it can find and try to locate them image after image, with sub-pixel precision. This is done through cross-correlation methods and is usually quite robust and insensitive to noise. The third step is to register all images to the first image taken as a reference. This is done through re-sampling methods in image space, and produces much less aliasing than Fourier space-based methods, linear interpolation, or just integer pixel moves. The only visible consequence is that noise (high frequencies) is smoothed out by the re-sampling process, but photometry is conserved. Once this is done, the last step is to stack all frames to a single one, using again a 3d-filter to remove spurious values. Post-processing is applied to this image to remove detector row saturation effects for example, then the result may be sent to an image displayer.

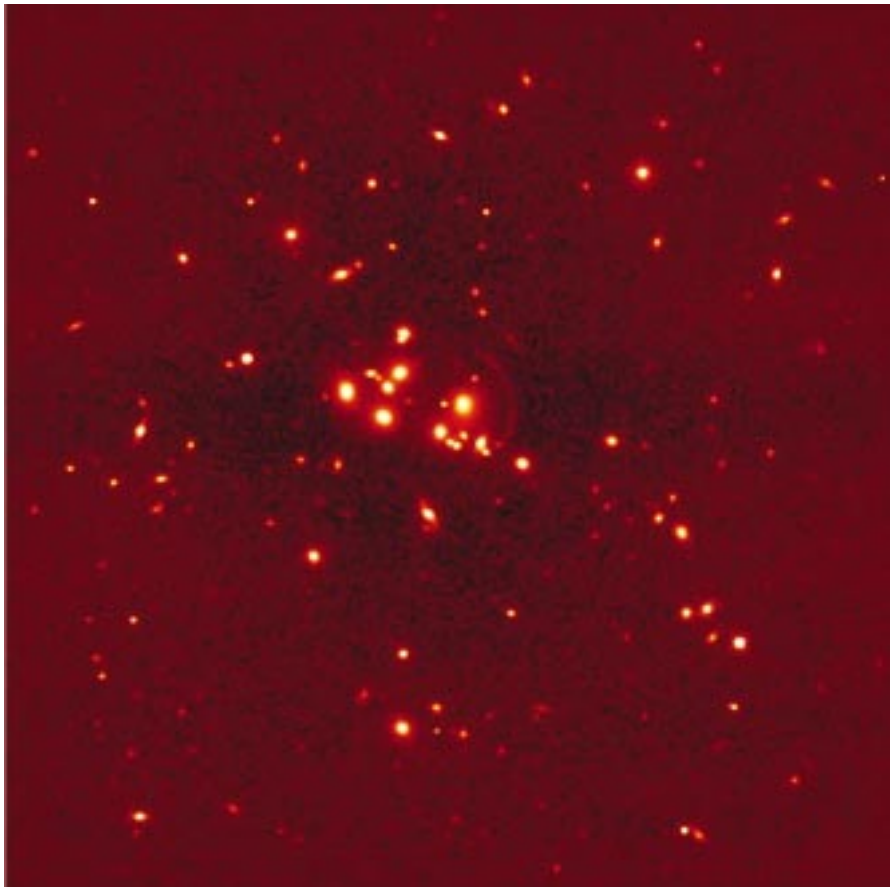

Figure 2.

Figure 2 shows an image produced in November 1998 with ISAAC, the Galaxy cluster CL2244-02 with gravitational arcs (see press release dated 26 November 1998 on the ESO web site, and the December 1998 *Messenger* issue). This image is the jittered combination of 60 input frames in Ks band; it was obtained with default settings for all parameters. This is a typical output from the ISAAC pipeline in the control-room, for that kind of data.

This algorithm proves to be very reliable and usually complete for typical fields acquired so far with SOFI or ISAAC. There are still some incorrectly processed cases though, mostly for images where all bright objects are located on the edges of the first frame (the reference), but that should be solved with e.g. point-pattern matching algorithms in later releases of the pipeline. For more detailed information about the algorithm and what can be fine-tuned, readers are referred to the following document: “jitter imaging data reduction: algorithms and implementation”.

The URL is http://www.eso.org/projects/dfs/papers/jitter98/

The software running automatically on both SOFI and ISAAC pipelines takes about 25 minutes (on a fast workstation with large amounts of memory) to reduce a batch of 60 frames, i.e. roughly 250 megs of data in input, and can run on virtually any POSIX-compatible machine. Supported OS’s so far are Solaris, HPUX, Linux, IRIX, AIX, DEC OSF/1, and any station that offers POSIX compatibility and an ANSI C compiler.

2. Spectroscopy Mode

The spectroscopy pipeline is made of MIDAS procedures making use of the LONG and ECHELLE packages, with some calls to eclipse routines to speed up pure image processing routines, and to perform standard star database search. It is likely that we will redevelop in C identified parts of the algorithm that are not likely to change and need CPU speed.

Calibrations

Various calibration procedures are performed for trend analysis purposes; they are mainly used by the instrument scientist. They include a control of the slit position with respect to the detector, calibration of the spectroscopic dispersion relation with calibration lamps, analysis of known spectral lines to correct for spectrum tilts or curvature in the spatial direction, and spectroscopic flat-fields.

Observations

Spectroscopic observations performed with the *NodOnSlit* template produce spectra on two different positions A and B obtained by a shift of the telescope along the slit. Each set of images is averaged to a single image, and both sets are subtracted from each other. Available outputs are images of (A-B), (B-A), and a combined image of those two. The combined image is actually the most important one for the observer, since extraction will take place on this 2d-spectrum image. The pipeline goes on from this point, extracting the brightest spectrum from this image, performs flux and wavelength calibrations when adequate calibration data are available, and outputs the results to a FITS table.

The brightest spectrum is to be seen as a checkpoint: since it is usually a reference object, it might be useful to check out that the acquisition actually performed as expected at least on this object. This spectrum is available to the user in the control room, together with the combined 2d image so that spectrum extraction can proceed from that point (partly) by hand.

Notice that spectroscopy recipes should be distributed as a part of MIDAS in a subset dedicated to pipeline routines. Some are supporting an interactive mode that actually allows giving more indications about how the procedure runs and lead them to proceed directly to the solution for the spectra of interest.

Acknowledgements

All ISAAC pipeline data reduction algorithms are based on the ISAAC calibration plan (ESO document VLT-PLA-ESO-14100-1384) by Pierre-Alain Duc and Jean-Gabriel Cuby. All procedures have been improved tremendously following the advice from Chris Lidman. Numerous discussions with Alan Moorwood, Almudena Prieto, Paola Amico, Pascal Ballester have helped a lot to clarify the requirements and improve the spectroscopy parts. The jitter process has received constructive and helpful comments from too many people to quote them all here; we thank them for their contributions.

ndevil@eso.org

Commissioning FEROS, the New High-resolution Spectrograph at La Silla

A. KAUFER, O. STAHL, S. TUBBESING, Landessternwarte Heidelberg-Königstuhl
P. NØRREGAARD, Astronomical Observatory Copenhagen
G. AVILA, P. FRANCOIS, L. PASQUINI, A. PIZZELLA, ESO

Introduction

On November 30, 1998, the second commissioning phase of the new Fiberfed Extended Range Optical Spectrograph (FEROS) was completed at the ESO 1.52-m telescope at La Silla.

The instrument had been installed by a small team from the Heidelberg, Copenhagen and La Silla observatories starting in mid-September – just two years after the contract signature between the FEROS consortium and ESO. FEROS saw its first stellar light at the end of the installation phase on October 6th.

An overview of the design and of the expected capabilities of the FEROS instrument has been presented in a previous paper [Kaufer et al., 1997, *The Messenger* 89, 1]; a more detailed description of the opto-mechanical design is found in [Kaufer & Pasquini, 1998, Proc, *SPIE* Vol. 3355, p. 844]. In the present article, the major technical results from the two commissioning phases which followed the first light event are reported.

The Spectrograph Environment

Figure 1 shows the FEROS spectrograph inside its temperature and humidity controlled room, which was erected by the La Silla infrastructure team at the place of the former Echelec spectrograph inside the coudé room of the ESO 1.52-m telescope. The feet of the optical bench are sitting on a platform coupled to the telescope pier but decoupled from the room's floor. The LN_2 supply tank is located outside of the spectrograph room in the neighbouring FEROS maintenance room and can be replaced every two weeks without entering the spectrograph room. Adding to these facts the very stable temperature which is maintained inside the room (ΔT < 0.2 K over 1 night), FEROS is located in a very stable environment – a crucial prerequisite for a long-term stability of the instrument as required for high-precision spectroscopic measurements.

From the spectrograph, the two fibers together with their metallic protection cable are led through the telescope's polar and declination axes, further inside the telescope's double tube, and eventually leave the telescope and enter the Boller & Chivens (B&C) Cassegrain spectrograph to end in the telescope's focal plane, which now hosts the new FEROS fiber head and the previous B&C long slit.

Instrument Performance

Table 1 summarises some of the main performances of FEROS as determined during the commissioning.

Efficiency

The detection efficiency of the complete system ESO 1.52-m telescope + fiber link + FEROS + Detector has been measured several times under photometric conditions using bright and faint CTIO standard stars [Hamuy et al., 1994, *PASP*, 106, 566]. Correction for the atmospheric extinction has been made according to the standard La Silla extinction tables. The typically achieved detection

Table 1: Measured performance of FEROS.

Wavelength Range	
in one exposure (object+sky)	360 – 920 nm (39 orders, 2 fibers)
Resolving Power	$\lambda/\Delta\lambda$ = 48,000 (2.2 pixels)
Entrance Aperture	2.7 arcsec (circular)
Detection Efficiency	1% at 360 nm, 16% at 440 nm, 17% at 550 nm
(with telescope and detector)	16% at 640 nm, 11% at 790 nm
Limiting Magnitudes at the ESO 1.52	16 mag in V, S/N = 9, t_{exp} = 2 h
	12 mag in V, S/N = 105, t_{exp} = 2 h
Radial-Velocity Accuracy	21 m/s rms (2-month time base)
Inter-order straylight	< 3%

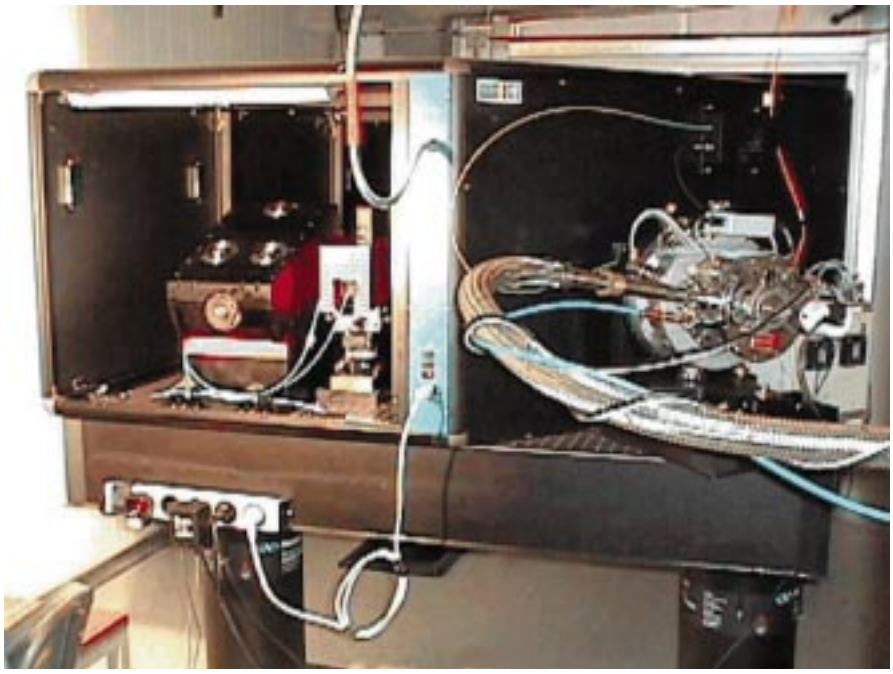

Figure 1: FEROS in the FEROS room at La Silla. One cover has been removed, which allows to see the echelle mount on the left with the fiber exit unit next to it. On the right is the detector system with the LN_2 supply line of the continuous-flow cryostat in the front.

efficiencies in the *UBVRI* colours are given in Table 1. The peak system efficiency of 17% considerably exceeds the performance of most (if not all) of the currently operating high-resolution spectrographs.

The high throughput together with the large simultaneous wavelength coverage from 360 to 920 nm in 39 orders for both fibers and the high resolving power of R = 48,000 reflect the outstanding performance of this new ESO instrument.

The measured spectrograph efficiency is consistent with the computations from the design and construction phase as can be seen in Figure 2. The efficiency in the very blue below 400 nm is lower than expected in the Final Design Report. This is due to the reflective coating of the mirrors which performs in this spectral range only at the lower limit of its specification. Since the optical path goes through four reflections on this coating, a drop of the efficiency in the blue becomes noticeable.

Spectral Resolution

The measured spectral resolving power of FEROS is R = 48,000 corresponding to 2.2 pixels of 15 µm. This resolution is achieved with the help of the two-beam two-slice image slicer [Kaufer, 1998, Fiber Optics in Astronomy III, ASP Conf. Series 152, 337]. The width and asymmetry of about 500 selected calibration lamp emission lines over the full echelle frame are routinely measured by the data reduction software. The FWHMs of the lines show a maximum degradation of < 15% in the extreme corners of the CCD. Along the dispersion direction a slight trend of the line widths is visible which presumably is due to a residual tilt of the CCD detector with respect to the field lens. The necessary alignment is planned to be carried out during an outstanding CCD upgrade (see below). The asymmetries of the lines are described by Gauss-Hermite polynomials and are below 1% for the odd and even terms.

Straylight and Ghosts

The inter-order straylight is primarily produced by the echelle grating and the roughness of the optical surfaces. The straylight distribution is found to be very local, i.e., it follows the intensity distribution of the spectral light source in the orders. This result was not clear *a priori* for the white pupil design used in FEROS. With this, we could determine the straylight level with the help of flatfield exposures by comparing the intensities in the orders with the intensities of the inter-order background: the straylight levels are found to be less than 3% all over the CCD.

The straylight contamination along the orders is difficult to determine. Therefore, we compared several very deep absorption lines of FEROS solar spectra with Kitt-Peak FTS spectra. After matching the resolution and pixelisation of the spectra, no considerable (> 2%) filling of the cores of the spectral lines was observed.

Several tests were carried out to identify possible ghost images produced in the optical system of FEROS. A spectrum of the emission line star η Carinae with a highly saturated Hα line revealed the presence of a focalised ghost image of this Hα line between two orders close to the centre of the CCD. The relative intensity level of this ghost was measured to 5×10^{-4} which is not critical.

Fiber Flatfield Stability

During the construction of FEROS, different teams reported on problems with the stability of flatfields in fiber-fed high-resolution spectrographs [e.g. Baudrand et al., 1998, ASP Conf. Series 152, 32] limiting the maximum achievable S/N in stellar spectra down to about 200. Since it was not possible to pin down the reason for this degradation, FEROS had to

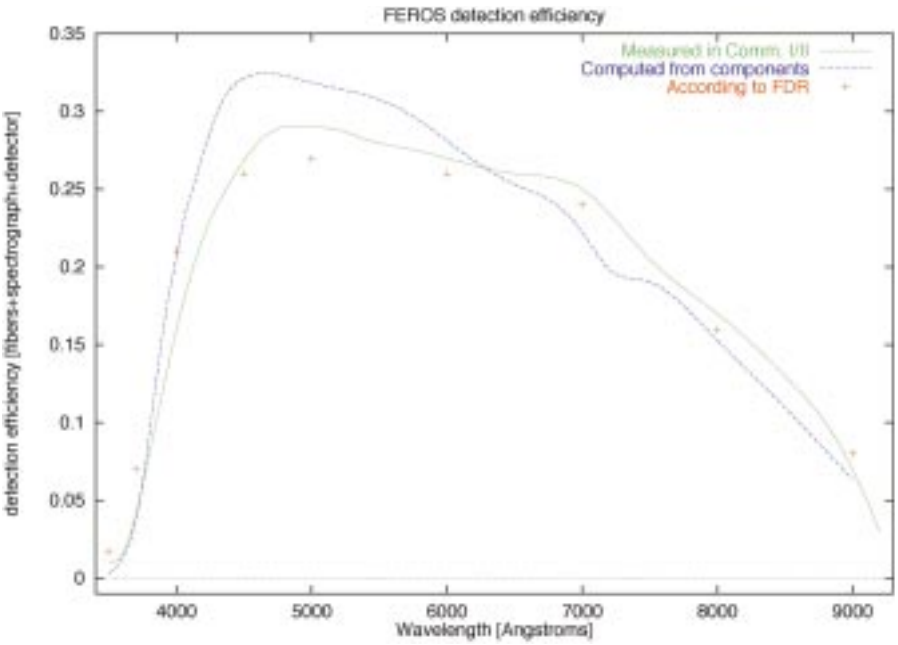

Figure 2: Efficiency of FEROS fibers + spectrograph + detector. The efficiency curve is derived from a spectrum of the standard star HR 9087. For the atmospheric extinction correction the standard La Silla extinction tables were used; for the telescope, an efficiency of 60% is assumed. The red crosses give the expected efficiency according to the FEROS Final Design Report (FDR); the blue curve is the total efficiency computed from the efficiency measurements of the individual components.

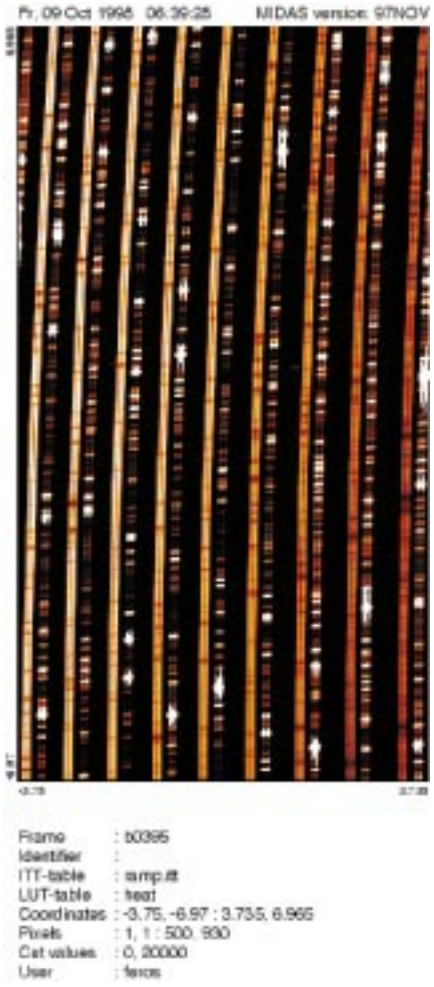

Figure 3: Central section of a raw spectrum of the radial-velocity standard τ Ceti observed in the Object-Calibration mode of FEROS: each stellar spectral order is accompanied by the spectrum of the calibration lamp which is exposed simultaneously over the full exposure time of the object.

prove its high S/N capabilities during the commissioning observations. For this purpose, a series of spectra spread over the whole night, i.e., at different telescope positions, and with high photon counts have been obtained for the bright B8 Ia star β Ori. The S/N measured in the reduced single spectra is close to 700, which is consistent with the S/N expected from pure photon statistics. Averaging of 5 single β Ori exposures increased the S/N to about 1400.

High-Precision Radial Velocities

To obtain a high long-term accuracy in radial-velocity measurements, FEROS has been equipped with the possibility to record simultaneously with the stellar spectrum the spectrum of the Thorium-Argon-Neon calibration lamp on the second fiber. This allows to monitor the residual motions of the spectrograph during the night and during the exposure. To explore the capabilities of this so-called Object-Calibration (OC) mode, the bright solar-type radial-velocity standard star τ Ceti (Δv_{rad} < 3 m/s) and the famous 51 Peg (Δv_{rad} = 57 m/s, P = 4.2 days) were observed regularly during the two commissioning periods. Figure 3 shows a section of the first raw echelle spectrum of τ Ceti obtained in the OC mode with FEROS.

Figure 4 shows the radial-velocity curve of τ Ceti with 130 measurements over a period of 55 days. The radial velocities are obtained by simple order-by-order crosscorrelation of the 39 echelle orders of the object and of the simultaneous calibration fiber with respect to a corresponding reference spectrum. Neither special masks or templates for the star or for the calibration lamp have been used, nor the full wavelength calibration solution. With this simple approach, a radial-velocity dispersion of 21 m/s rms is achieved for this supposely constant star. For 51 Peg, 30 measurements have been obtained and the residuals to the well-determined orbital curve show a rms of 29 m/s.

It is worth noting that the instrument was not working under the best and most stable conditions during the commissioning periods since numerous disturbing tests and optimisations had to be carried out during daytime. Therefore, we suppose that with the potential improvements from a dedicated software and from an improved stability of the environment, FEROS should be able to join the small club of instruments working in the < 10 m/s domain. However, this is out of the scope of the FEROS contract and commissioning and, therefore, no further steps will be made in this direction by the FEROS consortium.

Alternatively, the second fiber is fed by the sky background nearby the object fiber (the fixed distance between the fibers is 50 arcsec). The Object-Sky (OS) mode in principle allows to subtract all sky contributions from the object spectrum, e.g. the night-sky emission lines in long exposures. The sky subtraction capabilities of FEROS were tested by following an O star with few and broad lines with multiple 5-minute exposures at the end of the night into the twilight. The top two spectra of Figure 5 show the spectra recorded in the object and sky fiber shortly before sunrise with the stellar spectrum heavily contaminated by the bright sky background. After subtraction of the sky spectrum ('object – sky') the stellar spectrum is completely recovered. As comparison, the stellar spectrum obtained during the night ('object') is shown. Before subtracting the on-line reduced one-dimensional object and sky spectra, a constant factor of 0.95 had to be applied to the intensity scale of the sky spectrum. This factor reflects the slightly different flatfield illumination of the two fibers.

This result together with the reported FEROS flatfield capabilities is of high relevance, since the use of fibers in high-resolution spectroscopy has often been questioned on the basis of these problems. It is as well worth noticing that the FEROS system is very similar to the UVES fiber link as it will be mounted on the UT2 of the VLT. Therefore, we are confident that in this respect the FEROS commissioning results can be scaled to the VLT and UVES.

CCD System

The thinned and back-illuminated 2k × 4k 15µm pixel EEV CCD with its excellent quantum efficiency (measured peak QE = 98% at 450 nm) contributes considerably to the high detection efficiency of FEROS. In combination with the Copenhagen CCD controller, a read-out noise of 3.7 and 3.5 e^-/pixel for channel A and B is reached, respectively. Together with its high full-well capacity of 130,000 e^-/pixel and the very low blooming as observed at strongly saturated

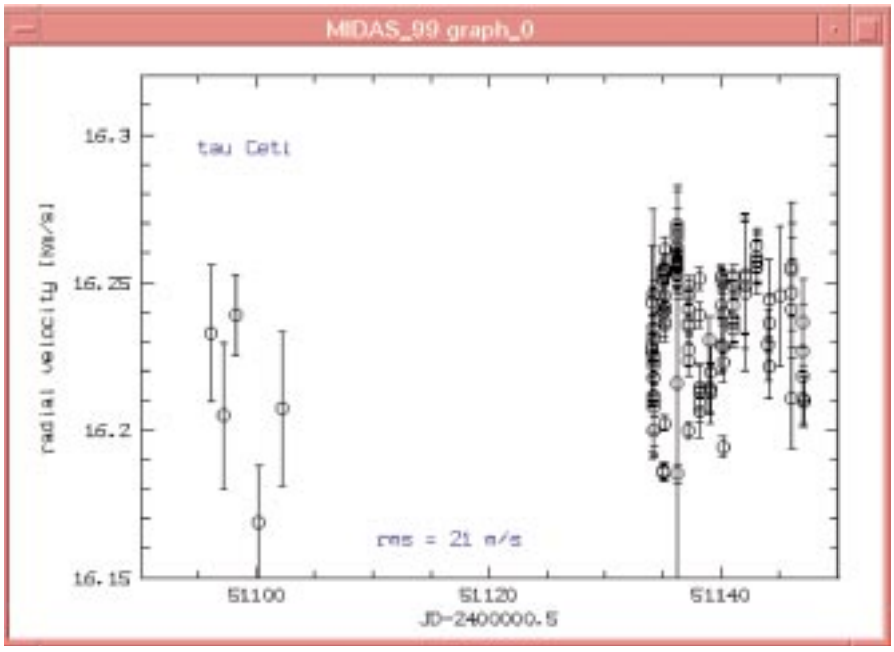

Figure 4: Radial velocity curve of the constant solar-type star τ Ceti.

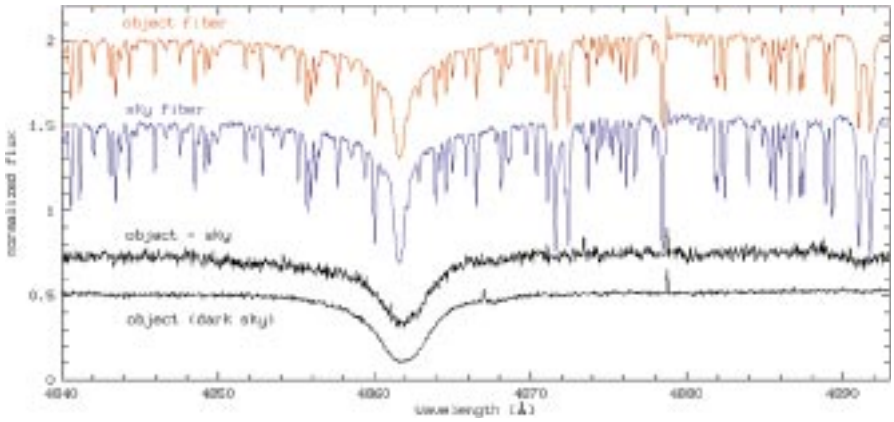

Figure 5: Skylight subtraction capability as tested on the bright O9 II star HR 3219 during the morning twilight.

spectral lines, the FEROS CCD seems to match perfectly the requirements of the instrument for both, low and high S/N observations.

Unfortunately, the CCD currently shows very bad cosmetics with several strong and numerous weak bad columns, the latter with the tendency to cluster into several neighbouring bad columns. Due to the high filling factor of the 2-dimensional echelle spectrum on the detector and the given orientation of the main dispersion direction along the 4k CCD columns, a considerable fraction of the 39 spectral orders is affected by the bad columns. The problem behind was traced down by the Optical Detector Team in Garching, which found that the cooling of the CCD chip is insufficient, i.e., the specified operating temperature of –120°C is not reached by the continuous-flow dewar of FEROS. This would explain why the numerous bad columns do not freeze out leaving the CCD with the two bad columns as reported by the manufacturer. An explanation by insufficient cooling goes in line with the observed high dark current of the FEROS CCD. Long dark exposures show strong structures with peak values for the dark current of 10 to 20 e^-/hour/pixel. The structures in the dark frames are found to be stable over several weeks, which allows to correct long science exposures for this structured background. Obviously, the high dark current is at the moment the limiting factor for FEROS for long low-S/N exposures since the noise contribution from the dark current becomes considerably higher than the very low read-out noise of the system.

To improve the performance of the CCD system, an upgrade of the dewar is planned for February 1999. The aim is to increase the heat conduction from the chip to the cold-head and to minimise the heat conduction through the electrical cabling. We hope that when you read these lines, FEROS is already back to operation and now presents its full performance with the upgraded CCD system.

To complete this section it is worth mentioning that the FEROS spectra taken with the thinned 2k × 4k EEV CCD show the unavoidable strong fringes in the red starting at about 700 nm. The amplitudes of the fringe patterns are strong with measured maximum values of more than ± 20%. Thanks to the fiber feed and the long-term stability of the FEROS spectrograph, the fringes are corrected to a level of clearly better than 1% just by flat-fielding. This is also true for science exposures taken at different positions on the sky and using the flatfields taken in the afternoon during the initialisation of the online data reduction software.

Data-Reduction Software and Pipeline

FEROS was delivered with a dedicated data-reduction software (DRS) developed at Heidelberg. This DRS is implemented in the ESO-MIDAS system as a new context named `feros` and will be distributed with the MIDAS package from version 98NOV on. The DRS is designed as a very general echelle-reduction software but is optimised for FEROS in the sense that it takes into account the double fiber feed of the spectrograph, the use of the two fibers with a double image slicer, and the strong curvature of the orders caused by the prism crossdisperser.

In addition to the standard routines for echelle data reduction, the FEROS DRS includes the possibility for standard and optimum extraction of the orders with and without cosmic rays spots clipping. For this, the advantage of the stable fiber feed can be used to define the necessary cross-order profiles just on the high S/N flatfield instead of the science frames. The tests during the commissioning showed that the gain in S/N with the optimum extraction corresponds to the theoretically expected – even for the complex wavelength dependent image-slicer cross-order profiles.

Further, the wavelength calibration is working with a global approach, i.e., a single multi-parameter function including the order number as one parameter is fitted to the positions of all automatically identified emission lines of the Thorium-Argon-Neon calibration lamp. This approach leads to a very stable over-all wavelength solution. The residuals between the known wavelengths of the identified lines and the fitted wavelengths show a stable rms value of < 3 mÅ. The residuals display no trends with position and wavelength, which is a good indication that the used global fit formula (which is directly based on the grating equation) includes all relevant terms.

An important feature for the data reduction of highly stable fiber-linked echelle spectrographs is the well-defined blaze function for each echelle order. Since the light paths through the spectrograph for object and calibration exposures are to a high level exactly the same, the blaze correction can be done by flatfielding only. The quality of the blaze correction is best checked by the match of the flux levels of the overlapping regions of the contiguous echelle orders. In case of FEROS it is found that the match is on a level of better than 1%. This is a prerequisite to

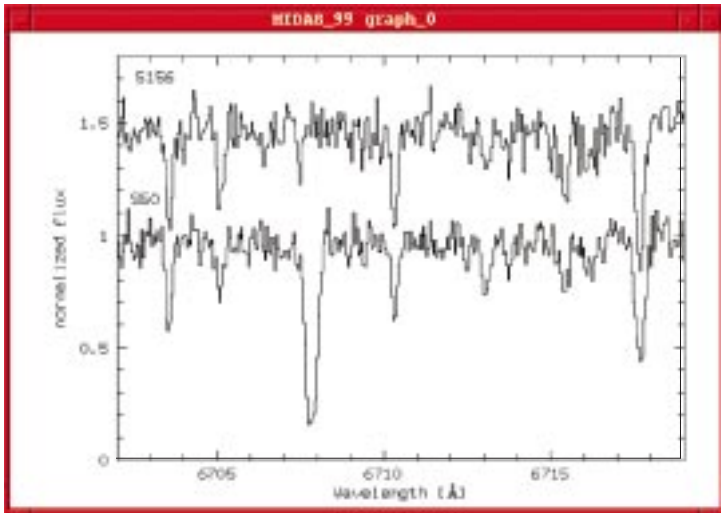

Figure 6: Spectra of two K giant stars in the metal poor cluster Berkeley 21. Both stars have a V magnitude of 15.6 and a V – I around 2 mag. The exposure times are 2 × 1 hour for each object; the S/N is estimated to > 20 in this spectral region.

PLEASE NOTE: An on-line searchable database with all FEROS spectra obtained during the commissioning period and the first guaranteed time (dataset not complete yet) is now available on the WWW:

http://www.lsw.uni-heidelberg.de/~akaufer/Feros/ferosDB/search.html

Note that the data obtained during the commissioning period are Public.

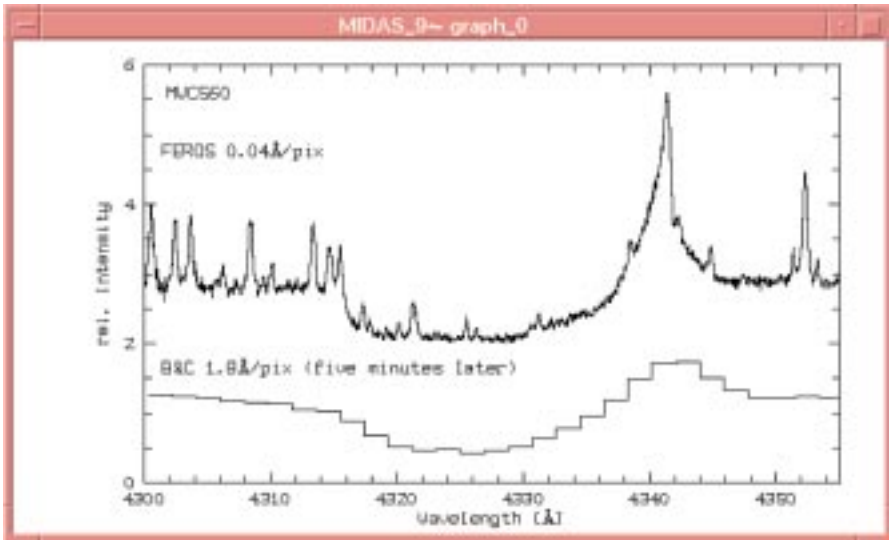

Figure 7: Spectra of the symbiotic star MWC 560 as obtained with FEROS (top, t_{exp} = 15 min) and shortly after with the B&C (bottom, t_{exp} = 30 sec). In between, only the slit unit was moved between the corresponding two positions.

apply routinely the merging of the wavelength calibrated echelle orders into a single and complete one-dimensional spectrum as done by the FEROS on-line DRS.

The FEROS on-line DRS pipeline as installed at the ESO 1.52-m telescope is an extension to the `feros` context. The on-line DRS is initialised with a set of calibration exposures taken daily before sunset. The initialisation programme provides the DRS with all frames (e.g. extracted flatfields) and tables (e.g. order positions, dispersion coefficients) for the coming night. During the observations, each incoming spectrum is archived on tape and processed according to its descriptor information, e.g., science frames are completely reduced into a flatfielded, wavelength-calibrated, barycentric-corrected, and merged one-dimensional spectrum, which allows the observer to inspect the spectrum about 6 minutes after the shutter is closed (using one-channel CCD readout and optimum extraction). Figure 6 shows the spectra of two faint metal poor stars which have been reduced by the on-line DRS with optimum extraction.

Observing with FEROS

The new FEROS instrument has been integrated in the existing telescope and B&C instrument environment in the ESO 1.52 control room. The user will find one additional Linux PC controlling the new common calibration unit for B&C and FEROS and the FEROS CCD, which uses the Danish BIAS software as known from the earlier days of DFOSC at the Danish 1.54-m telescope. The B&C exposures are still defined on the nearby HP 1000 system. Both, FEROS and B&C transfer their CCD frames to the HP instrument workstation where the FEROS on-line DRS and the B&C quick-look software are running in parallel on two different workspaces.

The change between the two instruments is very simple and requires only a manual movement of the new slit unit between the two corresponding positions. Figure 7 gives a nice demonstration of the possibility to use both instruments shortly one after the other. The figure shows the Hβ line of the symbiotic star MWC 560 as obtained in high spectral resolution with FEROS and in low resolution with the B&C a few minutes later after a change of the slit unit. The change between the two instruments is currently not offered to the observers but it is easy to imagine scientific programmes which could gain from this symbiosis of these two in a certain sense complementary instruments. For example, for the first time high-quality high-resolution spectrophotometric programmes could be carried out easily by combining flux-calibrated low-resolution B&C spectra with the spectral details as obtained from FEROS.

The experience from several test observing nights with FEROS at the ESO 1.52-m telescope showed that some effort is needed to reach always the maximum possible performance of FEROS in combination with the ESO 1.52-m. Particularly, it turned out that a proper focusing of the telescope on the fiber apertures is crucial to feed a maximum of light to the fibers. This is due to the use of microlenses in the focal plane which convert the slow f/15 telescope beam into a quite fast f/4.5 beam that is naturally more sensitive to defocus. Also bad seeing of more than 1.5 arcsec considerably affects the efficiency of the telescope + instrument system. Together with a bad telescope focus quickly half of the photons from the object are lost for the spectrograph.

Apart from the focus, the expected S/N for different environmental conditions is quite reliably estimated with the FEROS exposure-time calculator (ETC).

Further Information

All information concerning the status of the instrument (e.g. the CCD upgrade) and the preparation and execution of observations with FEROS (e.g. the ETC and the User Manual) can be found on the corresponding 2p2-team homepage[1]. In addition, this page provides links to more pictures and reports on the installation and commissioning phases of the FEROS instrument.

Acknowledgements

Commissioning being at the end of the 'food chain', we would like to thank here all the people actively involved in the FEROS installation and commissioning at La Silla: Our special thanks go to the 2p2-team, Wolfgang Eckert and his mechanics team, the detector group, the optics lab with Alain Gilliotte and Roberto Tighe, and Fernando Luco and the infrastructure support team.

Further big thanks go to the FEROS PI, Bernhard Wolf, and the FEROS teams in Heidelberg and Copenhagen, and the detector group in Garching. It is thanks to all their efforts that it was possible to build FEROS and to get it operational so quickly.

[1]http://www.ls.eso.org/lasilla/Telescopes/2p2T/Elp5M/FEROS/index.html

A.Kaufer@lsw.uni-heidelberg.de

Monitoring of the Atmospheric Sodium above La Silla

N. AGEORGES, National University of Ireland, Galway; Physics Department, Galway, Ireland
N. HUBIN, ESO

1. Introduction

This work corresponds to preparatory work for the laser guide star adaptive optics system planed for the VLT at Paranal. In this framework ESO and the National University of Ireland, Galway, are collaborating within the Training and Mobility of Researcher programme on "Laser guide star for 8m class telescopes", funded by the European Commission.

In Laser Guide Star (LGS) Adaptive Optics (AO), a laser is used to excite the mesospheric (90 km altitude) sodium

(Na) layer and thereby creates an artificial star that can be used as reference for the AO wavefront sensor. The intensity of the artificial star depends strongly on the amount of Na present in the atmosphere. It has been shown that this quantity varies seasonally but also on a day-to-day basis (see e.g. Ageorges et al., 1998, and references therein). However, the only existing measurements in the southern hemisphere have been done some 20 years ago in Brazil (Clemesha et al., 1978). No information exists on the absolute amount of sodium in the atmosphere in Chile. La Silla is at a different latitude than Paranal but measurements there will be good estimators of the amount of atmospheric sodium one can expect above Paranal.

Experiences to measure the column density and details of excitation of scattering properties of sodium atoms in the atmospheric sodium layer are very important to refine the design parameters of laser and assess the power requirement.

The observations aimed at determining the absolute averaged sodium density in the atmosphere above La Silla and the night and day-to-day variations. The data were obtained during one and a half night granted DDTC time in July 1998, on EMMI at the NTT. For this study, unreddened young bright stars of A or B type, closer than 50 pc to avoid any contamination of the spectrum by interstellar sodium, have been selected.

2. Observations

The minimum resolution to resolve the atmospheric sodium D lines from nearby contaminating water lines is of 50,000. This thus implied the choice of the echelle grating #14, which has a pixel size of 40 mÅ.

To get 15% error on the measure of the D_1 equivalent width, one would like a signal-to-noise ratio (SNR) of 1000, with:

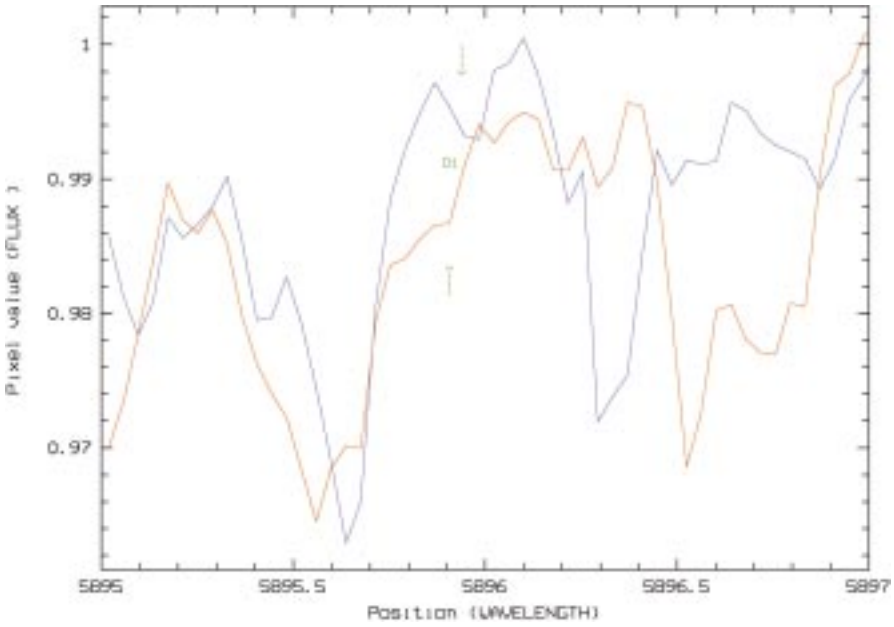

Figure 1: Spectrum of θ Cap (blue). It is the sum of 28 spectra corresponding to 5870 seconds of integration on source. The D_1 line is clearly resolved at 5895.96 Å. Overplotted (in pink) is the spectrum of β Lib, corresponding to 2325 seconds on source.

$$SNR = \frac{DQE \times \delta\lambda \times N_{obj} \times t}{\sqrt{(DQE \times \delta\lambda \times N_{obj} \times t) + (DQE \times \delta\lambda \times N_{sky} \times t) + DN^2}} \quad (1)$$

where DQE is the dectector quantum efficiency (0.65 for EMMI), δt the width of a spectral resolution element (in Å), N_{obj} the number of photons per second per Å per spatial resolution element incident on the detector from the object, N_{sky} same as N_{obj} but for photons from the sky, t the integration time (in seconds) and DN the detector noise per resolution element. Since we are considering only bright stars ($m_V < 6$), the sky contribution is negligible and will thus not be considered in this calculation.

The detector of interest is the CCD #36, which has a read-out noise of 5 electrons/pixel and a dark of 1.7 electrons/pixel/hour, so that $DN = N \times 5 + (1.7/3600) \times t$, with N the total number of exposures. This term is however negligible since the observations are dominated by the photon noise. It is thus reasonable to approximate the signal to noise ratio by:

$$SNR \approx \sqrt{(DQE \times \delta\lambda \times N_{obj} \times t)} \quad (2)$$

The slit has been selected to have 1″ width and 6.5″ length on the sky, corresponding to an expected resolution of 60,000.

For EMMI at the NTT and the echelle grating used, Dekker et al. (1994) quote the arrival of 1 photon/Å/sec at 5500 Å for a $m_V = 16.6$ star, at an airmass of 1. This number is multiplied by 57444 when observing a star with $m_V = 4.7$. Knowing the pixel size and the pixel scale of 0.27″, this gives $N_{obj} = 620.4$ photons/Å/sec. Taking the quantum efficiency of the detector into account, 403.3 electrons/Å/sec are arriving on the detector. Since the linearity of the detector is 50,000 ADUs, and the gain 2.2 electrons/ADU, up to $1.1\ 10^5$ electrons can be received without leaving the linear regime. One can thus integrate for ≈ 273 seconds when observing a $m_V = 4.7$ star, without saturating the detector. To reach the desired signal-to-noise ratio, we will then have to make, e.g., 23 exposures of 4 minutes, which represents 2 hours on the source when taking the overheads into account.

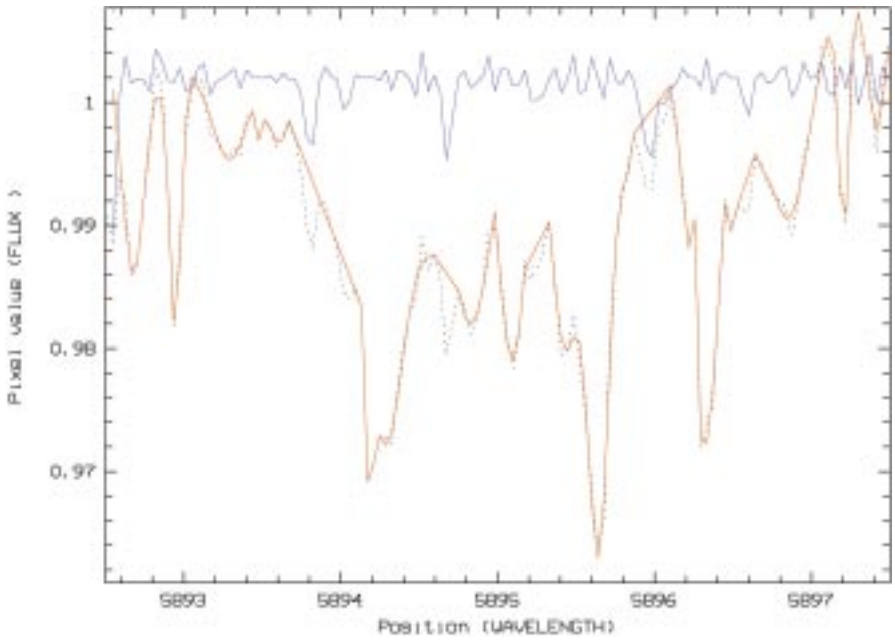

Figure 2: Spectrum θ Cap. The dotted black line is the original spectrum, the model fitted is in pink, and the resulting spectrum is overplotted in blue (with an artificial offset of 1).

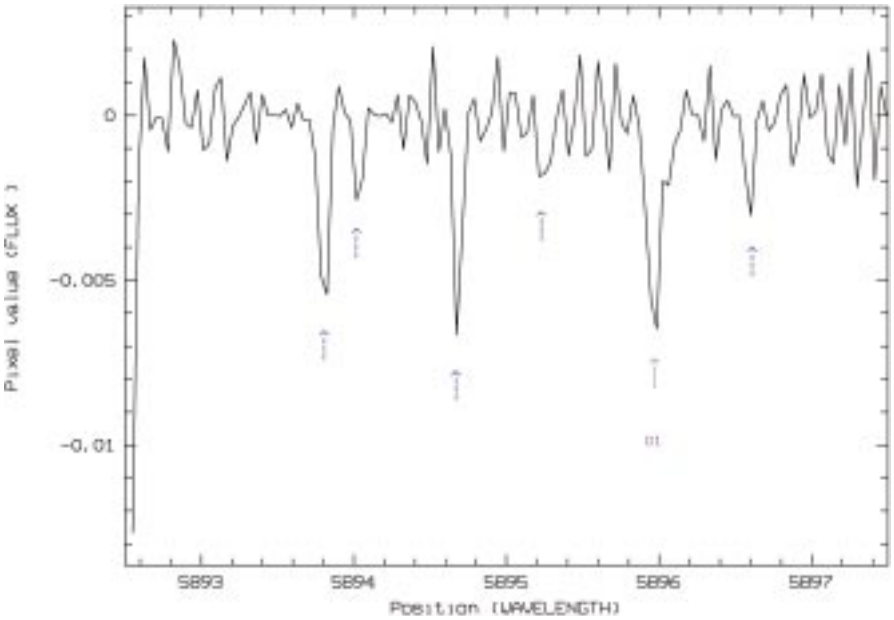

Figure 3. Final spectrum of θ Cap, resulting from the difference between the observed spectrum and the modelled one. Blue arrows indicate lines that were not identified and are thus remaining. The pink arrow points at the atmospheric sodium D_1 line, whose equivalent width is 0.5 mÅ.

3. Results

Only 3 sources could be observed and, unfortunately, mostly because of bad weather, one could never spend enough time on source to reach the desired signal to noise. Indeed, β Lib, θ Cap and ι Cen were observed respectively for a total of 2325, 5870 and 210 seconds on source.

Figure 1 represents spectra obtained with EMMI at the NTT. Each spectrum has been flatfielded individually, wavelength calibrated and finally coadded to the others to create this image. The data reduction has entirely been done under the echelle context of MIDAS. All further data analysis concerns only the θ Cap data, since it has the highest integration time, i.e. the best signal on source.

Since the Moon was 80% full during the observation, strong solar lines reflected off the Moon interfere with the observed spectrum. The best illustration is visible in Figure 1 where at 5895.55 for β Lib and 5895.65 for θ Cap appears a Doppler shifted solar sodium line. Most of the other lines identified in the spectrum correspond to atmospheric water contribution.

To calibrate the spectrum from the atmospheric contribution, except the mesospheric sodium, lines have been identified, fitted and suppressed. The contaminating lines to be suppressed have been identified thanks to the table of atmospheric and solar lines (essentially from Lundström et al., 1991 and Moore et al., 1966). Calibration of future observations are planned to be done in two ways: observe a blank sky to determine the exact position of the atmospheric lines; and compare spectra of at least 2 different sources, observed the same night, to identify the lines of solar origin thanks to their relative Doppler shift. It is also expected to be able to use a code creating a synthetic atmospheric spectrum.

The lines have been geometrically fitted with Gaussians and then merged into a spectrum corresponding to our model of the data (see Fig. 2). As can be seen in Figure 3, the signal to noise of the result is dependent not only on the total integration time but also on the quality of the fitting. We derived an equivalent width of $\approx$ 0.5 mÅ at 3.5 σ.

4. Discussion

Further analysis is on-going to determine the sodium column density present in the atmosphere at the time of the observation. From this information, one can derive the minimum laser power necessary to obtain a given magnitude for the laser guide star. This is one of the main information of interest in our study.

Due to the dynamic range of the CCD and the minimum exposure time needed on source to reach the requested SNR, the time resolution on the atmospheric sodium is at best 2 hours, with this type of observations. It is thus impossible to study short time-scale variations of the mesospheric sodium column density. However, this kind of study has to be pursued over at least a year period to determine the 'absolute' yearly minimum expected in the Na column density. Spectroscopic observations are thus very good for statistical studies of the atmospheric sodium.

Among the observing facilities present at La Silla, the CES, which is now fibre coupled to the 3.6-m, is the best solution in that it offers a resolution of up to 220,000. This would then allow both the Na D_1 and D_2 lines to be resolved from neighbouring water lines. One has thus a double check on the results.

The observations presented here also serve to refine the specifications of a portable atmospheric sodium layer monitor presently under study. This type of system could be developed for Paranal to make a site study and give some input to the VLT observing scheduler for LGS AO observations.

5. Acknowledgements

We would like to thank G. Mathys for his excellent advice before observing and N. Hurtado, J. Miranda and M. Pizarro for their support during all the time of the observations. Special thanks go to O. Hainaut and P. Ballester for their significant help during the data reduction.

NUIG and ESO are part of the EU TMR Network 'Laser Guide Star for 8m-class Telescopes' (contract no. FMRX-CT96-0094). NA is grateful to the EU for financial support.

References

Ageorges N., Hubin N., Redfern M., 1998, ESO-OSA proceedings, Sonthofen Sept. 7–11.

Clemesha B.R., Kirchhoff V.W.J.H., Simonich D.M., Takahashi H., 1978, *Geophys. Res. Let.* **5**, 873–876.

Dekker H., D'Odorico S., Fontana A., 1994, *The Messenger* **76**, 16–20.

Lundström I., Ardeberg A., Maurice E., Lindgren H., 1991, *A&A Suppl. Series* **91**, 199-208

Moore C.E., Minnaert M.G.J., Houtgast J., 1966, The Solar Spectrum 2935Å to 8770Å.

N. Ageorges
nancy@physics.ucg.ie

The Wide Field Imager at the 2.2-m MPG/ESO Telescope: First Views with a 67-Million-Facette Eye

D. BAADE[1], K. MEISENHEIMER[2], O. IWERT[1], J. ALONSO[3], TH. AUGUSTEIJN[3], J. BELETIC[1], H. BELLEMANN[2], W. BENESCH[2], A. BÖHM[2], H. BÖHNHARDT[3], J. BREWER[3], S. DEIRIES[1], B. DELABRE[1], R. DONALDSON[1], CH. DUPUY[1], P. FRANKE[2], R. GERDES[1], A. GILLIOTTE[3], B. GRIMM[2], N. HADDAD[3], G. HESS[1], G. IHLE[3], R. KLEIN[2], R. LENZEN[2], J.-L. LIZON[1], D. MANCINI[4], N. MÜNCH[2], A. PIZARRO[3], P. PRADO[3], G. RAHMER[1], J. REYES[1], F. RICHARDSON[3], E. ROBLEDO[3], F. SANCHEZ[3], A. SILBER[1], P. SINCLAIRE[3], R. WACKERMANN[2], S. ZAGGIA[4]

[1]*ESO, Garching;* [2]*Max-Planck-Institut für Astronomie, Heidelberg*
[3]*ESO, La Silla;* [4]*Osservatorio Astronomico di Capodimonte, Napoli*

1. Introduction

The basic capabilities of the Wide Field Imager (WFI) were described in a previous *Messenger* article (No. 93, p. 13; see also Table 1) which also includes a brief account of the contributions by the three participating institutes, namely ESO (Garching and La Silla), the Max-Planck-Institut für Astronomie in Heidelberg, and the Osservatorio Astronomico di Capodimonte in Napoli. Table 1 summarises the most important characteristics. A first fairly complete version of the user manual is now offered via the WFI home page on the Web (URL: http://www.ls.eso.org/lasilla/Telescopes/2p2T/E2p2M/WFI/WFI.html). The same page also provides access to some examples of pictures obtained with the instrument. An exposure time calculator is available under the URL: http://www.eso.org/observing/etc/

Following the completion of the 2.2-m Telescope Upgrade Plan (cf. *The Messenger*, No. 93, p. 19 and No. 94, p. 12), the WFI was installed on La Silla as the only instrument offered at the 2.2-m MPG/ESO Telescope. Since January 18, it is used by ESO Visiting Astronomers and MPI-A observers. Every night, the WFI's 67 million pixels produce an amount of data comparable to that generated by all other ESO telescopes on La Silla plus the VLT UT1!

2. Installation

A team of engineers from Heidelberg and Garching arrived on La Silla on December 8. Nine boxes with a total weight of almost one ton, in which the partly disassembled instrument, a handling cart, tools, spare parts, etc. had been packed after the system integration tests during the second half of November in Garching, were already waiting for them. Because of its sensitivity to mechanical shocks, the dewar head with the fully assembled science mosaic and the tracker CCD was transported as hand luggage by one of the Commissioning Team members. The weight (33 kg) and dimensions (80 cm × 80 cm × 25 cm) of the aluminium container made this travel a small adventure of its own.

Figure 1: The Wide Field Imager mounted in the Cassegrain focus of the 2.2-m MPG/ESO telescope on La Silla. The authors apologise for the obscuration by foreground objects (from left to right: H. Böhnhardt, J. Alonso, J. Brewer, E. Robledo, N. Haddad, J. Reyes, O. Iwert, A. Böhm, R. Donaldson, K. Meisenheimer, R. Klein, T. Augusteijn, D. Baade). However, although being excellent at taking images, the WFI does not render itself very suitable for being imaged because the instrument housing is deep black.

Table 1: The Wide Field Imager in a Nutshell

Field of view:	(34 × 33) arcmin^2
Pixel scale:	0.24 arcsec/pixel
Detector:	mosaic of eight 2k × 4k CCD's
Filling factor:	96.2%
Read-out time:	27 seconds
Read-out noise:	4.5 ± 0.1 e$^-$/pixel
(Inverse) gain:	2.0 ± 0.1 e$^-$/ADU
Dynamical range:	16 bit
Full-well capacity:	> 200.000 e$^-$
Telescope aperture:	2.2 m
Telescope focus:	Cassegrain (f/8)
Instrument F ratio:	5.9
Useful wavelength range:	atmospheric cut-off through 1 µm
Limiting magnitude (*B* band):	23 mag (5-σ detection in 2 min. at 1″ seeing)
Overall intrinsic image quality:	0.4 arcsec
Overall geometrical distortions:	≤ 0.1%
No. of simult. mountable filters:	50
Slitless spectroscopy:	4.5 (5.7) nm resolution at 400–640 (650–850) nm
Raw data format:	FITS (with extensions), 142 Mbyte/file

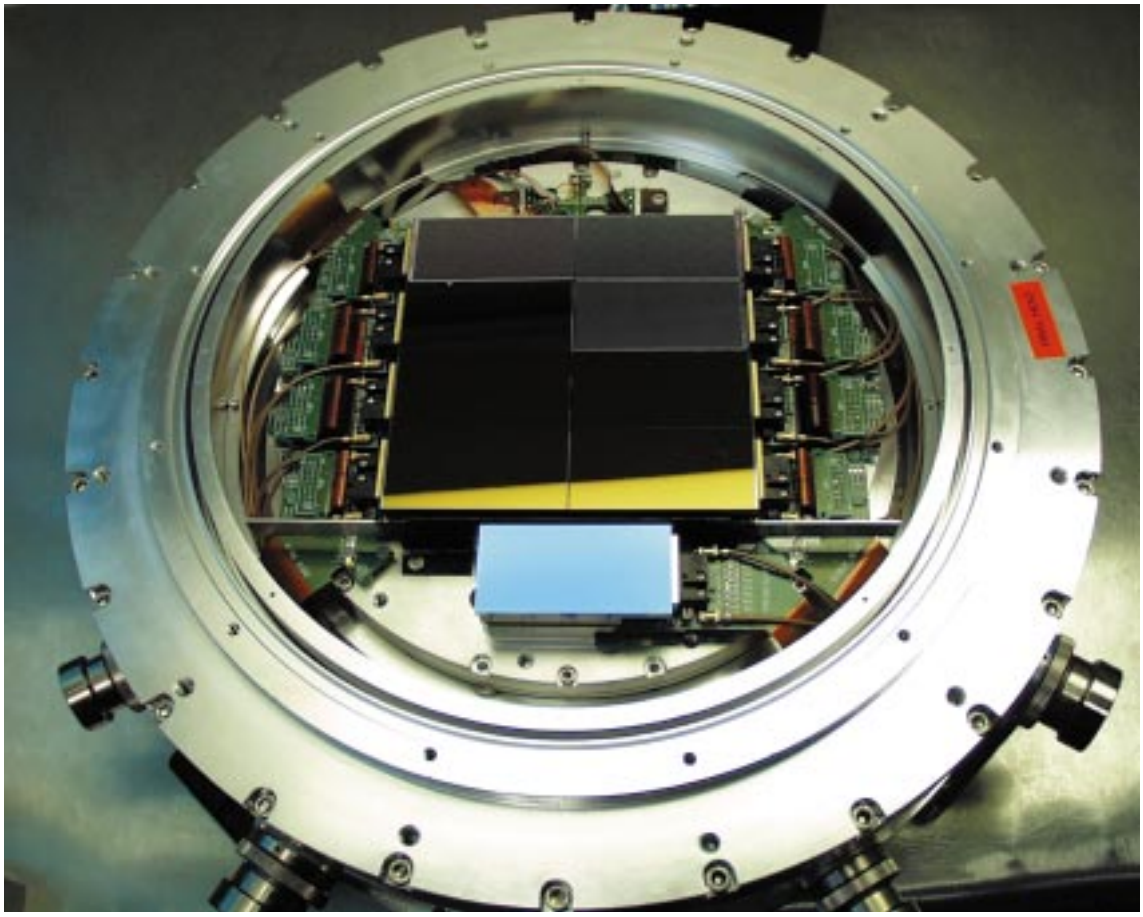

Figure 2: A close-up view of the WFI detector head.

After 4 busy days and with a lot of support from La Silla staff, everything was reassembled. The dewar had been pumped to a pressure of 10^{-6} mbar, the instrument was mounted to the telescope, telescope and instrument were balanced, all software had been installed, and for the first time also the communication with the instrument (DAISY+) and telescope control software had been established. All subsystems had been carefully checked, and no degradation with respect to the tests in Garching had been detected. Nevertheless, the suspense among the about 15 people present in the control room was very noticeable when only 30 minutes before December 13 the Start Exposure button was pressed for the first time. The telescope had been left pointing to an arbitrary field close to the zenith. But the image that appeared within little over half a minute on the Real Time Display (RTD) was greeted with much joy and enthusiasm.

The relief was not compromised by the discovery that the autoguiding of the telescope had failed. It was due to the predictable error in a sign, which was corrected in 5 minutes. That thereafter the autoguider system worked flawlessly was an impressive and instant proof of concept, because for the first time the tracker CCD, FIERA (ESO's CCD controller), the FIERA software, DAISY+, the shutter control electronics and software, and the telescope control hard- and software had all been chained together for a complicated real-time operation.

Days and nights of many engineering tests followed. A number of imperfections were discovered and eliminated one by one. All problems were sufficiently tractable that the 3 bottles of sparkling cooling liquid, which one of the software (!) engineers had put into one of the boxes only minutes before they were closed and shipped to Chile, were not needed. Miraculously, their contents turned out to be perfectly fit for human consumption and, therefore, reached their final destiny during a small farewell and Merry-Christmas party for the engineers, who started to return to Europe a few days before Christmas.

3. Commissioning and Science Verification

Now the astronomical testing and characterisation of the instrument could begin. The temptation to point the telescope at a number of aesthetically attractive large objects such as HII regions, nearby galaxies, globular and open star clusters, galaxy clusters, planetary nebulae, and the Moon was difficult to resist. And it was very impressive to see one image after the other show up on the RTD almost in poster quality even without any processing (a 3-colour composite image of the edge-on spiral galaxy NGC 4945 is shown on pp. 20–21; the corresponding caption is on p. 19). The equivalent of nearly four dark nights was used for *B*-filter observations to cover patch *C* of the EIS project (*The Messenger* No. 91, p. 49 and No. 92, p. 40) fully and three quarters of patch *D* for a total of 10.5 square degrees.

The application of the instrument for real scientific projects enabled the detection of a small number of further insufficiencies before the arrival of the first guest observers. Most of these problems could be solved, but some still persist. However, the important baseline conclusion is that the ESO and MPG communities now have access to a state-of-the-art wide-angle camera with excellent optical quality over the entire field of view and a very good mosaic of thinned, back-side illuminated CCD's with fast and low-noise readout electronics. In every respect, the WFI is rivalled only by very few similar instruments at other observatories. It would require too much space to mention all the salient points here. But they are described in depth in the user manual, and interested readers should kindly refer to it. Moreover, all ESO Commissioning and Science Verification data will be made accessible via the ESO Science Archive. Their availability will be announced on the ESO WWW pages.

A sore point for the Science Verification efforts and subsequent guest observers has been, and partly still is, that especially the standard broad-band filters were delivered very late and/or with major defects. Up-to-date status information is posted on the WFI home page mentioned above. We are very grateful to Dr. G. Luppino and the Institute for Astronomy of the University of Hawaii for the loan of a V filter formerly used with the UH8k camera. This camera was in January 1999 replaced with the even larger CFH12k instrument in the prime focus of the CFHT, and we take this opportunity to congratulate our colleagues on the successful commissioning of this impressive new Gigabyte-generating machine (cf. URL: `http://ftp.cfht.hawaii.edu/News/CFH12K-011399/cfh12k_neus.html`). Finally, we cordially thank the many colleagues in Garching, Heidelberg and La Silla, who have contributed to the project and very effectively supported the commissioning run.

Dietrich Baade (dbaade@eso.org)

The La Silla News Page

The editors of the La Silla News Page would like to welcome readers of the thirteenth edition of a page devoted to reporting on technical updates and observational achievements at La Silla. We would like this page to inform the astronomical community of changes made to telescopes, instruments, operations, and of instrumental performances that cannot be reported conveniently elsewhere. Contributions and inquiries to this page from the community are most welcome. *(J. Brewer, O. Hainaut, M. Kürster)*

News from the NTT

O. R. HAINAUT

The last three months have again been very quiet, with a total technical down time of 1.7%. As the telescope behaved very well, we had enough time to continue improving the system to make it even more reliable and user-friendly. To mention just a few of these improvements that are visible for the observer:

– In the framework of the implementation of the calibration plan, a large collection of calibration Observation Blocs (OBs) have been installed, including OBs for photometric standards for EMMI and SuSI, and for spectrophotometric standards for all EMMI's grisms (no more "how long should be the exposure time for LTT6248 with Grism #1?"). Flat-fields, biases, darks, and wavelength calibrations are also defined. These OBs, in combination with the new "Calibration Request Form" (to order day time calibrations) make easy the calibration of the most complex observing modes. For SofI, a large series of photometric standards have been measured. Information about all these calibrations is available on our web page (from the ESO web, follow the links to La Silla, NTT, Observations, then Calibrations).

– The differences of focus between the active optics image analyser and the scientific instruments were calibrated: so, when an image analysis is performed, the telescope is also focused. We are now running the active optics in parallel with the observations whenever it is possible (i.e. when a suitable guide star is available, and when the scientific exposures are longer than 5 minutes), so the optics is maintained in its optimal configuration, including the focus.

– P2PP version 1.2.1 was installed; this solves the problem of the long OB cloning time, which was quite frustrating for short exposures, and even worse when one had fetched the wrong OB.

There were lots of changes in the Team over the past months: Chris Lidman was transferred to Paranal, where he will work on ISAAC. The Team and the observers, will miss his extensive knowledge of SofI and his excellent support at the telescope. Fortunately, he had time to fully train the NTT fellows, Vanessa Doublier and especially Leonardo Vanzi, who will be the SofI instrument scientist until Chris' replacement is contracted. Norma Hurtado, the Telescope and Instrument operator who was well known, among other things, for her vigorous musical tastes, has also been transferred to Paranal, where she now drives UT1. Although we miss her expertise and her humour, we have already found an excellent replacement: Ariel Sanchez, who was formerly at the 3.6-m, joined the Team in 1999. And finally, after 6 years at the NTT, Philippe Gitton left ESO. Philippe joined the La Silla Observatory as a Cooperant (while I was myself finishing my cooperation), then was hired as an engineer. His contribution to the NTT in general and to the NTT upgrade was enormous; to mention only the most obvious, the Active Optics was tested, tuned, improved, fixed by Philippe, who left us with a reliable and efficient system.

New SOFI Grisms – NTT and IR Teams

C. LIDMAN

A new grism, with a resolving power of one to two thousand, was installed and tested over the new year. To cover most of the 0.8 micron to 2.5 micron range, the grism is used in orders 3 to 8 and with the broad-band filters (*Z*, *J*, *H* and *Ks*) as order-sorting filters. The details are listed in the following table. The resolution is listed for the 0.6 arcsecond slit.

For orders 3 and 4, the usable range is defined respectively by the *Ks* and *H* filters. For higher orders, it is defined by order overlap.

Order	Dispersion (Angstroms)	Usable Range (microns)	Resolution
3rd	4.63	2.00–2.30	2200
4th	3.44	1.49–1.81	1500
5th	2.71	1.20–1.28	1400
6th	2.22	1.17–1.24	1400
7th	1.87	0.89–0.93	1400
8th	1.58	0.86–0.95	1400

We expect this grism to be most useful in orders 3 and 4. The higher orders will be less useful. Those observers who wish to use the grism in higher orders should contact the NTT team (nttt@eso.org).

A New Control Room for the 3.6-m Telescope

M. STERZIK

The 3.6-m telescope team started the year 1999 with the move of the control room. Our new control room is now located in the third floor of the telescope building, in a spacious room that has been freshly refurbished for this purpose. The general design is kept modern and functional, but a warm and friendly atmosphere in the room is generated by wooden panelling and wooden doors.

The central area of the room is dominated by the huge operations console. We decided to use the same U-shaped desk that is well known from the NTT and VLT control rooms. The VLT-compliant operation of the telescope control system, adapter and autoguider, and the instruments require the extensive use of workstations and X-terminals in order to monitor and control all subsystems. One wing of the desk is dedicated entirely to telescope operations. The other wing is assigned to the visiting astronomers, allowing them to perform all necessary tasks from the preparation of observations to a first online data inspection and analysis. All our instruments can be operated from the new control room except the CES, which is still in the "old" CAT control room until its new VLT-compliant instrument control system becomes available later this year.

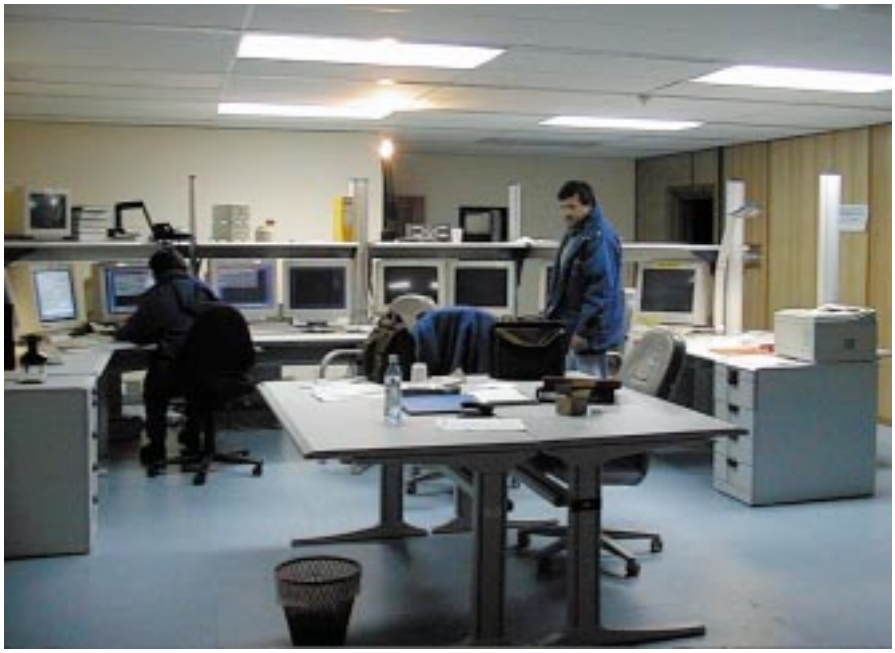

The size of the room allowed us to separate the generic control room from a more private area (for the few relaxed moments with music, tea or coffee) with a long bookshelf.

I am convinced that our users will enjoy, and benefit from this qualitative enhancement of their working environment.

On the technical side, I am glad that we can now offer a significantly improved telescope pointing behaviour as compared to the past year. Tightening the M2 mirror support structure allowed us to eliminate several high order harmonic terms in the pointing model. At present, we achieve about 8 arcsec rms pointing accuracy, a figure that is expected to decrease further once the new "Heidenhain" strip encoders can be used for axis control.

VLT DATA FLOW OPERATIONS NEWS

The NTT Service Observing Programme: On the Efficiency of Service Observing

P.A. WOUDT and D. SILVA, ESO

Abstract

A number of articles have recently appeared in the ESO Messenger reporting on the past experience of the NTT service observing programme in Periods 58, 59 and 60 (Silva and Quinn 1997, Silva 1998). In this paper, the third in this series, we report on the results of a statistical analysis of the efficiency of service observing during Period 60. We have compared service observing (SO) with the classical 'Visitor' Mode (VIS), and with the other main programme executed at the NTT during this period, the ESO Imaging Survey (EIS). To obtain an insight into the efficiency of service observing, we examined the Period 60 NTT observing logs in detail. We have only compared nighttime operations, and do not include pre-observing preparations into our analysis.

The observations in Service Mode suffered significantly more from adverse weather conditions at La Silla than both the VIS and EIS observations. On average, the down time during Service Mode (both weather and technical down time) is more than double the down time during either the VIS and EIS Mode, 23.7% versus 10.9% and 10.4% respectively. Irrespective of these adverse weather conditions during Service Mode, it can be

maintained that service observing is an efficient way of managing telescope time.

Introduction

Briefly stated, it has been argued (e.g. Silva 1998) that service observing has three main advantages over classical observing:

Science efficiency is maximised. Execution priority is given to the programme with the highest OPC rank that matches the current observing conditions. This scheme maximises the likelihood that the highest ranked programmes will be fully completed during the current ESO Period, i.e. complete scientifically useful datasets are efficiently produced.

Operations efficiency is maximised. Operations efficiency can be optimised by sharing calibration data between similar science observations, and by having experienced staff observers obtaining the data.

Data re-use is maximised. By acquiring uniform datasets with adequate calibration, data can be re-used efficiently in the future for projects other than the original OPC approved project.

Silva (1998) concluded that most of these objectives were achieved during the Period 60 NTT Service Observing Programme. However, what conclusions can be drawn by comparing Period 60 NTT Visitor Mode and Service Mode operations? In particular, what were the relative scientific and operations efficiencies of these two observing modes, and what lessons can be applied to the VLT service-observing programme? These questions are addressed and answered in this article.

Observing at the NTT During Period 60

During Period 60 at the NTT, 37.5 nights (= 21% of all the available time) were allocated to service observing, 27.5 nights (= 16%) were allocated to the ESO Imaging Survey (EIS) and 52 nights (= 29%) were given to observers executing their programme in Visitor Mode. The remaining 60 nights (= 34%) were used for various tests, e.g. testing the pointing model of the telescope, or for the commissioning of new instruments such as SOFI and SUSI2.

In order to analyse and compare all the different observing modes in an unbiased way, we have taken the NTT observing logbook[1] as the basis for the current discussion. All the records required, such as starting time, exposure time, the nature of the exposure, i.e. calibration, focus se-

(Continued on page 22)

[1]Unfortunately, for a few nights (2 nights in Visitor Mode) the logbooks were incomplete. These nights have been totally excluded from the current analysis. A further 4 nights in Visitor Mode were not included as they were scheduled in April 1998 and night logs were not readily available. For both the EIS and SO Mode, we have retrieved 100% of the night logs, for Visitor Mode we based our analysis on 88% of all the VIS programmes.

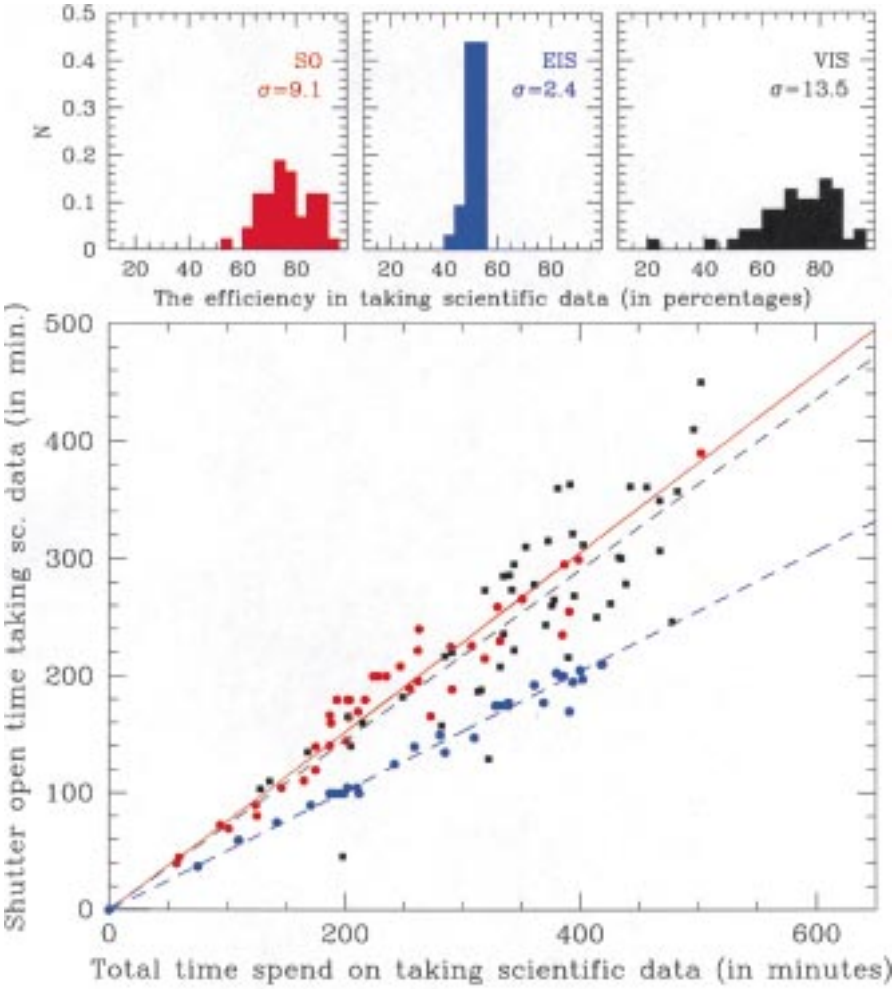

Figure 1: The bottom panel indirectly shows the efficiency of gathering scientific data for each of the different observing modes (SO = black squares, VIS = red dots, EIS = blue dots). If a programme was 100% efficient, i.e. all the time spent on a target was used to gather photons, that programme would lie on the x = y line. The top three histograms show the spread in efficiency as observed for each of the different observing modes.

NGC 4945 in 3 Colours

The picture on the following two pages of this nearby edge-on spiral galaxy was assembled from five 15-minute red-light (printed red), four 5-minute B-band (printed green), and five 1000-second U-filter (printed blue) exposures taken during the Science Verification phase of the Wide Field Imager at the 2.2-m telescope on La Silla. At the recession velocity of NGC 4945 of 560 km/s, the red filter centred at 665 nm with a full width at half maximum of 1.2 nm does still not include the Hα emission line of the interstellar hydrogen. The original resolution of 1 arcsec corresponds to roughly 19 pc at the distance of 3.9 Mpc of the Centaurus group of galaxies, to which this galaxy with a starburst/Seyfert nucleus belongs. East is to the left and North to the top.

In addition to NGC 4945 itself, only a few more distant galaxies can be recognised as such in this reproduction. The vast majority of the point-like sources are anyway stars in the Milky Way. Only around NGC 4945 are a fair number of them that are actually globular clusters belonging to this galaxy.

The applied image processing was on purpose kept to an absolute minimum of sophistication in order to subject the intrinsic quality of the data to the hardest test possible: Mean bias and sky background levels were subtracted as a constant, but separately for each CCD. No flatfielding was applied but all cosmetic defects and the inter-chip gaps were removed by median filtering of the stack of exposures obtained with each filter. The geometric registration of the images was accomplished by translations only, i.e. no rotation or other resampling was applied.

The total number of data points used is about 10^9; their information content corresponds to more than 70×10^9 photons (above the sky background). But only a part of the image corresponding to 28×20 arcmin is shown. It is printed at a scale of roughly 4 arcsec/mm and was rebinned to 0.48 arcsec/pixel to match the resolution of the printer (200 dpi). A similar print of the complete 33 arcmin × 33 arcmin field of view, that preserves the full 0.24-arcsec pixel sampling, would need to measure 100 cm × 100 cm, i.e. 8 times more in area.

dbaade@eso.org

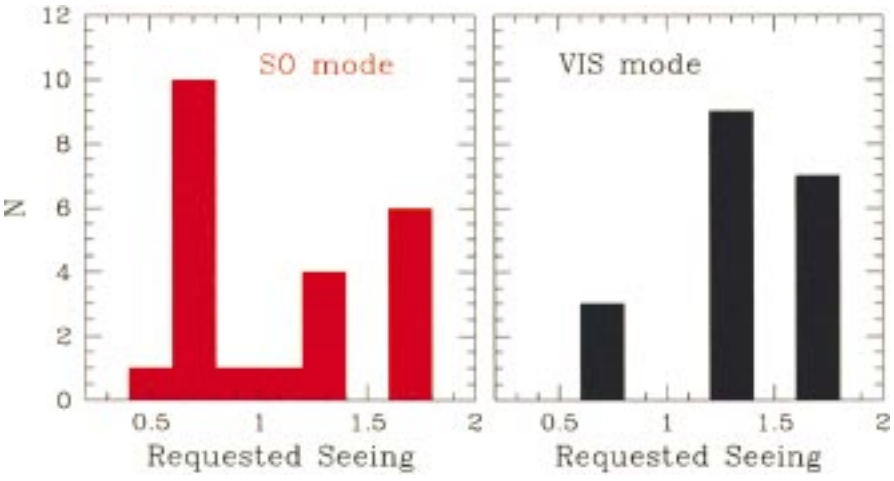

Figure 2: The distribution of the requested seeing conditions for programmes in Service Mode (left panel) and Visitor Mode (right panel). The programmes plotted in the bin (< 1.8") correspond to programmes without any specified seeing constraints.

(Continued from page 19)

quence, or scientific data, are stored in a uniform way. Records are kept of the seeing at La Silla from the DIMM2 instrument (*http://www.ls.eso.org/lasilla/seeing/html/DIMM2.html*). These records show that on average the ESO Imaging Survey experienced marginally worse seeing, compared to both the VIS and SO Mode (see also Table 1).

Weather and technical down time are verified for each night by comparing the observing logbook with the electronic night reports submitted by the observers (*http://www.ls.eso.org/lasilla/Reports/html/Opreport.html*). In all cases, the down time as observed from the NTT logbook was used in the statistical analysis. For each night, the total available time was subsequently split up into the following categories:

- Image analysis and Focus
- Switching instrument: EMMI ↔ SUSI
- Switching observing mode on shared nights: EIS ↔ SO, or VIS ↔ SO
- Calibration data
- Science data
- Weather down time
- Technical down time
- Target of Opportunity, or telescope tests

With regard to the "Image Analysis", "Calibration" and "Science" data, one can compare the time spent executing an Observation Block (Silva 1998) with the requested integration time. This will give an idea of the efficiency in executing such an Observation Block, i.e. how much time is spent on pointing the telescope, reading out the CCD, in relation to the shutter open – shutter closed time.

On the Efficiency of Service Observing

The main goal of this study is to determine how efficiently the NTT is used during Service Mode compared to classical observing; to see where time losses occur during the night time operations, how these losses can be reduced, and to find an answer to some frequently asked questions regarding service observing.

- Is service observing at a good meteorological site preferred over classical observing?
- Are visiting astronomers less efficient on their first night of observing?
- How will service observing be different at the VLT?

These questions are at the heart of the current analysis.

• First-night efficiency in Visitor Mode

It is generally assumed that observers in Visitor Mode are less efficient on their first night of observing, i.e. the observer still has to get acquainted with the set-up of the telescope. One argument in favour of service observing is that all the observations are done by observers familiar with the telescope, the instruments and the operations, and hence no valuable time is lost during the night.

From the data presented in Table 2, we find no evidence that Period 60 observers in VIS Mode were less efficient during their first night of observing. This is based on 19 individual VIS programmes out of a total of 23 VIS programmes that were given time in Period 60. The remaining 4 VIS programmes were excluded because the observing log was incomplete. The observed differences between the first night characteristics and the overall averaged performance are statistically insignificant; this is likely due to the high level of experience of the VIS Mode observers at the NTT during Period 60.

We also compared first-night performance for the SO and EIS Mode, and also here no significant changes are observed. Table 2 summarises the difference between first-night and overall performance for each of the individual modes. In Table 2 the difference (in percentages) is given between the first-night characteristics and the overall characteristics, e.g. observers in VIS Mode spent on average 1.9% less (hence the negative sign in Table 2) of the total available time on standards during the first night, compared to the overall observing run. The difference in operational overhead, calibration data, scientific data and down time should add up to zero.

The main difference is observed in the down time for both SO and EIS Mode. These modes have had, on average, better weather conditions during the first nights. This has, logically, resulted in spending more time on taking calibration data. Note that one service observing run (5/6 – 9/10 November 1997) is excluded from this particular analysis, because the first night on this run was totally unusable due to adverse weather conditions.

Summarising, there is no evidence from the NTT Period 60 logs, that observers in Visitor Mode use the telescope less efficiently on their first night. This could, however, be solely due to the high level of observational experience of these observers. Over the last five years, 80% of all the NTT Period 60 visiting astronomers had used one or more of the telescopes at the La Silla observatory, and over the last three years, 30% of the NTT Period 60 visiting astronomers had used the NTT previously.

• Various sources of time losses

Time lost due to bad weather conditions is beyond the control of any observer. All observatories try to minimise time lost to other problems. At the NTT during Period 60, there were some reoccurring sources of time loss, which could be avoided, or at least minimised in the future. The two main sources of time loss were the long CCD readout times, and switching from EMMI to SUSI during one night (mainly, but not exclusively, done during SO Mode).

The long CCD readout time of the CCD only became a serious problem when the scientific programme required many short exposures, such that the time spent on

Table 1: A summary of the observing conditions for the three different modes.

	VIS	SO	EIS
Number of nights	52	37.5	27.5
Average Seeing †	0.89 ± 0.28 (39)	0.86 ± 0.18 (16.5)	1.03 ± 0.31 (17.5)
> 50 % down time *	6.3 %	17.4 %	8.8 %

† In brackets the number of nights is given on which the quoted, average image quality (in arcseconds) is based.

* This shows the percentage of nights when more than half of the night was lost due to either adverse weather conditions, technical problems, telescope tests, or Targets of Opportunity.

Table 2: First-night performance compared to the overall performance for VIS, SO and EIS Mode.

	VIS	SO	EIS
	(Numbers quoted in percentages)		
Operational overhead	–1.9 ± 2.5	+1.0 ± 3.9	+1.1± 1.6
Calibration data	+0.4 ± 2.8	+3.0 ±10.4	+5.3 ±10.0
Scientific data	+1.0 ±11.4	+1.0 ±10.1	+2.7:±16.0
Scientific data (–overhead)	–0.3 ± 9.1	+0.2 ± 6.1	+1.0 ± 8.2
Efficiencycy †	–1.8 ± 3.9	+1.0 ± 6.3	–0.3 ± 1.4
Down Time *	+0.5 ±12.0	–4.9 ±11.8	–9.1 ±17.1

† The efficiency is defined as the fraction of the time spent on taking scientific data excluding the overheads such as pointing and reading out the CCD, compared to the total time taking scientific data.

* The Down Time is defined as the total time that the telescope is not used for the programme in question, either due to adverse weather conditions, technical problems, targets of opportunity, or telescope tests.

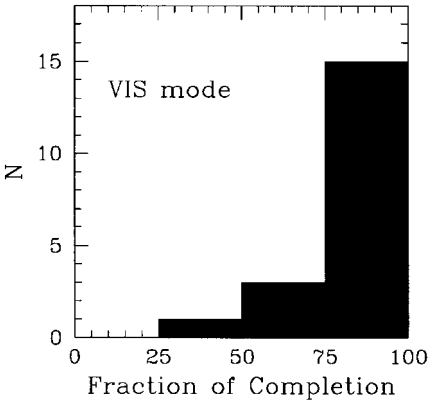

Figure 3: The distribution of the fraction of completion of the programmes in Visitor Mode based on the weather statistics (see text for a more detailed description). Fifteen programmes in VIS Mode lie in the interval of 75% to 100% completion.

gathering photons is equivalent to, or smaller than, the readout time. One programme in VIS Mode suffered severely from this effect. Of all the time spent on taking scientific data (i.e. on target) for this programme, only 43% of the time the shutter was open to gather photons, compared to the overall average of VIS Mode efficiency of 72.5%. This was by far the least efficient programme in this sense, only because of the short exposure times of the science objects. The ESO Imaging Survey also suffered slightly from this effect, with exposure times that were only double the CCD readout time (see also 'the overhead on science observations' for a further discussion). Of course, this problem would have been eliminated if FIERA CCD controllers had been available for EMMI during the EIS project as originally envisioned.

The other main source of time loss was due to switching between instruments during the night (sometimes more than once). Typically, it took between 30 and 40 minutes per switch before data acquisition resumed. A significant fraction of this time was spent on the focussing of the telescope. During Period 60, both EMMI and SUSI were offered until December 1, 1997. After this date, only EMMI was available. During two SO runs before December 1, 1997, the instrument switches took 6.0% and 9.3% of all the available time, respectively. Unless switching to a higher-priority programme, the advantages of reacting to changing weather conditions by switching to a different instrument are often lost due to decreased available science integration time.

One additional problem that arose during service observing in Period 60 was the lack of OPC-approved bright-time programmes. This problem presented itself in a nasty way during the fifth SO run in Period 60 (1/2–7/8 January 1997). There were time slots during the night for which no SO programme was available. Although this time was used for calibration observations and technical tests, it could have been used for science if programmes had been available. Therefore, it was not scientifically productive. This problem did not re-occur during Period 60.

The technical down time is generally very low, 2.9%, 1% and 4.3% of all the available time during VIS, EIS and SO Mode observing, respectively. In addition, a small fraction of the time was made available for the Targets of Opportunity, mostly during service observing (1.5%, 2.7% and 3.9% of all the available time during VIS, EIS and SO Mode observing respectively). In Table 3, a summary of these numbers is given. From Table 3[2], one can see most clearly that one of the main differences between the various observing modes was the time lost due to bad weather conditions. On average, service observing has suffered 10% more from bad weather, whereas both EIS and VIS modes suffered similar weather losses.

[2]In Figure 4 of Silva (1998), four nights that were completely lost due to bad weather conditions were by mistake not included in the pie diagram. The numbers quoted in Table 3 are the correct ones for Service Mode at the NTT during Period 60.

• The overhead on science observations

In Column 9 of Table 3, we present the efficiency in executing an Observation Block. This efficiency is defined as the fraction of the time requested by the observer for executing an Observation Block over the time actually needed to gather the data (including moving the telescope on target, reading out the CCD).

In the lower panel of Figure 1, the efficiency is indirectly plotted for each night of observing in each of the individual modes (black squares correspond to Visitor Mode, red dots represent the Service Mode and the blue dots show the results of the EIS Mode). The solid and dashed lines correspond to the efficiency listed in Column 9 of Table 3. The efficiency of the EIS Mode lies below that of both the VIS and SO modes. This is solely due to the precept goals of the EIS, namely large areal coverage, rather than going deep to faint magnitudes. In other words, although the EIS project achieved its main technical goal (areal coverage), it came at the cost of high operational overhead caused by old-generation CCD controllers. The original plan, of course, was to eliminate this overhead by using FIERA CCD controllers and a drift-scan technique. Alas, new CCD controllers for EMMI were not available in time for use during the EIS project.

From Table 3 and Figure 1, it can be

Table 3: Splitting up the night

I.A. (1)	S.I. (2)	S.M. (3)	Ops. (4)	Cal. (5)	Sci (6)	Sci-o (7)	Sci ov. (8)	Elf (9)	Wea (10)	Techn (11)	ToO (12)	Test (13)	Down (14)	
ALL	6.3	0.9	0.4	7.6	10.6	63.5	43.1	20.4	67.9	12.1	3.0	2.6	0.6	18.3
SO	7.0	1.5	0.4	8.9	9.7	52.1	39.7	12.4	76.2	19.4	4.3	3.9	1.7	29.4
EIS	7.4	0.0	1.0	8.5	12.3	66.1	33.7	32.5	51.0	9.1	1.3	2.7	0.0	13.1
VIS	5.0	1.0	0.0	6.0	10.3	71.2	51.6	19.6	72.5	8.0	2.9	1.5	0.0	12.5

(1) Image analysis, (2) Switching instruments, (3) Switching observing mode, (4) Operational overhead, (5) Calibration data, (6) Science data, (7) Science data minus overhead, (8) Overhead on the science data, (9) Fraction of time needed over time used for science data, (10) Weather down time, (11) Technical down time, (12) Target of Opportunity, (13) Tests of the telescope, (14) Total fraction of "down time" (= column 10+11+12+13).

maintained that service observing minimises the time to move to a target and gather the data, and in this sense it is the most efficient way of observing, closely followed by the Visitor Mode observing. Moreover, the spread in efficiency in Service Mode observing is much smaller than the spread observed in VIS Mode efficiency, as can be seen in the top panels of Figure 1 (2.4%, 9.1% and 13.5% for EIS, SO and VIS Mode, respectively). The histogram of the Service Mode efficiencies shows a close to Gaussian distribution, whereas the VIS mode histogram displays a clear non-Gaussian distribution, with a long tail towards lower efficiencies. The lack of this tail in the Service Mode histogram, and the smaller spread, indicate that service observers acquire the data in a more consistent way. Naturally, the EIS project has the smallest distribution because of their uniform observing strategy.

• Completion of the programmes

In a report on service observing at the NTT, Silva (1998) showed (Fig. 5) the fraction of completed programmes during service observing in Period 60. Completed means that the data passed the quality control and that all the requested observing Blocks have been successfully executed. Unfortunately, the data gathered in Visitor Mode are not subjected to a quality control and it becomes very difficult to judge from our current analysis if an observer in VIS Mode is satisfied with the quality of the obtained data. We estimated the Visitor Mode completion in two ways:

• Seeing. Does the image quality during the observing run (seeing on the DIMM2 telescope) conform to the image quality requested by the observer?

• Down time. What is the fraction of (weather) down time?

It turns out that the seeing requirements of the visiting astronomers were not so strict, and hence this parameter becomes a poor indication of the completion of a VIS Mode programme; 86% of the programmes experienced better seeing than requested and for the remaining 14% the seeing was comparable to, or marginally worse than, the initial request. In Figure 2, it can be clearly seen that the OPC-approved programmes in Service Mode (left panel in Figure 2) have a much more stringent seeing requirement, e.g. 10 programmes requested a seeing better than 0.8″, compared to their classical counterparts (right panel in Fig. 2). It shows that those programmes requiring good observing conditions have generally been assigned to be completed via service observing.

The fraction of down time is a much better indicator for the completion of visitor programmes, assuming that the initial time requested is sufficient to complete the entire programme. Figure 3 shows the fraction of completion of the VIS programmes. It cannot be directly compared to Figure 5 of Silva (1998) because of the lack of quality control, but does give an idea of the success rate of the Visitor Mode observing.

• In the long term

One final way of comparing the different observing modes and their respective efficiencies is to look at the scientific output. Has service observing resulted in making the astronomer more productive? What is the scientific impact of the NTT as a result of service observing? This, of course, can only be monitored over a larger time span, and it might still be too early to answer this question.

Out of all the programmes executed at the NTT during Period 60 (VIS and SO Mode), two papers have appeared to date in refereed journals, presenting data gathered at P 60. One paper is (partially) based on data taken during Service Mode (Sollerman et al. 1998), whereas the second paper presents data taken during Visitor Mode (Reimers et al. 1998).

Lessons Learned Redux

Silva (1998) ended with a review of lessons learned from the NTT service observing experience and how applying these lessons could improve service observing at ESO in the future. The additional analysis here reveals several new lessons.

It is obvious to all observers that, on any given night, minimising instrument-configuration changes minimises required calibration overheads and therefore maximises the amount of science acquisition time. The analysis presented here suggests that this paradigm can be extended to instrument switches. Although rapid instrument switching is possible at the NTT and will be possible at the VLT UTs, it is not clear whether this is the most efficient use of nighttime hours. During Period 60 service observing, instrument switching frequently consumed 10% or more of the night. The lesson is clear: unless the science priority is very high, switching between instruments on any given night should be avoided.

It is equally clear that the benefits of service observing become most significant for programmes that need special observing conditions (e.g. exceptionally good seeing or water vapour content) or have special scheduling constraints (e.g. rapid follow-up of transient events like gamma-ray bursters). Programmes that require worse than median conditions (as all the NTT Period 60 VIS programmes did) can typically be efficiently executed in Service or Visitor Mode. Nevertheless, it is important to schedule enough loosely-constrained programmes in Service Mode that the entire range of observing conditions delivered on nights dedicated to service observing can be used efficiently.

Acknowledgements

We wish to thank Elisabeth Hoppe of the VISAS office and the NTT Team for their assistance with collecting the data needed to complete this analysis.

References

Reimers, D., Jordan, S., Beckmann, V., et al. 1998, *A&A*, **337**, L13.
Silva, D. 1998, *The Messenger* **92**, 20.
Silva, D. and Quinn, P. 1997, *The Messenger* **90**, 12.
Sollerman, J., Leibundgut, B. and Spyromilio, J. 1998, *A&A* **337**, 207.

Patrick Woudt (pwoudt@eso.org)

“First Light” of UT2 !

Following the installation of the main mirror in its cell and a 20-hour working session to put the complex secondary mirror and its support in place, the UT2, now Kueyen, achieved (technical) first light in the morning of March 1, 1999, when an image was obtained of a bright star. It showed this telescope to be in good optical shape and further adjustments of the optical and mechanical systems are expected soon to result in some “astronomical” images.

The announcement of this important event was made by the ESO Director General during the opening session of the VLT Symposium that was held in Antofagasta during March 1–4, 1999.

(Excerpt from ESO Press Release 06/99 – http://www.eso.org/outreach/press-rel/pr-1999/pr-06-99.html)

The Lunar Occultation of CW Leo – a Great Finale for TIMMI

B. STECKLUM, Thüringer Landessternwarte, Tautenburg, Germany
H.-U. KÄUFL, ESO, Garching, Germany
A. RICHICHI, Arcetri Observatory, Firenze, Italy

Although TIMMI (Käufl et al. 1992), ESO's thermal infrared multi-mode instrument, had been decommissioned after Period 61, it got its very last chance on November 11th, 1998. The measurement was a special one, recording the lunar occultation of the well-known carbon star CW Leo[1], and the present contribution summarises these observations.

When TIMMI was under construction, perhaps none of its builders anticipated that the burst read-out mode implemented for technical reasons would ever yield scientific results. This mode offered the possibility to acquire an image sequence of 509 frames at rates up to 125 Hz. Thus, it was well suited to record fast transient phenomena such as occultations. When the authors discussed this capability a few years ago, it turned out that measurements of lunar occultations may yield an angular resolution of about 30 milliseconds of arc (mas) at the wavelength of about 10 µm, similar to that expected for the VLTI. This would enable detailed studies of the distribution of circumstellar dust around evolved stars. Consequently, proposals were submitted which aimed at the derivation of the angular diameter of asymptotic-giant-branch (AGB) stars. Despite some difficulties that led to the loss of a few events, several light curves were acquired for infrared sources with 12 µm fluxes in the range of 5 . . . 50 Jy. Since the required time resolution is in the order of 20 . . . 40 ms, the measurements had to be performed in staring mode, i.e. without applying the chopping/nodding technique commonly used to eliminate the overwhelming thermal background. Furthermore, as a consequence of the limited number of frames, the predictions had to be accurate to within typically 15 . . . 20 seconds to catch the event, a condition that was not always met (primarily due to the positional errors for infrared sources, which went undetected in optical surveys). Moreover, the comparatively small FOV of TIMMI (18″ × 18″) in combination with the poor tracking of the telescope (close to the Moon or during daytime the auto-guider does not work!) always provided for sufficient challenges for the observing team.

These measurements allowed the derivation of a few angular diameters and were crucial to assess the dependence of the attainable angular resolution on the signal-to-noise ratio. First results were presented at the ESO workshop Science

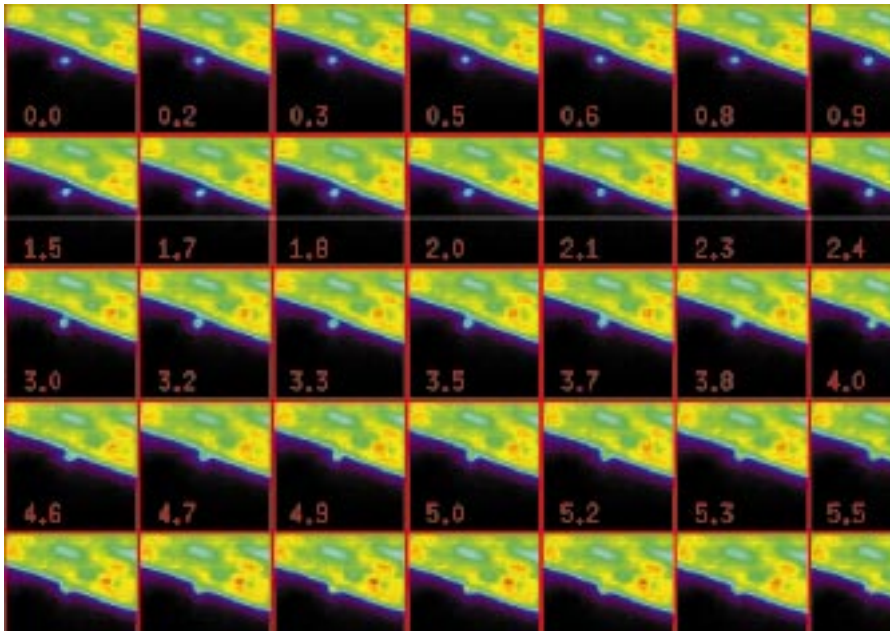

Figure 1: Sequence of the disappearance of CW Leo using linear intensity scale. Each frame is the average of three individual images.

[1]In the Strasbourg-ESO Catalogue of Galactic Planetary Nebulae (Acker et al., 1992), CW Leo is listed as a possible planetary nebula).

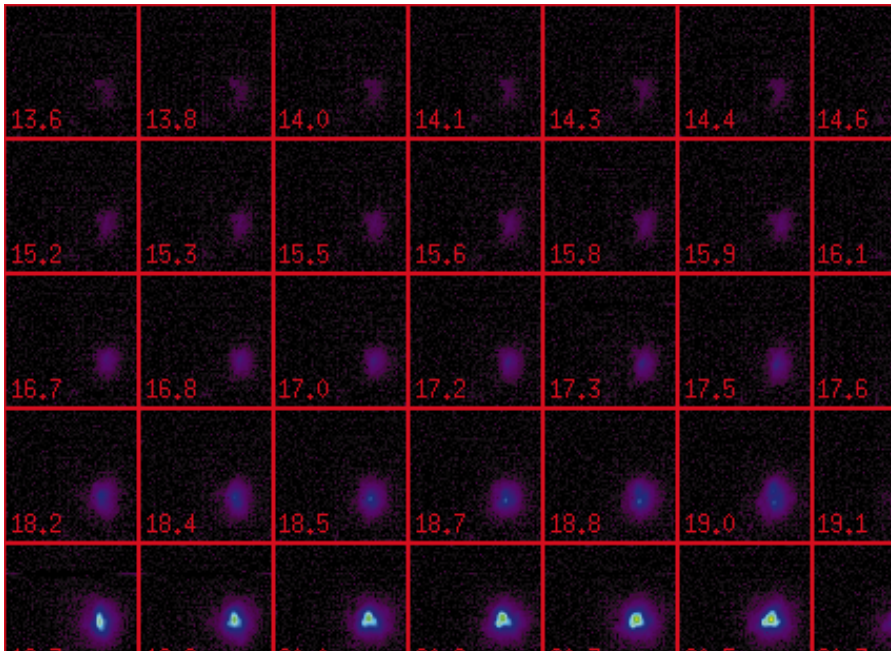

Figure 2: Sequence of the reappearance of CW Leo using a square-root intensity scale. Each frame is the average of three individual images. The elongation of the source is due to the uncovering of the western halo while the central peak is still occulted.

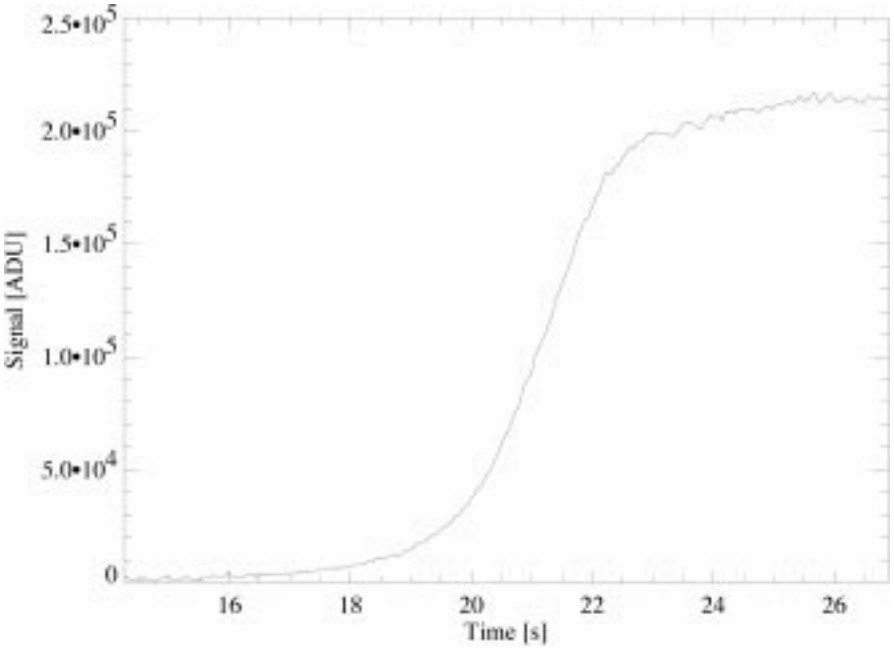

Figure 3: Light curve of the reappearance of CW Leo. Some disturbances at almost full signal level are due to scintillation.

with the VLTI (Stecklum et al. 1997). The prospects of this observing technique that intrinsically yields one-dimensional information in combination with the VLTI has been discussed recently (Käufl et al. 1998).

Monthly lunar occultations of a certain celestial object that is close enough to the ecliptic occur during a cycle that lasts up to 1.5 years when the Moon sweeps through that area in the sky. The forecast showed that an occultation of CW Leo, aka IRC+10216, the brightest celestial object at $\lambda \approx 10$ µm in the northern hemisphere, would occur for a visibility area including La Silla in fall 1998. Notably, the visibility regions for the current cycle of CW Leo do not include many major observing sites. Moreover, the next event visible from ESO observing facilities will be in 2008. Thus, it was our definite goal to observe the 1998 event in order to reveal the fine structure of the thermal emission from the dense dust envelope. A pioneering mid-infrared measurement also employing the lunar occultation technique by Toombs et al. (1972) revealed the presence of a core with a diameter of about 0.4″, which is surrounded by a 2″ halo. More recent observations by Sloan and Egan (1995) applying the deconvolution of slit-scanned profiles yielded evidence for two shells at the resolution of 0.7″. In the near-infrared, speckle interferometry revealed the presence of bright blobs in the dust shell located within 0.4″ (Haniff & Buscher 1998, Weigelt et al. 1998). The large net polarisation observed at 1 µm (Shawl & Zellner 1970) implies that these features are due to scattering rather than thermal emission. Thus, it is hard to assess the overall structure of the envelope from the morphology of these regions. From dynamical models of dust formation (Winters et al. 1995), an onion-like structure of the dust shell is predicted. Such a morphology has been observed already in Planetary Nebulae (e.g. in the Cygnus Egg nebula aka CRL 2688) and it has been suggested that CW Leo is already in the transition phase to such an object (e.g. Skinner et al. 1998). The shells around CW Leo are also a good test case for the thermonuclear evolution models for AGB stars, work that has been pioneered by Iben & Renzini (1983). Although the presence of circumstellar matter at angular distances up to $\sim 1'$ has been established by CCD imaging (Crabtree et al. 1987) and interferometric radio observations (Groenewegen et al. 1998), the large dust column density precludes the detection of the innermost shells at optical and near-infrared wavelengths. It was the main objective of the authors to trace the thermal emission from these discrete dust layers in order to prove that the model of Winters et al. (1995) for the prescription of dust formation on the AGB is basically correct.

The fact that the observations could be scheduled was not certain though the science case was tempting. Finally, all we would need was two times 30 seconds of observing time to measure both dis- and reappearance. Thus, we are happy to acknowledge that TIMMI was made available to us for this special event and appreciate the support of the 3.6-m telescope team. The occultations occurred on daytime (about 1.5 hours before local noon) after a long set-up night. About two hours before the main events, a chance to check everything was given by the occultation of HD 84194 which went fine. This star is offset by about 1.3° from CW Leo, and we wanted to use it as "parking star" when CW Leo would be hidden by the Moon. Since the huge brightness of CW Leo rendered it possible to record the disappearance at the bright (i.e. hot) limb of the Moon as well, two different settings of the detector electronics were prepared. The successful observation of the disappearance became clear when the initial images appeared on the screen showing the Moon steadily approaching CW Leo and finally occulting it. The major part of this image sequence is displayed in Figure 1. However, some nervousness arose when we were unable to find the offset star after the storage of the data was finished. After all, it was approximately 9:30 local time in the morning and the re-acquisition of a suitable

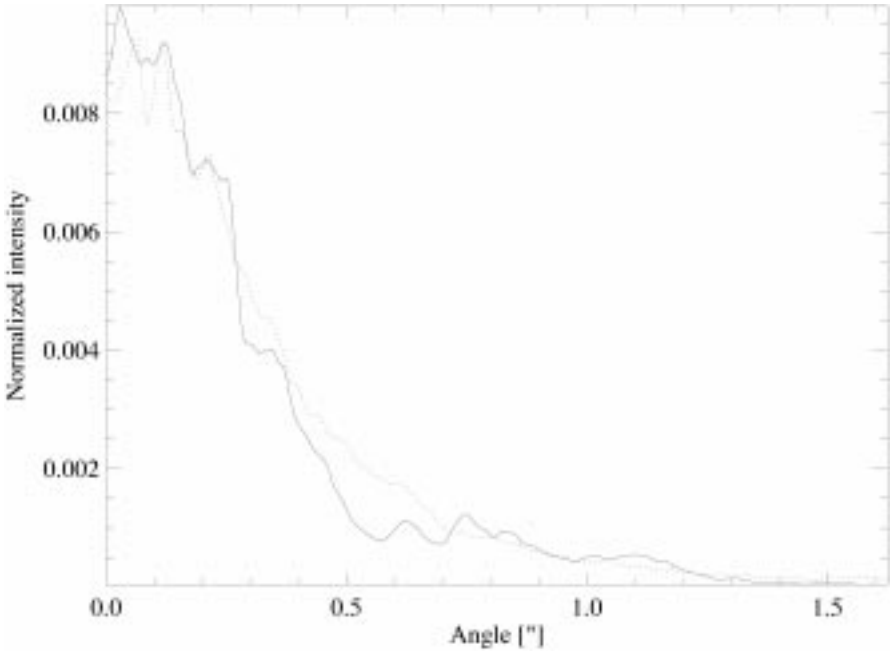

Figure 4: Reconstructed intensity profile splitted into eastern (dotted line) and western part (solid line). Four coinciding local peaks can be recognised, which presumably trace individual dust shells.

guidestar had to rely entirely on infrared imaging with TIMMI. Luckily, the nearby bright variable R Leo could be acquired and, after correcting the telescope co-ordinates on this source, the "parking star" could also be acquired. The detector setting was then changed for the reappearance for which the lunar background should be negligible. The final keystroke to start the burstmode for the reappearance was entered on $14^h\ 10^m\ 09^s$ UT. The data acquisition was active for 25 seconds and soon after, the individual images of the sequence were displayed. Excitation was rising when after 300 frames the screen still showed pure background. But then the intensity scaling of the display changed, indicating an increasing signal that soon overwhelmed the background level. With great joy we realised that the reappearance was caught late but not too late. Figure 2 shows the corresponding stack of frames. A more realistic impression can be obtained by watching the MPEG movies available at these URLs:

http://www.ls.eso.org/lasilla/Telescopes/360cat/timmi
http://www.tls-tautenburg.de/research/cw_leo.html and
http://www.arcetri.astro.it/~luna/irc10216.html

The first result presented here is based on the preliminary light curve of the reappearance shown in Figure 3. The one-dimensional brightness profile of CW Leo was derived by deconvolving this light curve with a point-source model according to the Fresnel prescription of diffraction at the lunar limb, taking into account all observational circumstances (spectral and temporal bandwidth, etc.). The deconvolution procedure utilises a maximum-entropy algorithm, which is the same as in Stecklum et al. (1995). The resulting brightness distribution has a FWHM of 0.6″, which confirms previous estimates. The eastern part is more wiggly, presumably due to scintillation, which influenced the last part of the light curve. Figure 4 provides a superposition of the eastern and western parts of the brightness profile. It can be recognised that there are step-like features in the profile, which occur almost symmetrically on either side. At least four such steps can be distinguished. Although the reduction of the data just started, we are confident that these features are not spurious but represent imprints of the innermost dust shells. Furthermore, the profile looks rather flat-topped and is much broader at its peak than the often-adopted angular diameter of the star of 40 mas. This indicates that either the photosphere is much more extended than previously believed or even hidden from direct view at mid-infrared wavelengths.

More in-depth conclusions will be drawn by comparing the final brightness profiles to model calculations. For us observers, the measurement was a breathtaking experience, and for TIMMI, it was a great finale. We'll miss you.

References

Acker, A., Ochsenbein, R., Stenholm, B., Tylenda, R., Marcout, J., & Schon, C., 1992, *Strasbourg-ESO Catalogue of Galactic Planetary Nebulae*, ESO.
Crabtree, D.R., McLaren, R.A., & Christian, C.A., 1987, in: *Late Stages of Stellar Evolution*, eds. S. Kwok & S.R. Pottasch, Kluwer Academic Publ., 145.
Groenewegen, M.A.T., van der Veen, W.E.C.J., Lefloch, B., & Omont, A., 1998, *A&A*, **322**, L21.
Haniff, Ch. & Buscher, 1998, *A&A*, **334**, L5.
Iben, I., & Renzini, A., 1983, *ARA&A*, **21**, 271.
Käufl, H.-U., Jouan, R., Lagage, P.O., Masse, P., Mestreau, P., Tarrius, A., 1992, *The Messenger* **70**, 67.
Käufl, H.-U., Stecklum, B., & Richichi, A., 1998, Proc. SPIE, 3350, p. 267.
Shawl, S.J. & Zellner, B., 1970, ApJ, 162, L19.
Skinner, C.J., Meixner, M., & Bobrowski, M., 1998, *MNRAS*, **300**, L29
Sloan, G.C. & Egan, M.P., 1995, ApJ, 444, 452
Stecklum, B., Henning, T., Eckart, A., Howell, R.R., & Hoare, M., 1995, *ApJ*, **445**, L153.
Stecklum, B., Käufl, H.-U., Richichi, A., 1997, in: Science with the VLTI, ed. F. Paresce, Springer-Verlag, 153.
Toombs, R.L., Becklin, E.E., Frogel, J.A., Law, S.K., Porter, F.C., & Westphal, J.A., 1972, *ApJ*, **173**, L71.
Weigelt, G., Balega, Y., Blöcker, T., Fleischer, A.J., Osterbart, R., & Winters, J.M., 1998, *A&A*, **333**, L51.
Winters, J.M., Fleischer, A.J., Gauger, A., & Sedlmayr, E., 1995, *A&A* **302**, 483.

Stecklum@methusalix.tls-tautenburg.de
(Bringfried Stecklum)
hukaufl@eso.org

The Reflex Cluster Survey: Observing Strategy and First Results on Large-Scale Structure

L. GUZZO[1], H. BÖHRINGER[2], P. SCHUECKER[2], C.A. COLLINS[3], S. SCHINDLER[3], D.M. NEUMANN[4], S. DE GRANDI[1], R. CRUDDACE[5], G. CHINCARINI[1,6], A.C. EDGE[7], P.A. SHAVER[8], W. VOGES[2]

[1]*Osservatorio Astronomico di Brera, Milano/Merate, Italy*
[2]*Max-Planck-Institut für Extraterrestrische Physik, Garching, Germany*
[3]*Liverpool John Moores University, Liverpool, U.K.*
[4]*CEA Saclay, Service d'Astrophysique, Gif-sur-Yvette, France*
[5]*Naval Research Laboratory, Washington D.C., U.S.A.*
[6]*Dipartimento di Fisica, Università degli Studi di Milano, Italy*
[7]*Physics Department, University of Durham, U.K.*
[8]*European Southern Observatory, Garching, Germany*

1. Introduction

As a modern version of ancient cartographers, during the last 20 years cosmologists have been able to construct more and more detailed maps of the large-scale structure of the Universe, as delineated by the distribution of galaxies in space. This has been possible through the development of redshift surveys, whose efficiency in covering ever larger volumes has increased exponentially thanks to the parallel evolution in the performances of spectrographs and detectors (see e.g. Da Costa 1998 and Chincarini & Guzzo 1998, for recent reviews of the historical development of this field).

While the most recent projects, as the Las Campanas Redshift Survey (LCRS, Shectman et al. 1996) and the ESO Slice Project (ESP, Vettolani et al. 1997) have considerably enlarged our view by collecting several thousands of redshifts out to a depth of $\sim 500\ h^{-1}$ Mpc[1], the quest for mapping a "fair sample" of the Universe is not yet fully over. These modern galaxy redshift surveys have indeed been able to show for the first time that large-scale structures such as superclusters and voids keep sizes that are smaller than those of the surveys themselves (i.e. $\sim$ 100–200 h^{-1} Mpc). This is

[1]Here h is the Hubble constant in units of 100 km s^{-1} Mpc^{-1}.

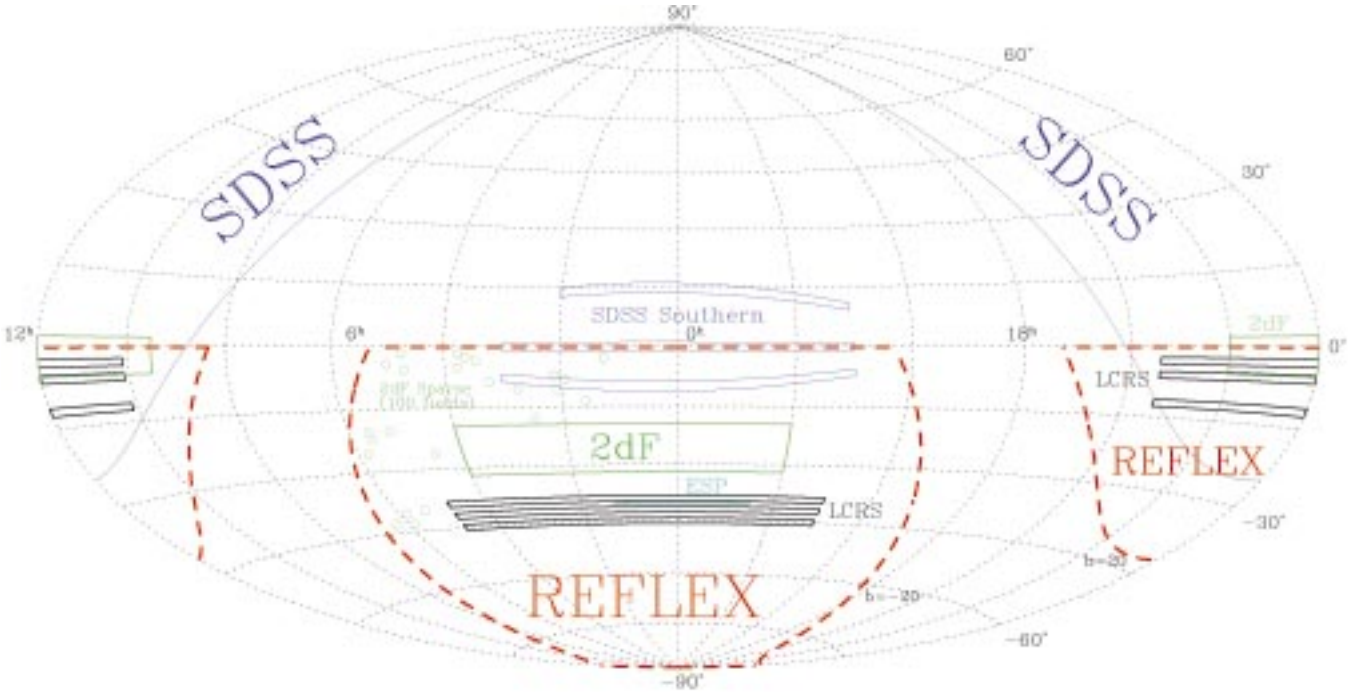

Figure 1: Aitoff view of how wide-angle redshift surveys with typical depth of $z \sim 0.2$ are covering the available sky (see Guzzo 1999 for details).

in contrast to the situation only a few years ago, when every new redshift survey used to discover newer and larger structures (a famous case was the "Great Wall", spanning the whole angular extension of the CfA2 survey, see Geller & Huchra 1989). On the other hand, it has also been realised from the ESP and LCRS results, among others, that to characterise statistically the scales where the Universe is still showing some level of inhomogeneity, surveys covering much larger areas to a similar depth ($z \sim 0.2$), are necessary.

To fulfil this need, on one side two very ambitious galaxy survey projects have started[2], the Sloan Digital Sky Survey (SDSS, Margon 1998) and the 2dF Redshift Survey (Colless 1999). The SDSS in particular, including both a photometric survey in five filters and a redshift survey of a million galaxies over the whole North Galactic cap, represents a massive effort involving the construction of a dedicated telescope with specialised camera and spectrograph.

Alternatively, one could try to cover similar volumes using a different tracer of large-scale structure, one requiring a more modest investment in telescope time, so that a survey can be performed using standard instrumentation and within the restrictions of public telescopes as those of ESO. This has been the strategy of the REFLEX Key Programme, which uses clusters of galaxies to cover, in the Southern Hemisphere, a volume of the Universe comparable to that of the SDSS in the North. Clusters, being rarer than galaxies, are evidently more efficient tracers for mapping very large volumes. The price to pay is obviously that of loosing resolution in the description of the small-scale details of large-scale structure. However, such information is already provided by the present generation of galaxy surveys.

The REFLEX cluster survey, in particular, is based on clusters selected through their X-ray emission, which is a more direct probe of their mass content than simple counts of galaxies, i.e. richness. Therefore, by using clusters as tracers of large-scale structure, not only do we sample very large scales in an observationally efficient way, but if we select them through their X-ray emission, we also have a more direct relation between luminosity and mass. Further benefits of the extra information provided by the X-ray emission have been discussed in our previous *Messenger* article (Böhringer et al. 1998). In the same paper, we also presented details on the cluster selection, the procedure for measuring X-ray fluxes, and some properties of the objects in the catalogue, as the X-ray luminosity function, together with a first determination of the power spectrum. Results on the cluster X-ray luminosity function have also been obtained during the development of the project from an early pilot subsample at bright fluxes (see De Grandi et al. 1999). Here we would like to concentrate on the key features of the optical follow-up observations at ESO, and then present more results on the large-scale distribution of REFLEX clusters and their clustering properties. Nevertheless, for the sake of clarity we shall first briefly summarise the general features of the survey.

2. The REFLEX Cluster Survey

The REFLEX (ROSAT-ESO Flux Limited X-ray) cluster survey combines the X-ray data from the ROSAT All Sky Survey (RASS), and ESO optical observations to construct a complete flux-limited sample of about 700 clusters with measured redshifts and X-ray luminosities. The survey covers almost the southern celestial hemisphere (precisely $\delta < 2.5°$), at galactic latitude $|b_{II}| > 20°$ to avoid high NH column densities and crowding by stars. Figure 1 (reproduced from Guzzo 1999), shows the region covered by the REFLEX survey, together with those of wide-angle galaxy redshift surveys of similar depth, either recently completed (ESP, LCRS), or just started (SDSS, 2dF).

Presently, we have selected a complete sample of 460 clusters to a nominal flux limit of 3×10^{-12} erg s^{-1} cm^{-2}. Due to the varying RASS exposure time and interstellar absorption over the sky, when a simultaneous requirement of a minimum number of source counts is applied, some parts of the sky may reach a lower flux. For example, when computing the preliminary REFLEX luminosity function presented in Böhringer et al. (1998), a threshold of 30 source counts in the ROSAT hard band was set, which resulted in a slightly reduced flux limit over 21.5% of the survey area. The important point to be made is that a full map of these variations is known as a function of angular position and is exactly accounted for in all the statistical analyses.

This first sample, upon which the discussion on clustering and large-scale structure presented here is based, has been constructed to be at least 90% complete, as described in Böhringer et al. (1998). Several external checks, as comparisons with independently extracted sets of clusters, support this figure. The careful reader may have noticed that the total number of objects in this sample has

[2]An earlier pioneering attempt in this direction was the Muenster Redshift Project, which used objective-prism spectra to collect low-resolution redshifts for a few hundred thousand galaxies (see e.g. Schuecker et al. 1996).

been reduced by 15 since the time of writing our previous *Messenger* report. This is the result of the ongoing process of final identification and redshift measurement: spectroscopy and detailed deblending of X-ray sources have led to a reclassification of 15 X-ray sources which either had AGN counterparts or fell below the flux limit. With these new numbers, as of today 95% of the 460 candidates in this sample are confirmed and observed spectroscopically. Final clearing up and measurement of redshifts for the remaining $\sim$ 20 candidates is foreseen for a forthcoming observing run next May. In the following, we shall simply refer to this complete sample as the "REFLEX sample". The distribution on the sky of the REFLEX clusters defined in this way is shown in Figure 2.

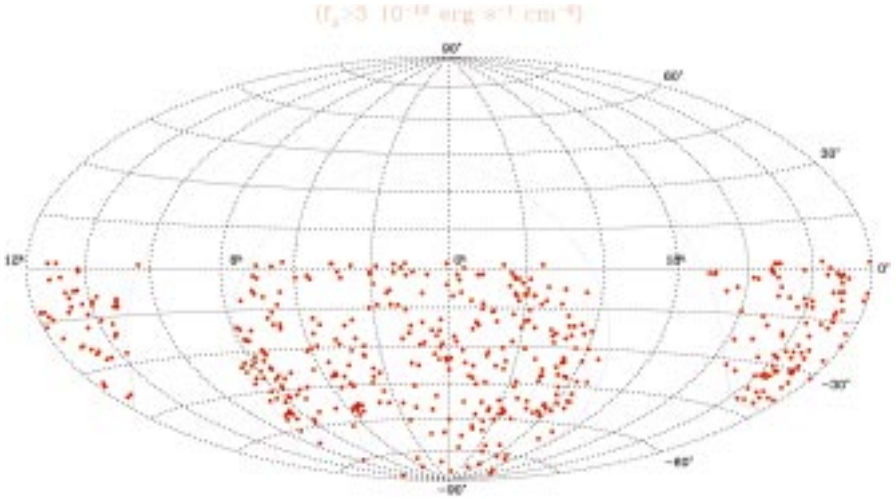

Figure 2: The distribution on the sky of the clusters in the REFLEX sample with $f_X \geq 3 \times 10^{-12}$ erg s^{-1} cm^{-2}. Note that the area around the Magellanic Clouds ($\alpha \sim 1^h$ and $\sim 5^h$, $\delta \sim -70°$), is not included in the survey.

3. Optical Follow-up Observing Strategy

The follow-up optical observations of REFLEX clusters were started at ESO in 1992, under the status of a Key Programme. The goal of these observations was twofold: (a) obtain a definitive identification of ambiguous candidates; (b) obtain a measurement of the mean cluster redshift.

First, a number of candidate clusters required direct CCD imaging and/or spectroscopy to be safely included in the sample. For example, candidates characterised by a poor appearance on the Sky Survey IIIa-J plates, with no dominant central galaxy or featuring a point-like X-ray emission had to pass further investigation. In this case, either the object at the X-ray peak was studied spectroscopically, or a short CCD image plus a spectrum of the 2–3 objects nearest to the peak of the X-ray emission was taken. This operation was preferentially scheduled for the two smaller telescopes (1.5 m and 2.2 m, see below), and was necessary to be fully sure of keeping the completeness of the selected sample close to the desired value of 90%. In this way, a number of AGN's were discovered and rejected from the main list.

Once a cluster was identified, the main scope of the optical observations was then to secure a reliable redshift. The observing strategy was designed so as to compromise between the desire of having several redshifts per cluster, coping with the multiplexing limits of the available instrumentation, and the large number of clusters to be measured. Previous experience on a similar survey of EDCC clusters (Collins et al. 1995) had shown the importance of not relying on just one or two galaxies to measure the cluster redshift, especially for clusters without a dominant cD galaxy. EFOSC1 in MOS mode was a perfect instrument for getting quick redshift measurements for 10–15 galaxies at once, but only for systems that could reasonably fit within the small field of view of the instrument (5.2 arcmin in imaging with the Tektronics CCD #26, but less than 3 arcmin for spectroscopy in MOS mode, due to hardware/software limitations in the use of the MOS masks). This feature clearly made this combination useful only for clusters above $z = 0.1$, i.e. where at least the core region could be accommodated within the available area.

The other important aspect of using such an instrumental set-up is that in several cases, after removal of background/foreground objects, one is still left with 8–10 galaxy redshifts within the cluster, by which a first estimate of the cluster velocity dispersion can be attempted. This clearly represents further, extremely important information related to the cluster mass, especially when coupled to the X-ray luminosity available for all these objects.

At smaller redshifts, doing efficient multi-object spectroscopy work would have required a MOS spectrograph with a larger field of view, i.e. 20–30 arcminutes diameter. One possible choice could have been the fibre spectrograph Optopus (Avila et al. 1989), but its efficiency in terms of numbers of targets observable per night was too low for covering several hundred clusters as we had in our sample. The best solution in terms of telescope allocation pressure and performances was found in using single-slit spectroscopy and splitting the work between the 1.5-m and 2.2-m telescopes. Clearly, this re-

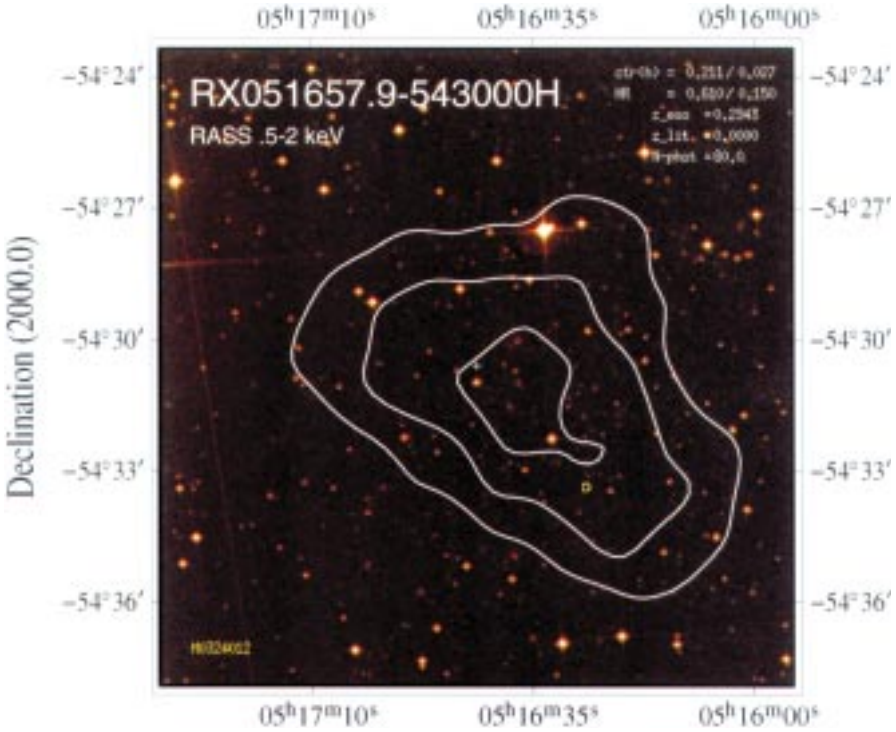

Figure 3: 15 × 15 arcmin identification image of a REFLEX cluster at z = 0.294. The optical image is from the Digitised Sky Survey (DSS), with superimposed the X-ray contours from the RASS. As suggested by the contours, this X-ray source shows a statistically significant extension.

Figure 4: Short CCD exposure (~ 60 sec, no filter) taken with EFOSC1 at the 3.6-m telescope, covering the central region of the REFLEX cluster of previous figure. The field side is 5.2 arcmin. Note the remarkable glory of faint galaxies around the central brightest members. The numbers indicate the positions of the slitlets for the MOS observations.

quired accepting some compromise in our wishes of having multiple redshifts, so that at the time of writing about 30% of the clusters observed at ESO have a measure based on less than 3 redshifts. The reliability of these as estimators of the cluster systemic velocity, however, is significantly enhanced by the coupling of the galaxy positions with the X-ray contours: we can clearly evaluate which galaxies have the highest probability to be cluster members. This is another advantage of a survey of X-ray clusters over optically selected clusters. At the time of writing, in about seven years of work, we have observed spectroscopically a total of about 500 cluster candidates, collecting over 3200 galaxy spectra.

Figure 3 shows one example of the identification images, used for the first confirmation of the candidates. These pictures are constructed for all our candidates by combining the Digitised Sky Survey plates of the ESO/SRC atlas (image) and the RASS X-ray data (contours). Although this cluster (RX051657.9-543000), lies at a redshift $z = 0.294$ (close to the redshift identification limit of REFLEX at $z = 0.32$), a sufficient number of galaxies is detected in the optical image even at the depth of the survey plates. This picture gives a clear example of how the X-ray contours "guide the eye" in showing which are the "best" galaxies to be observed. In this case we had a MOS observation, but had we observed only the central two galaxies within the X-ray peak, we would have obtained a correct estimate of the cluster redshift.

The same cluster is then visible in the direct EFOSC1 image of Figure 4. This is a short service exposure (less than one minute), taken in white light as a template for the drilling of the slits on the EFOSC1 MOS mask. The image shows a spectacular abundance of faint galaxies, one of the most impressive cases observed during our survey.

After looking at this latest picture, it is natural to ask what is, for example, the galaxy luminosity function of this cluster, or what are the colours of this large population of faint objects. This is clearly important information, which at the moment, however, is only available for a restricted fraction of REFLEX clusters (Molinari et al. 1998). To cover this aspect, a wide-field imaging campaign is going to commence in the next semester, starting first with those medium-redshift clusters that best match the WFI at the 2.2-m telescope.

4. The Large-Scale Distribution of X-Ray Clusters

The cone diagram of Figure 5 plots the distribution of REFLEX clusters in the South Galactic cap area of the survey, selecting only objects with $z < 0.2$ and $\delta > -55°$, to ease visualisation. One can easily notice a number of superstructures with sizes $\sim 100\ h^{-1}$ Mpc, that show explicitly the typical scales on which the cluster distribution is still inhomogeneous.

This inhomogeneity can be quantified at the simplest level through the two-point correlation function $\xi(s)$, that measures the probability in excess of random of finding a pair of clusters with a given separation (the variable s is used here to indicate separations in redshift space). A preliminary estimate of $\xi(s)$ for the REFLEX sample is shown by the filled circles in Figure 6. The dashed line shows for comparison the Fourier transform of a simple fit to the power spectrum P(k) measured from a subsample of the same data (see Böhringer et al. 1998). The estimates of $\xi(s)$ and P(k) were performed

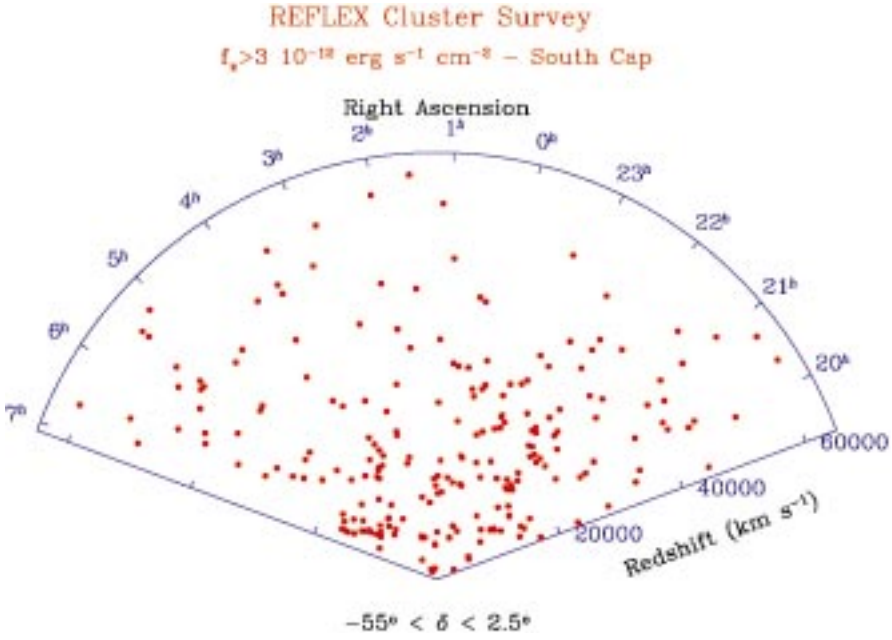

Figure 5: The large-scale distribution of REFLEX clusters within part of the South Galactic cap region. Only objects North of $\delta = -55$ are shown, to avoid excessive confusion by the projection along declination.

by taking into account the angular dependence of the survey sensitivity, i.e., the exposure map of the ROSAT All-Sky Survey, and the NH map of galactic absorption. The good agreement between the two curves is on one hand an indication of the self-consistency of the two estimators applied in redshift and Fourier space. Also, it shows a remarkable stability in the clustering properties of the sample, given that for the measure of P(k) the data were conservatively truncated at a comoving distance of 200 h^{-1} Mpc (Schuecker et al., in preparation), while the estimate of ξ(s) uses the whole catalogue (Collins et al., in preparation). On the other hand, this also indicates that the bulk of the clustering signal on ξ(s) is produced within the inner 200 h^{-1} Mpc of the survey, which is expected because this is the most densely sampled part of the flux-limited sample. We shall explore this in more detail when studying volume-limited samples, with well-defined lower threshold in X-ray luminosity.

Figure 6 shows that ξ(s) for clusters of galaxies is fairly well described by a power law out to 40 h^{-1} Mpc, and then breaks down, crossing the zero value around 50 h^{-1} Mpc. It is interesting to compare it with the two-point correlation function of galaxies, as we do in Figure 7. The galaxy data shown here (points) are obtained from two volume-limited subsamples of the ESP survey (Guzzo et al. 1999). They are compared to ξ(s) from the REFLEX clusters, given by the dashed lines. To ease the comparison, we preferred to plot the curves of ξ(s) as computed from the Fourier transform of P(k). This is given by the top line, while the bottom line has been re-scaled by a factor $b_c^2 = (3.3)^2$ in amplitude. This difference in amplitude, or bias, is expected, as clusters represent the high, rare peaks of the galaxy density distribution, and it can be demonstrated (Kaiser 1984) that their clustering has to be enhanced with respect to that of the general field. This quoted value of b_c, however, does not have a direct physical interpretation, as it is obtained from a flux-limited sample, and thus related to clusters having different mean intrinsic luminosities at different distances. One important aspect of selecting clusters through their X-ray emission is in fact that a selection in X-ray luminosity is closer to a selection in rnass, than if one used a measure like the cluster richness (i.e. the number of galaxies within a given radius and a given magnitude range, as in the case of the Abell catalogue). For this reason, the observation that ξ(s) has a different amplitude for volume-limited subsamples with different X-ray luminosity limits (i.e. a different value of b_e), has important implications for the theory (Mo & White 1996). The validity of a simple biasing amplification mechanism on these scales is explicitly supported by the very similar slopes of ξ(s) shown in Figure 7 by galaxies and clusters. A full discussion concerning the luminosity dependence of the amplitude of the correlation function is being prepared (Collins et al., in preparation).

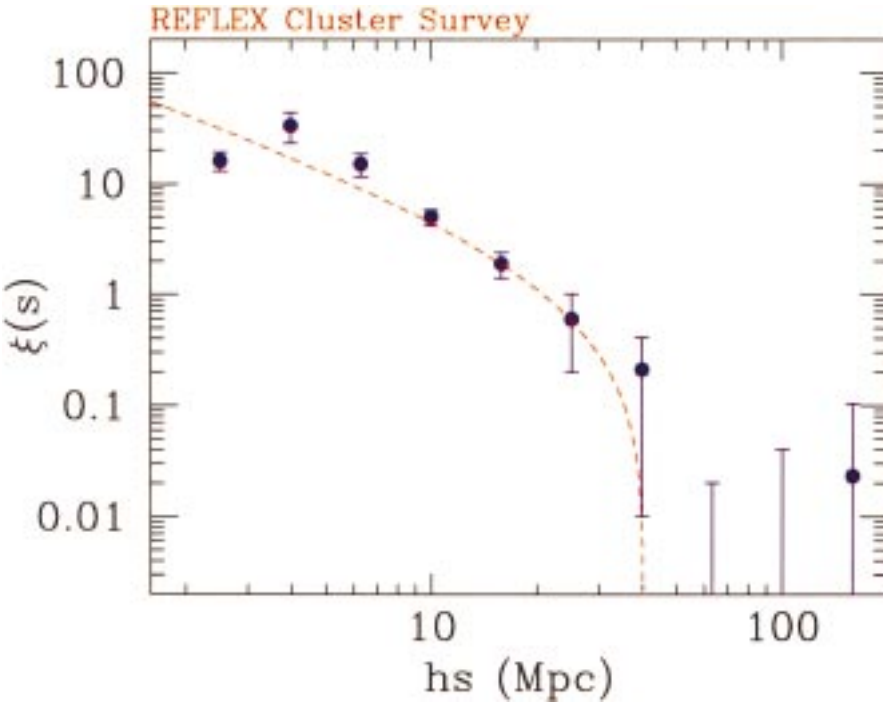

Figure 6: The two-point correlation function of clusters of galaxies in the REFLEX survey. The filled circles give the direct estimate, while the dashed line is computed by Fourier transforming the power spectrum of the survey data, that we showed in Böhringer et al. 1998.

5. Conclusions

We have discussed how after several years of work with the X-ray data from the RASS and with ESO telescopes, the REFLEX project has reached a stage where the first significant results on large-scale structure can be harvested. We hope to have at least given a hint of how the REFLEX survey is possibly the first X-ray selected cluster survey where the highest priority was given to the statistically homogeneous sampling over very large solid angles. This makes it an optimal sample for detecting and quantifying the spatial distribution of the most massive structures in the Universe, as can be appreciated from the high S/N superclusters visible in the cone diagram of Figure 5 out to at least $z \sim 0.1$.

We have also shown how these results have been reached without specially designed instrumentation. Started in May 1992, with the next May run it will be seven years that we have been observing and measuring redshifts for REFLEX clusters. Again, this long timescale is a consequence of the fact that the project is based on "public" instrumentation, and therefore subject to the share of telescope time with the general ESO community. Clearly, even in these terms, this could have never been possible at ESO without the long-term "Key Programme" scheme. In fact, it is exactly for surveys like REFLEX, i.e. large cosmology projects, that the concept of Key Programmes was originally conceived, under suggestion of those few people that at the end of the eighties

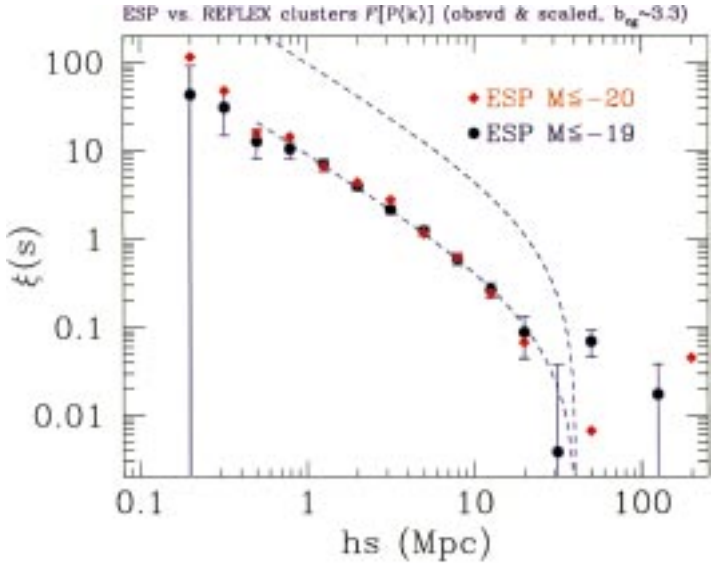

Figure 7: Comparison of the two-point correlation function of REFLEX clusters (top dashed line), to that of ESP galaxies (dots, Guzzo et al. 1999). The bottom dashed line is the REFLEX x(s) after scaling by an arbitrary bias factor of $b_c^2 = (3.3)^2$. The agreement in shape between galaxies and clusters is remarkable.

were starting doing large-scale structure work in continental Europe. If the aim of the Key Programmes was that of making the exploration of the large-scale structure of the Universe feasible for European astronomers, providing them with a way to compete with the dedicated instrumentation of other institutions, we can certainly say that, after ten years, this major goal has probably been reached.

References

Avila, G., D'Odorico, S., Tarenghi, M., & Guzzo, L., 1989, *The Messenger*, **55**, 62.
Böhringer, H. et al., 1998, *The Messenger*, **94**, 21 (astro-ph/9809382).
Chincarini, G., & Guzzo, L., 1998, in *Proc. of V^{eme} Colloque de Cosmologie*, H. De Vega ed., in press.
Colless, M., 1998, Phil. Trans. R. Soc. Lond. A, in press (astro-ph/9804079
Collins. C. A., Guzzo, L., Nichol, R. C., and Lumsden, S. L., 1995, *MNRAS*, **274**, 1071.
Da Costa, L.N., 1998, in *Evolution of Large-Scale Structure: from Recombination to Garching*, T. Banday & R. Sheth eds., in press (astro-ph/9812258).
De Grandi, S., et al., 1999, *ApJ* (Letters), in press (astro-ph/9812423).
Geller, M.J. & Huchra, J.P., 1989, *Science*, **246**, 897.
Guzzo, L., 1999, in *Proc. of XIX Texas Symposium*, (Paris – October 1998), Elsevier, in press.
Guzzo, L., et al. (The ESP Team), 1999, *A&A*, in press (astro-ph/9901378).
Kaiser, N., 1984, *ApJ*, **284**, L9.
Margon, B., 1998, Phil. Trans. R. Soc. Lond. A, in press (astro-ph/9805314).
Mo, H.J., & White, S.D.M., 1996, *MNRAS*, **282**, 347.
Molinari, E., Moretti, A., Chincarini, G., & De Grandi, S., 1998, *A&A*, **338**, 874.
Schuecker, P., Ott, H.-A., & Seitter, W.C., 1996, *ApJ*, **472**, 485.
Shectman, S.A., et al., 1996, *ApJ* **470**, 172.
Vettolani, G., et al. (the ESP Team), 1998, *A&AS*, **130**, 323.

G. Guzzo
guzzo@merate.mi.astro.it

NTT Service Mode Observations of the Lyman-Limit Absorber towards Q1205-30

J.U. FYNBO, B. THOMSEN, P. MØLLER, ESO

1. Introduction

The amount of information about the galaxy population at high redshift (z = 2–4) has increased tremendously in the last few years. Using the Lyman-break technique, several hundred high-redshift star-forming galaxies, Lyman-break galaxies (LBGs), have been detected and studied with imaging and spectroscopy (Steidel et al.,1996). Using the Hubble Space Telescope, detailed morphological studies of the LBGs have been carried out (Dickinson, 1998). It is, however, not yet known how complete the Lyman-break technique is in detecting high-redshift galaxies.

An independent route along which to study the galaxy population at high redshift is via the high column density QSO absorption-line systems. The advantage of high column density QSO absorption-line systems is that a wealth of information on the chemical evolution can be and has been obtained by studying the metallicity and dust content of the absorbers from high-resolution spectroscopic studies of the background QSOs (e.g. Lu et al., 1996). However, the spectroscopic studies will not tell us anything about the emission properties of the absorbing galaxies.

Only when combining the information obtained from the LBG studies (e.g. the luminosity function of LBGs), the absorption-line statistics for QSO absorp-tion-line systems and the properties of galaxy counterparts of QSO absorption-line systems can we hope to disentangle the observational selection biases which each of the different studies suffer from, and obtain a more complete insight into the nature of the high-redshift galaxy population.

We are currently undertaking programmes aimed at identifying galaxy counterparts of the two most gas-rich subgroups of QSO absorption-line systems, Damped Lyα Absorbers (DLAs) and Lyman-limit systems (LLSs). Three out of the five high-redshift DLAs that have been detected in emission at present are at approximately the same redshift as the background QSO. In order to examine whether $z_{abs} \approx z_{em}$ systems indeed are more active emitters (e.g. due to photoionisation by the QSO or induced star formation) we choose to study Q1205-30, since the spectrum of Q1205-30 published by Lanzetta et al. (1991) shows the presence of a strong LLS at the emission redshift of the QSO, which is z_{em} = 3.036.

In this paper we report on preliminary results of our analysis of the data obtained during NTT service observation in January, February and March 1998.

2. Locating Q1205-30

The coordinates of Q1205-30 have not been published (in the paper by Lanzetta et al. (1991) the reference to Q1205-30 is 'Hazard and McMahon, unpublished'). As the coordinates could not be obtained through private communication, we had to 'rediscover' Q1205-30. We found that one way in which this could be accomplished was by obtaining a copy of the prism plate of the area around RA 12^h05^m, DEC –30° from the UK-prism survey. After careful visual inspection of the plate UJ9085P we found a point source with an emission line consistent with being Lyα at $z \approx 3.0$ and measured its approximate coordinates from the plate. By examining the corresponding field in the Digital Sky Survey we measured the precise position of Q1205-30 to be RA 12 05 35.72, DEC –30 14 25.8 (1950).

3. Observations and Data Reduction

We have applied a narrow/broad-band filter technique in several earlier studies of galaxy counter parts of DLAs (e.g. Møller & Warren, 1993, Fynbo, Møller & Warren, 1999). This method is extremely well suited towards service observations since it requires many long integrations of the same field on the sky during dark time. We hence submitted a proposal for and obtained NTT service mode time to image the field of Q1205-30 using a special 20 Å (FWHM) narrow filter centred at 4906 Å which is the wavelength of redshifted Lyα, and in standard B and I filters. The data were obtained during January, February and March, 1998. The total integration times in each filter and the seeing in each of the combined frames are given in Table 1.

Also observed were two standard star fields from Landolt (1992) and the three spectrophotometric standard stars Eggr99, Feige 56 and L970.

The individual reduced images in each of the three filters were combined using the code described in Møller and Warren (1993), which optimises the signal-to-noise for faint objects. We reach 5σ limiting magnitudes of 26.0 in B(AB), 25.1 in I(AB) and 25.1 in the narrow band. At z = 3.036 a narrow-band AB magnitude of 25.1 corresponds to a Lyα flux of 1.0×10^{-17} ergs^{-1} cm^{-2}.

4. Results

4.1 The neighbourhood of Q1205-30

Figure 1 shows the result of the subtraction of the point-spread function (PSF)

Table 1: Journal of observations, NTT, 1998

Filter	Combined seeing (arcsec)	Exposure Time (sec)
CS 4906/20	1.4	64000
B	1.3	3600
I	0.96	5600

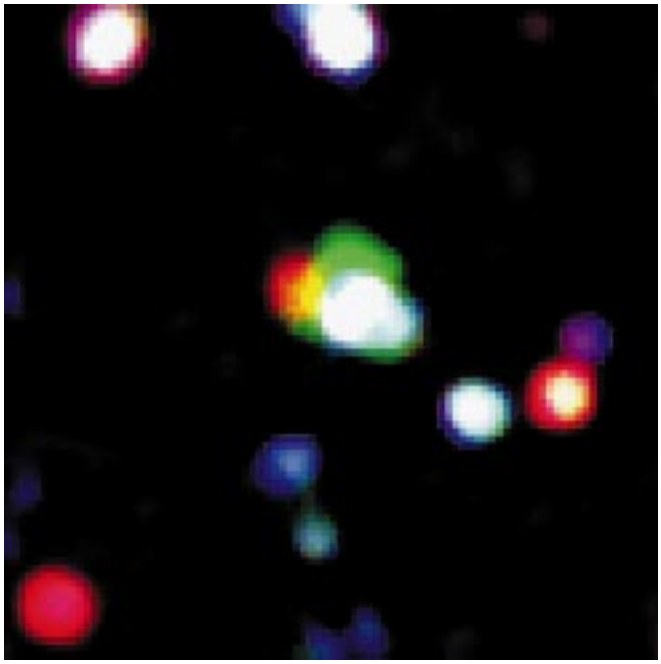

Figure 1: A composite colour image showing a 90 × 90 pixels, 32 × 32 arcsec^2, region surrounding Q1205-30. The colour coding is red (I-band), blue (B-band) and green (narrow-band). 95% of the QSO-flux has been subtracted in each filter in order to reveal excess emission close to the QSO line of sight. North is up and east is to the left.

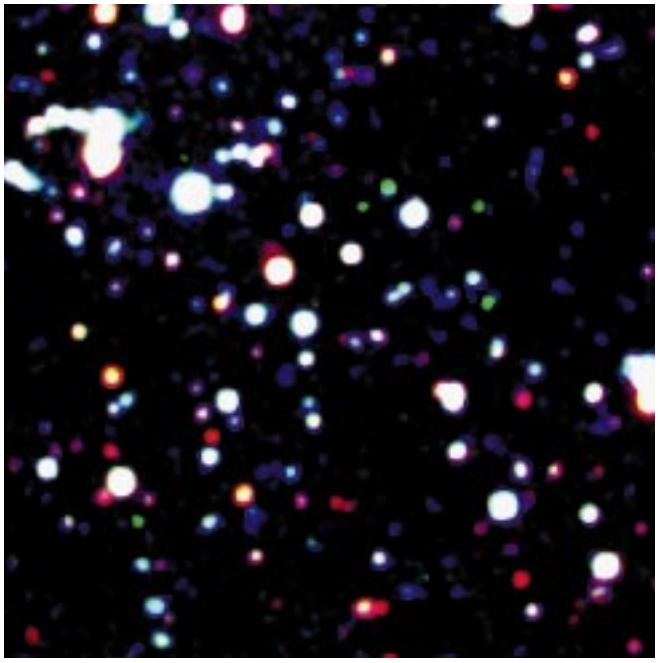

Figure 2: A composite colour image showing a 350 × 350 pixels, 123 × 123 arcsec^2, region containing a group of 5 candidate Lyα emission-line galaxies 70–150 arcsec west of Q1205-30. The colour coding is red (I-band), blue (B-band) and green (narrow-band). North is up and east is to the left. The emission-line galaxies are the green objects north-west of the centre and in the lower east corner. Q1205-30 is located about 120 arcsec east and outside this frame.

of Q1205-30 in the I-band. Seen is a red galaxy 3 arcsec east of the QSO, a fainter blue galaxy 2 arcsec west of the QSO and most importantly excess emission in the narrow band north of the QSO (green fuzz).

4.2 Lyα emitters in the field

In order to pick out galaxies in the field associated with the QSO/absorber system with Lyα line emission, we performed photometry in the three bands using the photometry package SExtractor (Bertin & Arnout, 1996). 473 galaxies were detected with a signal-to-noise ratio (SN) > 5 in the narrow band. Figure 3 shows the two-colour diagram *n(AB) – B(AB)* versus *n(AB – I (AB)* for these objects. Five galaxies with strong excess emission in the narrow-band filter compared to the B-band filter were found at separations from 80 to 150 arcsec west of Q1205-30. These five galaxies are shown in Figure 2. The Lyα fluxes range from 1.1×10^{-17} ergs^{-1} cm^{-2} to 4.0×10^{-17} ergs^{-1} cm^{-2}. Q1205-30 has a slight excess emission in the narrow-band filter compared to B. The weakness of this excess emission is the result of the blue wing of the Lyα emission line of the QSO being absorbed partly by the Lyman limit absorber.

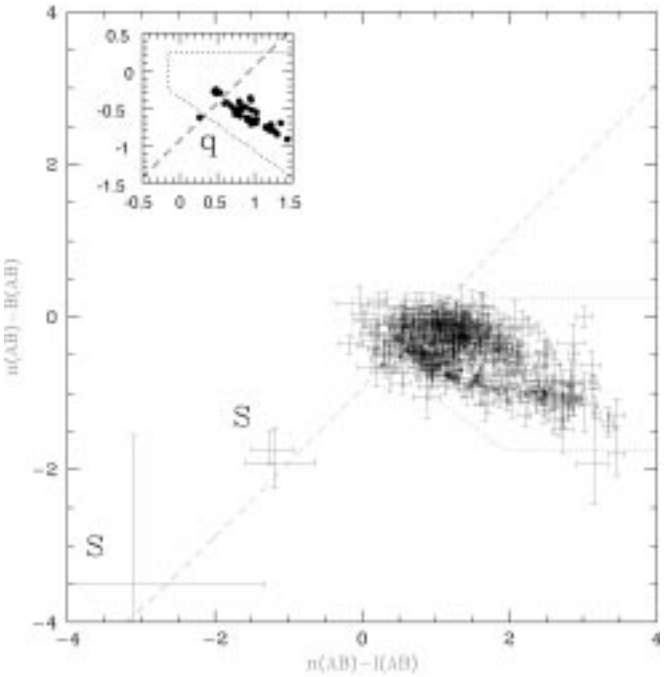

Figure 3: Two-colour diagram n(AB)—B(AB) versus n(AB)—I(AB) for objects detected with SN in the narrow-band frame > 5. The dashed line is a line of constant B – I in the continuum (chosen to be that of Q1205-30), but with a spectral feature in the narrow filter ranging from a strong absorption line in the upper right-hand corner to a strong emission line in the lower left-hand corner. Three of the five candidate emission-line galaxies are seen in the lower left corner (marked S). The remaining two are detected in neither B nor I. The dotted lines confine the expected region of objects with no special features in the narrow filter. The inserted diagram shows a blow up of the region of the plot containing Q1205-30 (marqued q) and objects with SN > 30.

5. Future Work

We need to perform spectroscopic follow-up observations in order to confirm the redshifts of the candidate emission-line galaxies and the three sources close to the QSO line of sight.

Acknowledgements

We wish to thank the NTT service observation team for providing us with these excellent data. J.U.F. wishes to thank the UK Schmidt Telescope Unit for generous help in the effort of locating Q1205-30.

References

Bertin E, Arnouts S. 1996, *A&AS*, **117**, 393B.
Dickinson M, 1998, preprint, astro-ph/980264.
Fynbo J. U, Møller P., Warren S. J., 1999, *MNRAS*, in press.
Landolt A.U., 1992, *AJ*, **104**, 340.
Lu L., Sargent W.L.W., Barlow T.A., Churchill C.W., Vogt S.S., 1996, *ApJS*, **107**, 475.
Møller P., Warren S., 1993, *A&A*, **270**,43.
Steidel C.C, Giavalisco M., Pettini M, Dickenson M., Adelberger K.L., 1996, *ApJL*, **462**, L17.

J.U. Fynbo (jfynbo@eso.org)

This month – March 1999 – sees the 90th anniversary of the first expedition in northern Chile to search for a good site for an astronomical observatory: the Curtis expedition.

Halfway from La Silla to Paranal – in 1909

H.W. DUERBECK [1, 3], D.E. OSTERBROCK [2], L.H. BARRERA S. [3] and R. LEIVA G.[4]

[1]Brussels Free University (VUB), Belgium; [2]Lick Observatory, University of California, Santa Cruz, California, USA; [3]Instituto de Astronomía, UC del Norte, Antofagasta, Chile; [4]Facultad de Ciencias, Universidad de Atacama, Copiapó, Chile

1. Prelude

Chile's national observatory was founded in 1852, with instruments left by the United States Naval Astronomical Expedition (1849–1851). Its head, Lt. James M. Gilliss, had set up its 16.5-cm refractor and a meridian circle on Cerro Santa Lucia, a hill in the middle of Santiago, to measure positions of Venus, Mars and southern stars, to improve the solar parallax (Gilliss 1855, Keenan et al. 1985).

A German scientist, Carl (Carlos) W. Moesta, became the first director of the new Observatorio Nacional, which had by then moved to downtown Santiago. He held this position until 1865 when he returned to Europe to become the Chilean consul in Dresden. His successor as director was his former assistant, José Vergara. After Vergara died in 1889, his assistant, Hubert (Huber) A. Obrecht, an Alsatian trained at the Paris Observatory, became director. He drifted more and more into teaching, and did little observing. Then Pedro Montt, a new president of Chile who was personally interested in astronomy, appointed the German Friedrich (Federico) W. Ristenpart as the new director, charged with reorganising the observatory. He took over at the end of 1908.

Meanwhile, in 1903, Lick Observatory established an observing station on Cerro San Cristobal, then near the outskirts of Santiago (Osterbrock et al. 1988). At Mount Hamilton, the new Lick director, William W. Campbell, had already begun a pioneering radial-velocity programme, which he realised required all-sky coverage. From Darius O. Mills, a California and New York banker, he obtained the funds to build a 0.94-m reflecting telescope and spectrograph, optimised for this programme, and to erect it in the southern hemisphere. This telescope remained in operation under Lick auspices until 1928, and more than ten thousand radial-velocity spectrograms were obtained with the Mills spectrograph there (Osterbrock 1984). A report on the more recent state of the San Cristobal Observatory can be found in a previous *Messenger* article (Sterken and Vogt 1982).

The first Lick astronomers to go to Chile were William H. Wright and his assistant, Harold K. Palmer. Heber D. Curtis, a professor of Greek and Latin turned astronomer, and Campbell's assistant at Lick Observatory since 1902, replaced Wright in charge of the southern station in 1906. He was to stay in Chile for three years. George F. Paddock, a University of Virginia graduate student, succeeded Palmer, also in 1906. During Curtis's term in Chile, Ristenpart took over as director of the National Observatory. In 1909 he offered Curtis a position as head of "astrophysics" (spectroscopy), but the American astronomer decided to return to Lick instead.

Just as Curtis was ending his term in Chile, Ristenpart's two new assistants, Richard Prager and Walter Zurhellen, arrived from Germany. They had been appointed to head the "Section of Calculations" and the "Section of Astrophotography", respectively. (After Curtis declined it, the "Astrophysics" position was never filled in Ristenpart's time.) Joseph H. Moore, sent down from Lick to relieve Curtis, reached Santiago a few weeks later; a rare photograph documents this early meeting of North American and European astronomers on Chilean soil (Fig. 1).

Figure 1: Lick and Observatorio Nacional astronomers at Lick Southern Hemisphere Station, June 1909. Standing, left to right, W. Zurhellen, F. W. Ristenpart, R. Prager; seated, H.D. Curtis, J.H. Moore, G.F. Paddock (Shane Archives).

Figure 2: Section of a map of the region of Copiapó, issued in 1909, at the time of Curtis's trip. The railway Caldera–Copiapo–Puquios runs from west to east. The north-south railroad system "Longitudinal", also depicted here, was under construction. Curtis's favourite site is in the upper right corner of the map, in the Llano de Varas (marked Llano), next to the railroad station "Carrera Pinto" (see Fig. 4). Of the many mines shown, only Dulcinea is still operating.

The fate of the European astronomers in the picture was a sad one. In 1912 Zurhellen resigned because of personal problems with his director. He joined the staff of Berlin-Babelsberg Observatory, only to be interned while on a solar eclipse expedition to Russia in 1914, just after the outbreak of World War I. Released a year later, he was killed in action in France in 1916. Ristenpart encountered more and more obstacles with the Chilean authorities. He knew his appointment would not be renewed, and became so frustrated that he committed suicide in 1913. The National Observatory, which under his directorship had moved from the downtown Quinta Normal to the southern suburb of Lo Espejo, remained there till the early 1950s, when it was moved to its present location on Cerro Calan. Prager, Ristenpart's faithful assistant, also went to Berlin-Babelsberg, where he remained for twenty-five years, preparing and editing a monumental variable-star bibliography. In the Nazi era he was forced to leave Germany and emigrated to the United States, where he found a position at Harvard College Observatory. He died there in 1945.

Curtis went back to Lick in 1909 to take charge of the 0.9-m Crossley reflector, to continue the survey of nebulae that James E. Keeler had begun. Curtis came to realise, from the direct photographs he obtained with it, that the spiral "nebulae" were really "island universes", or galaxies as we say, composed of stars, real nebulae, and "occulting matter" (dust), responsible for the dark lanes seen especially well in edge-on spirals like NGC 891 and in our Milky Way. He left Lick Observatory in 1920 to become director of Allegheny Observatory at the University of Pittsburgh. Ten years later he moved on to the University of Michigan, his alma mater, as director of its observatory (McMath 1942; Aitken 1943). Curtis is best known today as a participant in the "Great Debate" with Harlow Shapley, which took place at a meeting of the National Academy of Sciences in 1920. While Shapley was closer to right about the true size of the Milky Way, Curtis was correct in his concept of the Milky Way as a galaxy, and of the nature of spiral "nebulae".

2. The Curtis Report

Before deciding to locate the Lick station in Santiago, Campbell had considered possible sites in Australia, but the available climatic records and all the reports he obtained from astronomers indicated that Chile would be better for observing. He had decided to erect the Lick station in or near Santiago, where supplies, living quarters, food, and other necessities were readily available. In the early 1900s light pollution was not yet much of a problem, particularly with the slow photographic plates of those days which made spectrograms of sixth-magnitude stars the limit of convenient exposure times. But Campbell told Wright and then Curtis to collect information from travelling businessmen, mining engineers, and ranch owners on conditions elsewhere in the country where more clear weather might be expected. All three of them were well aware of the climatic analogies between California and Chile, both with high mountain ranges near their Pacific coasts. Wright, within a few weeks of his arrival, was already writing Campbell about the "land of little rains" around Copiapó to the north, more or less equivalent to San Diego and Baja California in the northern hemisphere. Curtis, who became well integrated into the Chilean community, learned much more about these regions and Campbell directed him to make a brief reconnaissance of the most promising area before returning to Lick. At that time, Campbell was considering sending visual double-star observer Robert G. Aitken to the southern hemisphere also, with a 0.6-m refractor, to complete his survey of the entire sky. Curtis's 22-page typed report on his hurried site survey, illustrated with photographs he took, still exists in the Mary Lea Shane Archives of the Lick Observatory.

It is interesting to compare Curtis's requirements with those of today. Of course, a good site had to be in a region with a clear climate, uninfluenced by the coastal fog and clouds. It had to have a good seeing and be somewhat shielded from bad storms. But it also had to be reasonably accessible in a period when cars were rare and airlines unknown. And it needed to have a supply of water, living supplies, and electricity. Curtis travelled by ship from Valparaiso to Caldera, the port of Copiapó. There he took the first Chilean railway, connecting Caldera, Copiapó, and several mining stations further inland (Fig. 2). These stations to the east of Copiapó were higher and beyond the range of the coastal fog. Curtis's first choice as a potential observatory location was a little hill (cerro) in the Varas Plain (Llano de Varas), easily accessible on foot or horseback from the nearest station, sur-

rounded by higher mountains. To our knowledge, this hill has no name; we refer to it as “Cerrito Curtis” in the following.

In his report to Campbell, Curtis (1909) wrote:

Very laudatory reports were given me of the great clearness at Púquios, the northern terminus [of the railway], 143 kilometers from Caldera. I went up there on April 8 [1909]; the trip takes about four hours [from Copiapó] and is up through a barren valley-cañon all the way. I remained there or in the vicinity for three days, till the next train back.

Púquios is the center for a number of copper mines; is a little town of perhaps four hundred inhabitants. It lies in a sandy plain not more than a mile in width and with precipitous mountains rising two or three thousand feet higher to N. and S. Accomodations were very primitive; though this region is almost destitute of flora and fauna large involuntary entomological collections were made. Púquios looks much like some Arizona adobe town stripped of its sage brush surroundings and with higher and more ragged mountains about. It has some small stores, a butcher shop, small drug store and a water supply piped down from the Llano de Varas. [...]

On the 9th I left for the smelter of the Copiapó Mining Co., known here as La Compañia Inglesa de Minas de Copiapó. It is distant about three miles by road from Púquios. The road is quite good, used constantly for mining freight, and an automobile ought not to have any trouble with it. The road passes up through a very narrow cañon to the northeast of the town. [...] Near the end of the Cañon are the mines and houses of la Descubridora. Farther on the cañon debouches into the southern end of the great Llano de Varas, a fine plain some ten miles long by three broad, sloping gently toward the west. It averages about 5200 (by barometer) feet above the sea [...]

The general effect is that of a shallow basin. Mountains not much higher, generally rounded and not precipitous. Some coarse herbage grows in the S. E. corner [. . .]

In the southern end of this plain water is obtained for the mines and for the town of Púquios, probably by seepage from the distant Cordilleras [...] At Posada del Gallo good sweet water is obtained from wells. Mr. W. L. Stevens, M. I. T., is in charge of the smelter and lives here with his family; he uses condensed water, and would furnish same to a station, for drinking purposes only. [...] The Cerro is a small elliptical hill about 200 feet above the plain and 250 above the smelter; it is perhaps 800 feet long and would perhaps furnish a site with sufficient atmospheric drainage [see photograph, Fig. 3]. *Water would have to be brought from Posada del Gallo or from the smelter. All the mines, etc., of this plain are in telephonic communication with Púquios, Copiapó and Caldera, and one telephone line passes almost through Posada del Gallo. The little Cerro is about one mile distant from Posada del Gallo and from the other railroad now in construction, which will reach this spot in five or six months more; this line is planned as a link in the proposed longitudinal railway system [...] Eventually freight can be brought more easily to the western edge of this plain from Copiapó than via Púquios.*

Figure 3: Cerrito Curtis, seen from the east. H.D. Curtis photographed this small, dark hill (to the right of the middle of the picture) and recommended it as a potential observatory site (Shane Archives).

The horizon from the Cerro is good, maybe 5° is cut off at one point at the south. The smelter has a dynamo and might be willing to furnish a small amount of electricity at night.

The night fogs of Copiapó almost never reach here, according to all reports. Not a cloud was visible day or night during my stay here and at Púquios; on all these days fog or cloud was present at Copiapó, coming in at twelve or one o'clock at night; on the day I was at the Llano the clouds were so thick at Copiapó that rain was hoped for and the clouds did not clear way till noon. Wind is generally light at night, sometimes brisk in the days, and almost always either northwest or southeast. In eight months residence Mr. Stevens states that he has on about three occasions seen the sky thickly overcast with clouds; the impression of all with whom I talked is that the overwhelming majority of all days and nights are perfectly clear [. . .]. [I] am inclined to prophecy that a site in the southern end of the Llano de Varas would average 300 clear nights per year.

[. . .] Best location, in my opinion, [is] the small cerro [. . .]. Roads across the plain to the railroad at the west or to tap present road from smelter at El Ingenio would need only the scratching away of a few loose rocks, as the hard plane can be traversed in any direction. A road up the cerro not long nor hard to make, as the slope is easy. Good horizons, and sufficiently far from smelter so as not to be disturbed by its smoke. About one mile from wells of sweet water; for a permanent station might pay to drive a well, as there is evidently water under this plain. About one mile from the railroad from Chulo, so that it would be easier to use this road than to bring in supplies via Púquios [...]

The sky at the Llano impressed me as very blue and pure; no whitening toward the horizon. The night sky at Copiapó about as usual; at Púquios very transparent and clear.

Three of us used Curtis's description and maps to identify it on the spot in 1997. About Púquios, the booming mining town of 1909, the modern tourist guide says: “at km 59 and 60 you can see the ruins and the graveyard of Púquios”. Nowadays, the Llano de Varas is more easily accessible over the well-paved route 51, connecting Copiapó and Diego de Almagro in the north. A road branches off to Carrera Pinto, and after a few hundred metres, one can see from the distance the southern end of the plain and a few hills, the most prominent being Cerrito Curtis, being at 69°55.27′ W. 27°6.31′ S, altitude 1760 m (Figs. 3 and 4). Our pickup truck could not get to the top, and we had to walk up the last 100 m on foot. From the top of the hill there is a marvellous view into the multicoloured, barren Llano de Varas stretching to the north, and the rugged mountains that surround it from the east through south to the west. Traces of mines and the ruins of the smelter can be seen; a few people still live in the mine near the railroad station Carrera Pinto (Fig. 4), and in the tiny hamlet, La Posada.

Although Cerrito Curtis was without doubt a better site than San Cristóbal, Curtis advised Campbell that he and his assistant were getting more clear nights there than they could use effectively, and that unless several more observers were sent down there would be no point in moving the Lick station. It would be much

Figure 4: Cerrito Curtis, seen from the west. The buildings to the right are the railroad station Carrera Pinto (in the NE corner of Fig. 2). The hill is seen as a small brownish elevation, in front of the higher mountain range, between the road sign in the middle and the telephone pole at left.

more expensive to supply the desert site, and few educated people, especially astronomers with families, would consider living there for years. A move would have been costly; Mills, the prospective donor, died in early 1910, and Campbell never succeeded in raising the money to send Aitken south with a refractor. Curtis's report was filed and almost forgotten. The Lick radial-velocity station remained on Cerro San Cristóbal until it was bought, in 1928, by Manuel Foster and donated to the Universidad Católica de Chile.

3. The Aftermath

The Lick experience was important when planning began for the large European and American southern-hemisphere observatories in the 1950's. Although Curtis's report languished in the files, Lick astronomers knew of the excellent observing conditions in Chile, and Walter Baade, a strong proponent of the ESO idea, had become well aware of them by word of mouth. In correspondence and certainly also in talks with Jan Oort, he insisted that the Europeans not rush into South Africa before carrying out serious site tests in Chile (Osterbrock 1998). But only after AURA had cast their dice for a Chilean mountaintop in the early sixties, ESO, with detailed climatological data of several South African sites at hand, changed its mind almost "at the last moment". ESO's earliest Chilean site tests of 1962 focussed on the mountain La Peineta (about 40 km north-east of Cerrito Curtis), as well as on two mountaintops in the neighbourhood of Cerro Tololo, near La Serena. In 1964, La Silla was chosen as the site for the European Southern Observatory (Blaauw 1991).

The observatories La Silla, Cerro Tololo and Las Campanas were erected in the mountains north and east of La Serena. These sites are about halfway from Santiago to the Llano de Varas; it in turn is about halfway from La Silla to Cerro Paranal and the VLT, as well as to Cerro Armazones where the observing station of the Universidad Católica del Norte is located. The whole region is still as clear, as dry, and probably even more deserted than it was when Curtis saw "his" Cerrito and envisioned an observatory ninety years ago.

We are grateful to A. Blaauw for his helpful comments on the manuscript, to the Mary Lea Shane Archives of the Lick Observatory, University Library, University of California, Santa Cruz, for permission to quote from Curtis's report, and to reproduce the three early photographs from its collection. H.W.D. acknowledges support from the German Academic Exchange Service (DAAD) which made his stay in Chile possible.

References

Aitken, R. G., 1943, Heber Doust Curtis, 1872–1942, *Biog. Memoirs Nat. Acad. Sci.*, **22**, 275.

Blaauw, A., 1991, *ESO's Early History*, European Southern Observatory, Garching.

Curtis, H.D., 1909, Report on Astronomical Conditions in the Region about Copiapo. Typewritten manuscript, dated April 17, 1909, in the Mary Lea Shane Archives of the Lick Observatory, University Library, University of California, Santa Cruz, CA., USA.

Gilliss, J.M. 1855, The U.S. Naval Expedition to the Southern Hemisphere, Vol. I. Washington: A.O.P. Nicholson (Printer); House of Representatives, 33d Congress, 1st Session, Ex. Doc. No. 121.

Keenan, P.C., Pinto, S., Alvarez, H., 1985, The Chilean National Astronomical Observatory (1852–1965), Facultad de Ciencias Físicas y Matemáticas, Universidad de Chile.

McMath, R.R., 1942, Heber Doust Curtis. *PASP* **54**, 69.

Osterbrock, D.E., 1984, James E. Keeler, Pioneer American Astrophysicist. Cambridge University Press, Cambridge.

Osterbrock, D.E., Gustafson, J.R., Unruh, W.J.S. 1988, Eye on the Sky: Lick Observatory's First Century, University of California Press, Berkeley.

Osterbrock, D.E. 1998, Walter Baade, *Observational Astrophysicist* (3): Palomar and Göttingen, 1948–1960 Part B. JHA **29**, 345 (see esp. 363 and note 120).

Sterken, C., Vogt, N. 1982, Radial Velocity Observations with the 36″ Telescope at Cerro San Cristobal, Santiago, Chile, *The Messenger* **28**, 12.

Hilmar W. Duerbeck <duerbeck@stsci.edu>
Don Osterbrock <don@ucolick.org>

Figure 5: Three of the authors on top of Cerrito Curtis (from left to right: R. Leiva, L.H. Barrera, H.W. Duerbeck).

The Questionnaire Survey for “La Silla 2000+”

B. NORDSTRÖM, Chair, ESO Users Committee

First, I wish to thank the many colleagues who have spent time and effort on answering the “Questionnaire on the Future of the La Silla Facilities 1999–2006”. I am happy to report that we received 254 answers, about twice as many as four years ago, when a similar survey was initiated. This is a very gratifying response, which testifies to the great interest in the future of La Silla in the community and lends important support to the recommendations we will prepare.

From the diagrams below you can see the distribution in age and nationality of those who contributed answers to the questionnaire. It is particularly noteworthy and encouraging that so many young colleagues submitted replies. There is also a well-balanced representation of answers from all Member States, Chile, and the ESO staff.

We are well aware that some people had difficulties submitting the questionnaire through the ESO Web server and apologise to those who did not succeed. To compensate for this, an email version of the form was provided and used by some.

A joint STC/UC/ESO Working Group will prepare a summary report and a set of recommendations, which will be presented to the Director General and eventually to the ESO Council. This WG consists of G. Burki, A. M. Lagrange, S. Ortolani, J. Melnick, and G. Monnet and is chaired by the writer.

The WG had its first meeting on February 4, 1999, and is now hard at work to take into consideration all the constructive and thoughtful comments about future instrumentation and science to be conducted at La Silla.

On behalf of the WG, I wish to thank all the colleagues who submitted replies, as well as the ESO REMEDY team who have been very helpful during the planning, execution, and analysis of the survey.

birgitta@astro.ku.dk

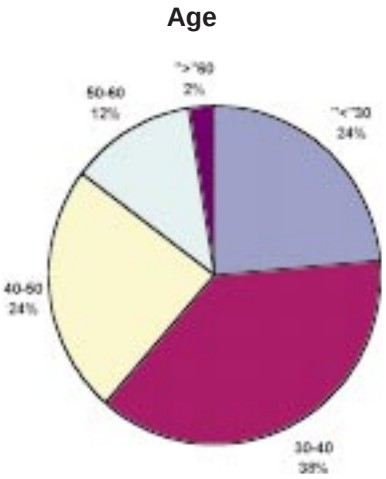

Figure 1: Distribution of ages.

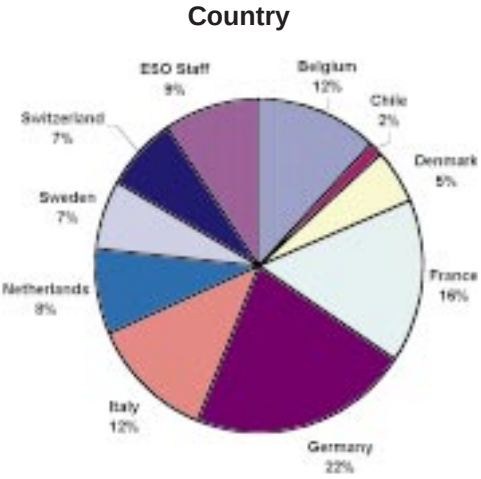

Figure 2: Distribution of nationalities.

ANNOUNCEMENTS

Catherine Cesarsky – ESO’s Next Director General

The ESO Council has appointed Dr. Catherine Cesarsky as Director General for a five-year period, succeeding Professor Riccardo Giacconi, whose term ends this year. Dr. Cesarsky will take up her duties on September 1, 1999, at the ESO Headquarters in Garching (Germany).

Dr. Cesarsky was born in France in 1943. She received a degree in Physical Sciences at the University of Buenos Aires and graduated with a PhD in Astronomy in 1971 from Harvard University (Cambridge, Mass., USA). Afterwards she worked at the California Institute of Technology (CALTECH).

In 1974, she became a staff member of the Service d’Astrophysique (SAp), Direction des Sciences de la Matière (DSM), Commissariat à l’Energie Atomique (CEA) (France). She headed the theoretical group of the SAp (1978–1985), was Head of SAp (1985–1993) and has been Director of DSM since 1994. The DSM encompasses, at the CEA, activities of basic research in physics, chemistry, astrophysics and earth sciences and comprises about 3000 scientists, engineers, technicians, etc.

Dr. Cesarsky is known for her successful research activities in several central areas of modern astrophysics. The first part of her career was devoted to the high-energy domain. This has involved studies of the propagation and composition of galactic cosmic rays, of matter and fields in the diffuse interstellar medium, as well as the acceleration of particles in astrophysical shocks, e.g. in connection with supernovae.

She then turned to infrared astronomy. She is the Principal Investigator of the ISOCAM camera onboard the Infrared Space Observatory (ISO) of the European Space Agency (ESA) and, as such, she leads the ISOCAM central programme. It studies, in a co-ordinated way, the infrared emission from a variety of galactic and extragalactic sources and is yielding new and exciting results on star formation and galactic evolution.

Dr. Cesarsky received the COSPAR (Committee on Space Research) Space Science Award in 1998.

She is a member of many national and international associations and organisations within physics, astrophysics and space sciences, and of related working groups and committees. She has assumed several chairs and presidencies in these, e.g., as Vice-President of the ESO Council and of the European Astronomical Society (EAS), and Chairperson of ESO's Observing Programmes Committee. She is Vice-President of the International Astronomical Union (IAU) since 1997. She has also been Editor-in-Chief of the European journal Astronomy & Astrophysics.

She is married and has two children.

(ESO Press Release 01/99 – 8 January 1999)

ESO Studentship Programme

The European Southern Observatory research student programme aims at providing the opportunities and the facilities to enhance the post-graduate programmes of ESO member-state universities by bringing young scientists into close contact with the instruments, activities, and people at one of the world's foremost observatories. For more information about ESO's astronomical research activities please consult Research Projects and Activities (*http://www.eso.org/projects/* or *http://www.eso.org/science/*).

Students in the programme work on an advanced research degree under the formal tutelage of their home university and department, but come to either Garching or Vitacura-Santiago for a stay of up to two years to conduct part of their studies under the supervision of an ESO staff astronomer. Candidates and their national supervisors should agree on a research project together with the potential ESO local supervisor. This research programme should be described in the application and the name of the ESO local supervisor should also be mentioned. It is highly recommended that the applicants start their Ph.D. studies at their home institute before continuing their Ph.D. work and developing observational expertise at ESO.

The ESO studentship programme comprises about 14 positions, so that each year a total of up to 7 new studentships are available either at the ESO Headquarters in Garching or in Chile at the Vitacura Quarters. These positions are open to students enrolled in a Ph.D. programme in the ESO member states and exceptionally at a university outside the ESO member states.

The closing date for applications is June 15, 1999.

Please apply by using the ESO Studentship application form now available on-line (*http://www.eso.org/gen-fac/adm/pers/forms/*)

European Southern Observatory
Studentship Programme
Karl-Schwarzschild-Str. 2, 85748 Garching bei München, Germany
ksteiner@eso.org

PERSONNEL MOVEMENTS

International Staff

(1st January 1999 – 31st March 1999)

ARRIVALS

EUROPE

BOITQUIN, Olivier (B), Data Analysis Specialist
KERBER, Florian (A), Instrument Scientist
WOLF, Sebastian (D), Scientific Applications Developer for UVES
ROGON, Thomas (DK), Scientific Applications Developer for IR Imaging
LOCKHART, John (UK), Database Administrator
LOMBARDI, Marco (I), Student
SPOON, Henrik (NL), Student

CHILE

MOUTOU, Claire (F), Fellow Santiago/Paranal

DEPARTURES

EUROPE

ANGELONI, Elisabetta (I), Software Engineer
VEROLA, Massimo (I), Software Engineer
LARTEY, Kathrin (D), Personnel Officer
RIGAUT, Francois (F), Head, Adaptive Optics Group
RAVENSBERGEN, Martin (NL), Electronics Engineer
BARZIV, Orly (GR), Student,
BERNARDI, Mariangela (I), Student

CHILE

GITTON, Philippe (F), Optical Engineer
PERSSON, Glenn (S), Software Engineer, SEST

Local Staff (Chile)

(1st July 1998 – 28th February 1998)

ARRIVALS

MATHIEU, Michelle, Administrative Secretary, 7/1/98
EHRENFELD, German, Mechanical Engineer, 7/9/98
NIEVAS, Hernan, Electrónic Technician, 7/13/98
VARAS, Humberto, Safety Engineer, 7/20/98
GUTIERREZ, Pablo, Electronic Engineer, 8/10/98
BARRIGA, Pablo, Electronic Engineer, 9/7/98
IBAÑEZ, Patricio, Optical Instrumentation Engineer, 10/5/98
VALLEJO, Karen, Administrative Secretary, 10/6/98
MORALES, David, Accounting Clerk, 10/13/98
FISCHMANN, Nicolas, Logistics & Procurement Officer, 11/23/98
PAZ, Magda, Application Programmer, 12/1/98
SCHEMRL, Anton, Data Handling Administrator, 12/1/98
SILVA, Soledad, Executive Bilingual Secretary, 12/1/98
MORENO, Nicolas, Telescope Instrument Operator, 12/4/98
LAGARINI, Andrea, Executive Bilingual Secretary, 12/7/98
MENA, Alejandra, Executive Bilingual Secretary, 12/7/98
JARA, Maria Fca., Bilingual Secretary, 12/21/98
OSORIO, Maria Isabel, Technical Secretary, 1/1/99
GONZALEZ, Andres, Telescope Instruments Operator, 1/1/99
WENDEROTH, Erich, Telescope Instruments Operator, 1/1/99
GARCIA, Enrique, Electronics Technician, 2/22/99

DEPARTURES

GODOY, Angela, Bilingual Secretary, 7/30/98
PIZARRO, Oscar, Night Assistant, 7/30/98
ROJAS, Norman, Driver, 9/15/98
RODRIGO, Manuel, Scient. Inst. Oper. / Night Assistant, 9/15/98
REYES, Oscar, Software Project Manager, 9/30/98
RIVERA, Andres, Detector Engineer, 10/30/98
CORRALES, Esperanza, Bilingual Secretary, 10/30/98
GUERRA, Carlos, Precision Mechanic , 12/3/98
PIZARRO, Guido, Night Assistant, 12/23/98
ROSAS, Alfredo, Car Mechanic, 12/30/98
MONTES, Lucia, Bilingual Secretary, 1/12/99,
MARIN, Hector, Draftsman, 2/28/99,

List of Scientific Preprints

(January–March 1999)

1313. E. Brocato et al.: Predicted HST FOC and Broad Band Colours for Young and Intermediate Simple Stellar Populations. *A&A.*
1314. H.U. Käufl et al.: Thermal Infrared Survey of LMC, SMC and Sagittarius Dwarf Galaxy. Contributed paper at the IAU Colloquium 192, Capetown, Sept. 7–11, 1998, *The Stellar Content of Local Group Galaxies.*
1315. H. Boehnhardt et al.: The Nuclei of Comets 26P/Grigg-Skjellerup and 73P/Schwassmann-Wachmann 3. *A&A.*
1316. J.Alves et al.: Correlation Between Gas and Dust in Molecular Clouds: L977. *ApJ.*
1317. M. Kürster et al.: Precise Radial Velocities of Proxima Centauri. Strong Constraints on a Substellar Companion. *A&A.*
1318. L.B. Lucy: Improved Monte Carlo Techniques for the Spectral Synthesis of Supernovae. *A&A.*
Computing Radiative Equilibria with Monte Carlo Techniques. *A&A.*
1319. C. Lidman et al.: The Redshift of the Gravitationally lensed Radio Source PKS 1830–211.

ESO, the European Southern Observatory, was created in 1962 to "… establish and operate an astronomical observatory in the southern hemisphere, equipped with powerful instruments, with the aim of furthering and organising collaboration in astronomy …" It is supported by eight countries: Belgium, Denmark, France, Germany, Italy, the Netherlands, Sweden and Switzerland. ESO operates at two sites. It operates the La Silla observatory in the Atacama desert, 600 km north of Santiago de Chile, at 2,400 m altitude, where fourteen optical telescopes with diameters up to 3.6 m and a 15-m submillimetre radio telescope (SEST) are now in operation. In addition, ESO is in the process of building the Very Large Telescope (VLT) on Paranal, a 2,600 m high mountain approximately 130 km south of Antofagasta, in the driest part of the Atacama desert. The VLT consists of four 8.2-metre and several 1.8-metre telescopes. These telescopes can also be used in combination as a giant interferometer (VLTI). "First Light" of the first 8.2-metre telescope (UT1) occurred in May 1998. UT1 will be available on a regular basis for astronomical observations from April 1999 on. Over 1000 proposals are made each year for the use of the ESO telescopes. The ESO Headquarters are located in Garching, near Munich, Germany. This is the scientific, technical and administrative centre of ESO where technical development programmes are carried out to provide the La Silla and Paranal observatories with the most advanced instruments. There are also extensive astronomical data facilities. In Europe ESO employs about 200 international staff members, Fellows and Associates; in Chile about 70 and, in addition, about 130 local staff members.

The ESO MESSENGER is published four times a year: normally in March, June, September and December. ESO also publishes Conference Proceedings, Preprints, Technical Notes and other material connected to its activities. Press Releases inform the media about particular events. For further information, contact the ESO Education and Public Relations Department at the following address:

EUROPEAN
SOUTHERN OBSERVATORY
Karl-Schwarzschild-Str. 2
D-85748 Garching bei München
Germany
Tel. (089) 320 06-0
Telefax (089) 3202362
ips@eso.org (internet)
URL: http://www.eso.org

The ESO Messenger:
Editor: Marie-Hélène Demoulin
Technical editor: Kurt Kjär

Printed by
J. Gotteswinter GmbH
Buch- und Offsetdruck
Joseph-Dollinger-Bogen 22
D-80807 München
Germany

ISSN 0722-6691

Minor Planet Mariotti

"Named in memory of Jean-Marie Mariotti (1955–1998), French astronomer, most recently in Garching at the European Southern Observatory. He led the pioneering project to establish optical interferometry with the new Very Large Telescope as a breakthrough new astronomical instrument for the next century. His interest was in the area of high angular resolution, and he was involved in interferometric projects both on the ground (e.g., FLUOR and VLTI) and in space (DARWIN). He hoped with these techniques to find low-mass companions, and ultimately planets outside our solar system. He had an extraordinarily effective mix of technical expertise and scientific eagerness."

The 'official' publication of this name giving is to be found in the MPC (Minor Planet Circular) nr 33151 of December 8th, 1998. These MPC's are published, on behalf of Commission 29 of the IAU, by: Minor Planet Center, Smithsonian Astrophysical Observatory, Cambridge, MA 012138, USA.

More info on the publication, or on their web page: http://cfa-www.harvard.edu/iau/mpc.hmbl.

The planet was originally discovered on March 25, 1971 by C.J. van Houghton and I. van Houten-Groeneveld, on Schmidt plates taken by T. Gehrels.

The planet is designated nr (7972) = 1171 T-1.

Contents